

**INVESTIGATING THE ROLE OF INVOLUTION MAMMARY FIBROBLASTS IN
PROMOTING POSTPARTUM BREAST CANCER**

By

Qiuchen Guo

A THESIS/DISSERTATION

Presented to the Cancer Biology Program
& the Oregon Health & Science University

School of Medicine

in partial fulfillment of
the requirements for the degree of

Doctor of Philosophy

MARCH 2017

Contents

| | |
|---|------|
| LIST OF FIGURES. | III |
| LIST OF TABLES. | V |
| LIST OF ABBREVIATIONS. | VI |
| ACKNOWLEDGEMENT. | VIII |
| ABSTRACT. | IX |
| CHAPTER I: BACKGROUND AND INTRODUCTION.# | 1 |
| • Postpartum Breast Cancer. | 1 |
| • Weaning-Induced Involution is Tumor Promotional. | 6 |
| ○ ECM Remodeling. | 9 |
| ○ Immune Modulation. | 11 |
| ○ NSAIDs Decrease Tumor Promotional Attributes of Involution. | 13 |
| • Collagen and Breast Cancer. | 17 |
| ○ The Role of Collagen in Promoting Breast Cancer. | 17 |
| ○ Main Types of Collagen In the Mammary Gland. | 18 |
| ○ NSAIDs decrease collagen during weaning-induced mammary gland involution. | 24 |
| • Introduction of fibroblast. | 26 |
| ○ Fibroblast definition and function. | 26 |
| ○ Fibroblast in wound healing. | 28 |
| ○ Fibroblasts in Cancer. | 29 |
| CHAPTER II. COLLAGEN CHARACTERIZATION DURING WEANING-INDUCED INVOLUTION. | 32 |
| • Abstract. | 33 |
| • Introduction. | 34 |
| • Results. | 37 |
| ○ De novo collagen synthesis during rodent mammary gland involution. | 37 |
| ○ Rat mammary collagen structural reorganization during weaning-induced involution. | 41 |
| ○ Collagen abundance and structural change in human breast tissue during postpartum involution. | 43 |
| • Discussion. | 46 |

| | |
|--|------------|
| • Method. | 48 |
| • Supplemental tables. | 53 |
| CHAPTER III. PHYSIOLOGICALLY ACTIVATED MAMMARY FIBROBLASTS PROMOTE POSTPARTUM MAMMARY CANCER.¹ | 55 |
| • Abstract. | 56 |
| • Introduction. | 57 |
| • Results. | 60 |
| ○ Involution mammary fibroblasts are uniquely activated. | 60 |
| ○ Ibuprofen inhibits involution fibroblast activation in vivo. | 64 |
| ○ Ibuprofen inhibits fibroblast activation in vitro. | 67 |
| ○ Fibroblasts recruit monocytes in a COX-PGE2 dependent manner in vitro. | 69 |
| ○ Ibuprofen inhibits tumor promotional capacity of involution fibroblasts. | 71 |
| • Discussion. | 76 |
| • Method. | 81 |
| • Supplemental Figures. | 90 |
| • Supplemental method. | 96 |
| CHAPTER IV. DISCUSSION AND FUTURE DIRECTIONS. | 98 |
| • Summary of key findings. | 98 |
| • Future perspectives and new questions. | 103 |
| ○ Understand the immune modulation function of fibroblasts during involution. | 103 |
| ○ Macrophage RNA-seq data discussion. | 107 |
| ○ 3D culture models development. | 109 |
| ➤ <i>The crosstalk between macrophages and fibroblasts in a 3D culture model.</i> | 110 |
| ➤ <i>A 3D culture model development for potentially studying involution.</i> | 113 |
| ○ Method. | 115 |
| • Significance. | 118 |
| REFERENCE. | 120 |

LIST OF FIGURES.

| | |
|---|-----|
| Figure 1- 1. The promotional and protective effects of pregnancy to breast cancer. | 2 |
| Figure 1- 2. Breast cancers are mainly diagnosed in aged patients, but within breast cancer patients diagnosed before 45 years of age, 47% of the cases are considered as PPBCs. | 3 |
| Figure 1- 3. Young women diagnosed with postpartum breast cancer are at increased risk for metastasis. | 4 |
| Figure 1- 4. H&E staining of rat mammary gland showing the morphologically changes during a complete pregnancy cycle. | 7 |
| Figure 1- 5. Rodent model of synchronized weaning-induced mammary gland involution. | 8 |
| Figure 1- 6. Immune cells increase in the mammary gland during involution. | 13 |
| Figure 1- 7. The COX/PGE ₂ pathway. | 14 |
| Figure 1- 8. Structures and functions of different types of collagens. | 19 |
| Figure 1- 9. Main types of collagen in the nulliparous rat mammary glands by ECM proteomics. | 20 |
| Figure 1- 10. Type I collagen and type III collagen have similar location pattern in the mammary gland. | 23 |
| Figure 1- 11. Comparison of LOX family members [119] | 27 |
| | |
| Figure 2- 1. De novo collagen synthesis during rat mammary gland involution. | 39 |
| Figure 2- 2. Fibrillar collagen abundance in rat mammary lobules in nulliparous and involuting hosts. | 40 |
| Figure 2- 3. Rat mammary collagen structural remodeling during weaning-induced involution. | 43 |
| Figure 2- 4. Breast collagen abundance and structural change during postpartum involution. | 45 |
| | |
| Figure 3- 1. Mammary fibroblasts are activated during weaning-induced gland involution. | 63 |
| Figure 3- 2. Systemic in vivo ibuprofen treatment during weaning-induced mammary gland involution decreases mammary fibroblast activation. | 66 |
| Figure 3- 3. In vitro mammary fibroblast activation by TGF β 1 is directly inhibited by ibuprofen. | 68 |
| Figure 3- 4. PGE ₂ directly stimulates fibroblast collagen and cytokine expression but not cell elongation. | 70 |
| Figure 3- 5. Mammary involution-fibroblasts are tumor promotional via a COX2 dependent mechanism that suggests immune modulation. | 73 |
| Figure 3- 6. Schematic overview of the potential tumor promotional contributions of mammary involution-fibroblasts. | 75 |
| | |
| Supplemental figure 1. PDGFR α is expressed dominantly by stromal cells surrounding mammary ducts and alveoli. | 90 |
| Supplemental figure 2. Effects of ibuprofen treatment on PDGFR α + cells in the InvD6 mammary gland. | 91 |
| Supplemental figure 3. TGF β 1 does not induce fibroblast α SMA expression in floating collagen cultures. | 91 |
| Supplemental figure 4. Fibroblast ex vivo adhesion and cell culture survival are independent of reproductive state. | 92 |
| Supplemental figure 5. Immunohistochemical characterization of tumor infiltrating immune cells. | 94 |
| Supplemental figure 6. FOXP3 and Ki67 IHC tumor analyses demonstrate no differences between fibroblast groups. | 95 |
| Supplemental figure 7. Characterization of monocyte derived cells by flow cytometry. A) Cells are gated by forward scatter and side scatter. | 96 |
| | |
| Figure 4- 1. Interleukins (A), TGF β s (B), C-X-C motif chemokines and C-C motif chemokines (C) gene expression in nulliparous-fibroblasts (blue) and involution-fibroblasts (orange). | 107 |
| Figure 4- 2. Two populations of macrophages are present in the mammary gland and have altered gene expression during involution compared with nulliparous. | 109 |

Figure 4- 3. M1 macrophages stimulate fibroblast collagen production in a 3D culture model 112
Figure 4- 4. Apoptotic EpH4 cells stimulate more fibroblast-macrophage interactions, especially in F-M2
co-culture conditions..... 113
Figure 4- 5. Fibroblasts support EpH4 cellular morphogenesis..... 115
Figure 4- 6. Average age when women have their first child in United States..... 118

LIST OF TABLES.

| | |
|---|----|
| Table 1. Breast cancer subtypes categorized by postpartum history..... | 5 |
| Table 2. Patients survival rate categorized by pregnancy status at the time of diagnosis..... | 6 |
| Table 3. The width of collagen fibers. | 44 |
| Supplemental table 1. Length of collagen fibers..... | 53 |
| Supplemental table 2. Straightness of Collagen Fibers..... | 54 |
| Supplemental table 3. Properties of Collagen Fibers..... | 54 |

LIST OF ABBREVIATIONS.

| | |
|--------------|--|
| α SMA | Alpha-smooth muscle actin |
| BMDMs | Bone marrow-derived macrophages |
| BMI | Body mass index |
| CAFs | Cancer associated fibroblasts |
| CD3 | Cluster of differentiation 3 |
| CD4 | Cluster of differentiation 4 |
| CD8 | Cluster of differentiation 8 |
| CD11c | Cluster of differentiation 11c |
| CD45 | Cluster of differentiation 45 |
| CD68 | Cluster of differentiation 68 |
| COX | Cyclooxygenase |
| CSF1R | Colony stimulating factor 1 receptor |
| CXCL | C-X-C Motif Chemokine |
| Dock1 | Dedicator of cytokinesis 1 |
| ECM | Extracellular matrix |
| EGF | Epidermal growth factor |
| FACIT | Fibril-associated collagen with interrupted triple helices |
| FACS | Fluorescence-activated cell sorting |
| FN | Fibronectin |
| FSP1 | Fibroblast specific protein 1 |
| GFP | Green fluorescent protein |
| HGF | Hepatocyte growth factor |
| HMD | High mammographic density |
| IGF | Insulin-like growth factor |
| IHC | Immunohistochemistry |
| IL-4 | Interleukin 4 |
| IL-6 | Interleukin 6 |
| IL-8 | Interleukin 8 |
| IL-10 | Interleukin 10 |
| IL-12 | Interleukin 12 |
| IL-13 | Interleukin 13 |
| JAK1 | Janus Kinase 1 |
| LIF | Leukemia inhibitory factor |
| LMD | Low mammographic density |
| LOX | Lysyl oxidase |

| | |
|---------------|--|
| LOXL1-4 | Lysyl oxidase like proteins 1-4 |
| MACIT | Membrane-associated collagen with triple helices |
| MEC | Mammary epithelial cell |
| MMP | Matrix metalloproteinase |
| MMTV | Mouse mammary tumor virus |
| MULTIPLEXIN | Multiple triple helix domains and interruptions |
| NF κ B | Nuclear factor kappa-light-chain-enhancer of activated B cells |
| NSAIDs | Nonsteroidal anti-inflammatory drugs |
| PD1 | Programmed cell death protein 1 |
| PDGFR | Platelet-derived growth factor receptor |
| PDL1 | Programmed death-ligand 1 |
| PGD2 | Prostaglandin D2 |
| PGE2 | Prostaglandin E2 |
| PGI2 | Prostaglandin I2 |
| PPBC | Postpartum breast cancer |
| PyMT | Polyoma middle T |
| SHG | Second harmonic generation imaging |
| STAT3 | Signal transducer and activator of transcription 3 |
| SV40 | Simian virus 40 |
| TACs | Tumor-associated collagen signatures |
| TAMs | Tumor associated macrophages |
| TGF β | Transforming growth factor |
| TNBC | Triple negative breast cancer |
| TNF | Tumor necrosis factor |
| TXA2 | Thromboxane |
| VEGF | Vascular endothelial growth factor |

ACKNOWLEDGEMENT.

I would like to thank my mentor Dr. Pepper Schedin for being a fearless leader to accept me as a Ph.D. candidate, with knowing that I need more help and training as an international student. She teaches me not only how to do science, but also to become a better scientist. Her inspiration and encouragement will last in my future scientific career.

I would like to thank the past and present Schedin lab members for welcoming me to become a family member of the Schedin lab and for their continuous help and support as a team. I want to thank Courtney Betts and Erica Goddard to be with me through my entire graduate school journey, and for their support during difficult times and also memories of fun time together.

I would like to thank my dissertation committees for their insightful suggestions and discussions regarding my project.

Finally, I would like to thank all my friends and family for their supports during this long journey to keep me moving forward.

ABSTRACT.

Postpartum breast cancer, which is breast cancer diagnosed within 5 to 10 years of childbirth, has poor outcomes compared to breast cancer in age-matched nulliparous or pregnant women, regardless of the breast cancer subtypes, tumor stage or year of diagnosis. In preclinical mouse models, tumor cells show increased proliferation, invasion and metastatic capacities when injected into the involuting mammary gland, compared with the nulliparous mammary gland. Investigations of the microenvironment of the involuting mammary gland that may contribute to tumor promotion reveal increased fibrillar collagen abundance. Collagen abundance and structure regulation is closely associated with breast cancer risk and progression, and here we hypothesize that increased collagen deposition and structure remodeling occurring during weaning-induced involution is similar to tumor associated collagen, referred to as TACS3, which independently predicts poor outcomes in breast cancer patients. TACS3 collagen is straightly aligned collagen fibers that are perpendicular to leading edge of the tumor, and is thought to facilitate local tumor cell escape and vascular invasion. Further, we hypothesize that pro-tumorigenic collagen remodeling during involution is mediated by a uniquely activated fibroblast that is normally present only during weaning-induced involution. Here, I identified the dominant collagens present in the rat mammary gland, and provide evidence for stage-specific regulation, deposition and organization of collagen between nulliparous, lactating and weaning-induced involuting mammary glands in both rats and women. A transient and significantly decreased gap area between ductal collagen fibers was found during involution, suggesting tightly packed collagen fibers under high tension. Moreover, increased percentage of fibers that were perpendicular to the mammary epithelium were found during involution, data consistent with the tumor-associated TACS3 collagen signature. Increased collagen abundance and structural remodeling indicate activation of mammary fibroblasts during involution, as fibroblasts are well-known for their function in

collagen production and remodeling. To test this hypothesis, I isolated and characterized PDGFR α + mammary fibroblasts from nulliparous and involuting hosts, and found increased gene expression of fibrillar collagens and collagen remodeling enzymes in the involution-fibroblasts compared with nulliparous-fibroblasts. Pathway analysis of the RNA-seq data showed involution-fibroblasts were also enriched for immune related pathways, with increased levels of cytokines and chemokines, such as TGF β 1 and CXCL12. Further, ibuprofen treatment during involution decreased fibroblasts activation, suggesting a cyclooxygenase-dependent activation in the involution-fibroblasts. Importantly, involution-fibroblasts showed increased tumor promotional capacities compared to nulliparous-fibroblasts, which was also decreased by ibuprofen treatment. Further investigation of the in vitro culture and in vivo tumor studies indicated a COX/PGE2 dependent immune modulation function of the involution fibroblasts, consistent with monocyte recruitment and CD8 T cell inhibition.

In summary, we found reproductive-state dependent mammary collagen deposition and organization, which may contribute to the individual differences in breast density observed in women. Physiologic regulation of fibrillar collagen deposition and organization may be a previously unrecognized modifier of breast cancer risk, as well as tumor outcome that deserves further investigation. Additionally, I found that collagen regulation during weaning-induced involution is at least partially contributed by fibroblast activation. Fibroblast characterization reveals critical functions of fibroblasts in the contribution of the tumor promotional microenvironment during weaning-induced involution, which involve ECM remodeling and immune modulation. The function of ibuprofen in targeting fibroblasts collagen I production and immunosuppressive functions during involution may provide new leads for the prevention and therapeutic treatment of postpartum breast cancer.

CHAPTER I: BACKGROUND AND INTRODUCTION.#

- **Postpartum Breast Cancer.**

Pregnancy can have both protective and promotional effects on breast cancer. It is well known that pregnancy has a long-term protective effect on breast cancer risk, primarily reducing incidence of postmenopausal breast cancer. It is hypothesized that pregnancy protects the gland through induction of terminal differentiation, since breast tissue is not fully differentiated or mature until pregnancy and lactation, and full maturation of mammary epithelium is protective against development of breast cancer in rodent models [1]. On the other hand, more recent studies have shown that there is a transient increased risk for breast cancer following childbirth, which peaks at ~6 years post-partum. The fact that pregnancy can both reduce and increase risk for breast cancer has been called the dual effect of pregnancy, and was first described by Janerich and Hoff in 1982 [2]. The duration of increased risk of breast cancer following pregnancy also positively correlates with age at the first birth, with age 35 as a crucial point, as the increased risk becomes permanent, rather than transitory, when a mother's first birth is after 35 years of age [3]. Further, the breast cancers diagnosed within 5-10 year postpartum, and defined as postpartum breast cancers (PPBCs), have increased risk of metastasis [3, 4].

#Most of the immune regulation function of TGF β in the introduction was re-printed with permission from the Journal of Clinical Medicine. (Guo Q, Betts C, Pennock N, Mitchell E, Schedin P. Mammary Gland Involution Provides a Unique Model to Study the TGF- β Cancer Paradox. J Clin Med. 2017 Jan 13;6(1).)

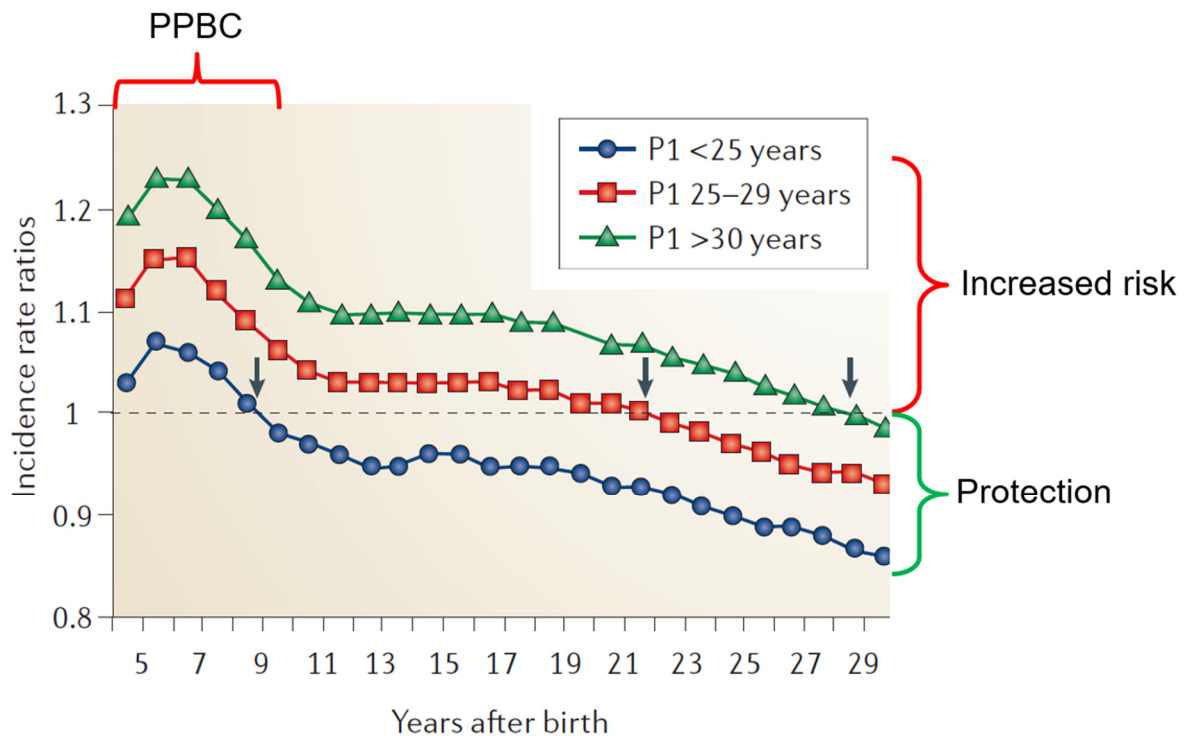


Figure 1- 1. The promotional and protective effects of pregnancy to breast cancer.

Breast cancer risk is influenced by productive history. In women of all age groups analyzed, there is a transient increased risk for breast cancer following giving birth compared with nulliparous women (incidence rate ratios=1) and then the breast cancer risk is gradually decreased. This transiently increased risk for breast cancer is positively correlated with the age at first birth. Women who are less than 25 years of age at first birth have approximately 10 years increased breast cancer risk following birth, and then reach pregnancy associated breast cancer protection. While, women who are more than 30 years of age at first birth have a prolonged increased risk for breast cancer, which lasts for nearly 30 years postpartum. Figure adapted and reprinted with permission from Nature Reviews Cancer (Schedin P. Pregnancy-associated breast cancer and metastasis. *Nat Rev Cancer*. 2006 Apr;6(4):281-91.)

Although breast cancer is most frequently diagnosed among women aged 50 and older [3], the diagnoses of invasive cases in young women with age less than 50 years are comparable with the older women (Figure 1-2A), suggesting an overall increased ratio of invasive breast cancer in young women. Further, a significant number of breast cancers in young women are associated with recent pregnancy [4] (Figure 1-2B). Based on breast cancer case records during 2009-2013, around 11% of new breast cancer cases per year are women with age under 45, and among those cases, around 50% patients are within 10 years postpartum, which are considered PPBC cases [4] (Figure

1-2B). According to data from National Vital Statistics System, a gradual increase from 23 to 26 years of age at first birth has been observed between 1980 and 2012 in United States. Importantly, this trend toward delayed childbearing is occurring worldwide [5]. Considering the fact that increasing age at first birth correlates with increased risk for breast cancer, more PPBC cases per year are expected and observed in several population studies, including Sweden, Japan, and United States [6-8].

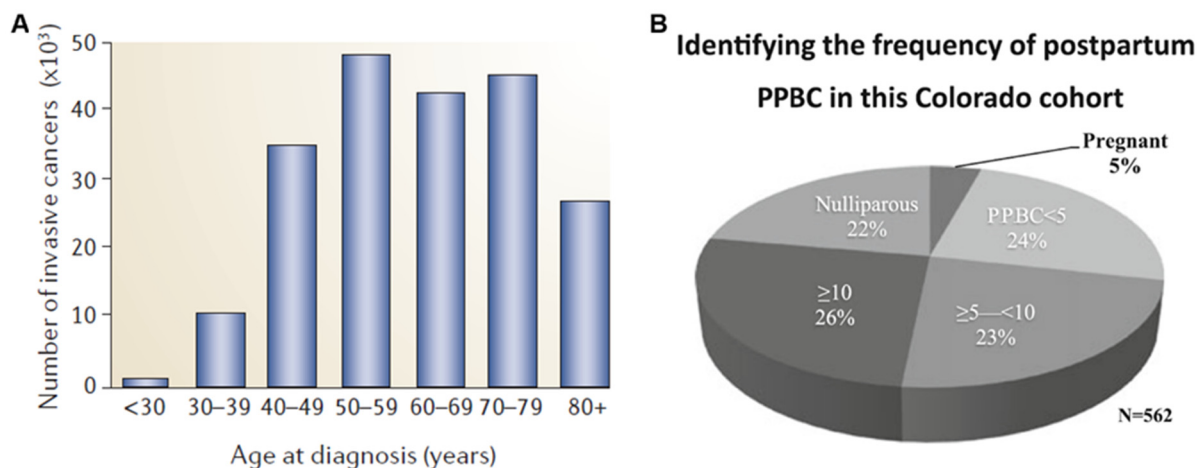


Figure 1- 2. Breast cancers are mainly diagnosed in aged patients, but within breast cancer patients diagnosed before 45 years of age, 47% of the cases are considered as PPBCs.

A. The numbers of invasive breast cancer cases diagnosis are grouped by age of the patients, indicating invasive breast cancers are diagnosed more in the 50-59 age group than all other groups. **B.** In Colorado young women’s breast cancer cohort, among breast cancer patients diagnosed within 45 years of age, 24% of the cases are within 5 years postpartum and 23% of the cases are 5 to 10 years postpartum, which are both consisted PPBCs. These data suggest that almost half of the young women’s breast cancer cases can be categorized into PPBC. Figure adapted and reprinted with permission from Nature Reviews Cancer (Schedin P. Pregnancy-associated breast cancer and metastasis. *Nat Rev Cancer*. 2006 Apr;6(4):281-91.) and (Callihan EB. et al. Postpartum diagnosis demonstrates a high risk for metastasis and merits an expanded definition of pregnancy-associated breast cancer. *Breast Cancer Res Treat*. 2013 Apr;138(2):549-59.)

The uniqueness of postpartum breast cancer that differentiates it from other breast cancers is the aggressiveness of the disease. In a University of Colorado young women’s breast cancer cohort, patients diagnosed within 5 years of a pregnancy were around 3 times more likely to have a metastatic recurrence and die from their disease, compared to nulliparous patients who had never

given birth [4](and unpublished data, Goddard et al. Schedin Lab.) (Figure 1-3). These data remained significant even after adjusting for poor prognostic clinical variables including breast cancer biologic subtype, stage, patients' age at diagnosis, and year of diagnosis [4](and unpublished data, Goddard et al. Schedin Lab.).

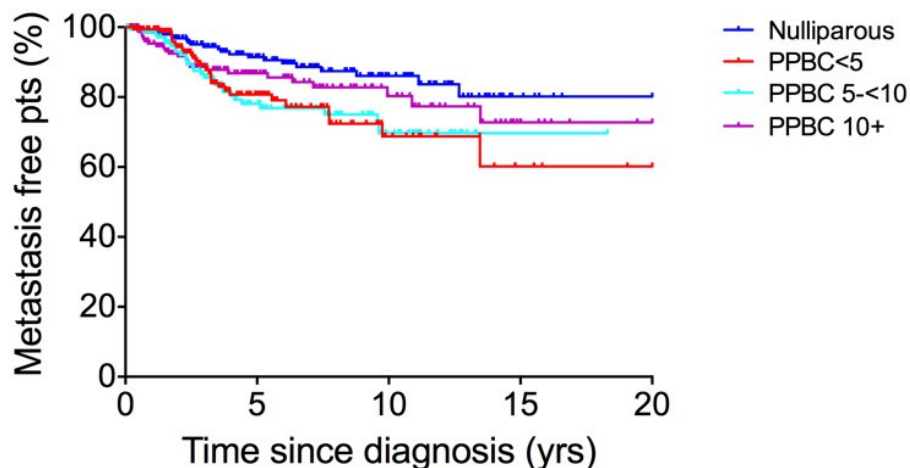


Figure 1- 3. Young women diagnosed with postpartum breast cancer are at increased risk for metastasis.

Time to metastasis Kaplan-Meier curve of young women's breast cancer cohort (n=705) (Log Rank Test, P=0.02). Analysis excluded patients with stage 0, stage IV, or stage unknown disease, and/or an unknown year of diagnosis (n=221 Nullip; n=175 PPBC<5; n=153 PPBC 5-<10; n=156 PPBC 10+). (Unpublished data from Erica Goddard, Solange Mongoue-Tchokote, Tomi Mori, Jeremy Johnston, Eryn Callihan, Pepper Schedin, Virginia Borges)

PPBC patients have decreased survival compared with the nulliparous patients with the same breast cancer subtypes [4](and unpublished data, Goddard et al. Schedin Lab.). What's more, analysis of the same patient cohort suggests that PPBC cases are also not enriched for the more aggressive subtypes of breast cancer, such as triple negative breast cancer (TNBC) or HER2 positive breast cancer (Table 1, unpublished data from Goddard et al, Schedin Lab), further supporting that the aggressiveness of the PPBC is not due to enrichment in poor prognostic biologic subtypes, but rather is being driven by extrinsic factors, such as host biology.

Table 1. Breast cancer subtypes categorized by postpartum history.

| Subtype | Nullip (n=232) | PPBC<5 (n=187) | PPBC 5<10 (n=164) | PPBC≥10 (n=168) |
|--------------|-------------------|-------------------|----------------------|--------------------|
| | % | % | % | % |
| TN | 15.1 | 18.2 | 13.4 | 17.3 |
| Her 2+ | 7.3 | 8.6 | 7.9 | 8.3 |
| Lum A | 37.5 | 42.3 | 43.3 | 36.9 |
| Lum B | 15.5 | 13.4 | 13.4 | 12.5 |
| Her2-Unknown | 24.6 | 17.7 | 22 | 25 |

Surprisingly, epidemiologic data suggest that a breast cancer diagnosis and treatment during pregnancy does not increase rates of metastasis over age-matched, stage matched nulliparous patients [9-11]. This is surprising given that pregnancy is characterized by dramatic increases in estrogen and progesterone levels, which have been reported to be intimately associated with breast cancer initiation and progression [12, 13]. Thus, it was anticipated that increased hormone levels during pregnancy would contribute to the aggressiveness of postpartum breast cancer. However, epidemiologic studies of breast cancer patient cohorts defeat this hypothesis [9-11]. Rather, epidemiologic studies report that the poor prognosis of postpartum breast cancer is limited to women diagnosed in the postpartum window, and is not observed in women diagnosed and treated during pregnancy [3, 4, 14] (Table 2). Further, the vast majority of young women diagnosed with breast cancer are either nulliparous or postpartum, with only 1-2% of young women's breast cancer diagnosed during pregnancy [9]. These data suggest breast cancers diagnosed during pregnancy potentially do not contribute largely to the number and poor outcome of the young women breast cancer patients.

Table 2. Patients survival rate categorized by pregnancy status at the time of diagnosis.

| Survival | non-pregnancy associated breast cancer | diagnosed during Pregnancy | <7-month post-partum |
|-------------------------|--|----------------------------|----------------------|
| 11 year ^[9] | 69% | 52% | 33% ($P=0.036$) |
| 10 year ^[10] | 66% | 53% | 35% |
| 5 year ^[11] | 81% | 78% | not determined |

Delayed diagnosis is another potential explanation for the poor survival rate of PPBC, as increased breast density during pregnancy and lactation limits the accuracy of self-exam and mammography [15, 16]. However, similar tumor sizes and stages are found between breast cancers diagnosed in nulliparous and PPBC patients [4, 17, 18], demonstrating poor prognosis of postpartum patients appears independent of delayed diagnosis. Together, these epidemiology studies indicate that unique biology in the postpartum window, independent of tumor intrinsic biology and pregnancy, are promoting breast cancer progression.

- **Weaning-Induced Involution is Tumor Promotional.**

Weaning-induced involution is proposed to be a primary contributor to the poor outcome of postpartum breast cancer patients, as the microenvironment of the involuting mammary gland is highly tumor promotional. In preclinical murine models of PPBC, tumor cells injected into the mammary fat pad at day 1 post-weaning formed significantly larger tumors with higher rates of metastasis compared to tumors injected into mammary glands of age-matched nulliparous controls [14, 19]. More specifically, tumor cells injected into involuting mammary gland not only grew faster but also had increased tumor cell local invasion, blood vessel invasion, lymphatic vessel invasion, higher numbers of circulating tumor cells, and increased lung metastasis [14, 19, 20]. Together, these data demonstrate a tumor promotional microenvironment in the mammary gland during weaning-induced involution, which may provide insight into the high metastatic rates observed in women with postpartum breast cancer.

The mammary gland is a dynamic organ that undergoes dramatic changes during each pregnancy cycle, and this intensive tissue remodeling process may contribute to the increased risk for postpartum breast cancer. In rodent models, before pregnancy, the mammary gland is predominantly adipose tissue with a low amount of glandular tissue. During pregnancy, with the stimulation of high levels of hormones (mainly estrogen, progesterone, and prolactin) and growth factors such as Insulin-like growth factor (IGF), mammary epithelial cells undergo remarkable proliferation and differentiation in preparation for milk production during lactation. After lactation, with milk cessation or after pregnancy in the absence of nursing, the mammary gland undergoes involution. During weaning-induced involution, unnecessary secretory epithelial cells are eliminated through a concerted, developmentally regulated cell death and tissue remodeling program, upon which, the mammary gland returns to a regressed stage, with morphology resembling the nulliparous mammary gland (Figure 1-4) [21-25].

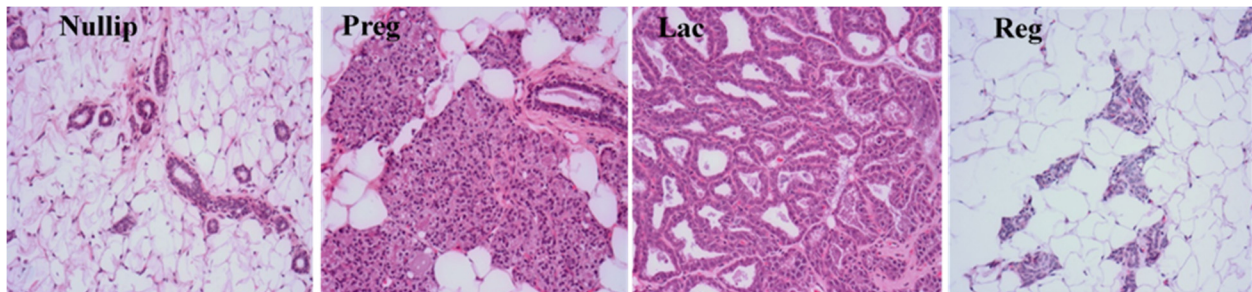


Figure 1- 4. H&E staining of rat mammary gland showing the morphologically changes during a complete pregnancy cycle.

Nullip: Nulliparous. Preg: Pregnancy. Lac: Lactation. Reg: Regressed.

Using rodent models, where the lactational load can be normalized and involution synchronized by standardizing pup removal, it is possible to obtain tissue from different stages of involution allowing for the cellular and molecular events of involution to be analyzed in detail (Figure 1-5). The hallmark features of involution include clearance of $\geq 80\%$ of the mature, secretory mammary

epithelium through programmed cell death mechanisms [22, 26], adipocyte repopulation [27], immune cell infiltration, and extracellular matrix (ECM) deposition consistent with wound healing [19, 28, 29]. Weaning-induced involution leads to regression of the mammary gland to a rudimentary state, which is histologically almost indistinguishable from the nulliparous mammary gland.

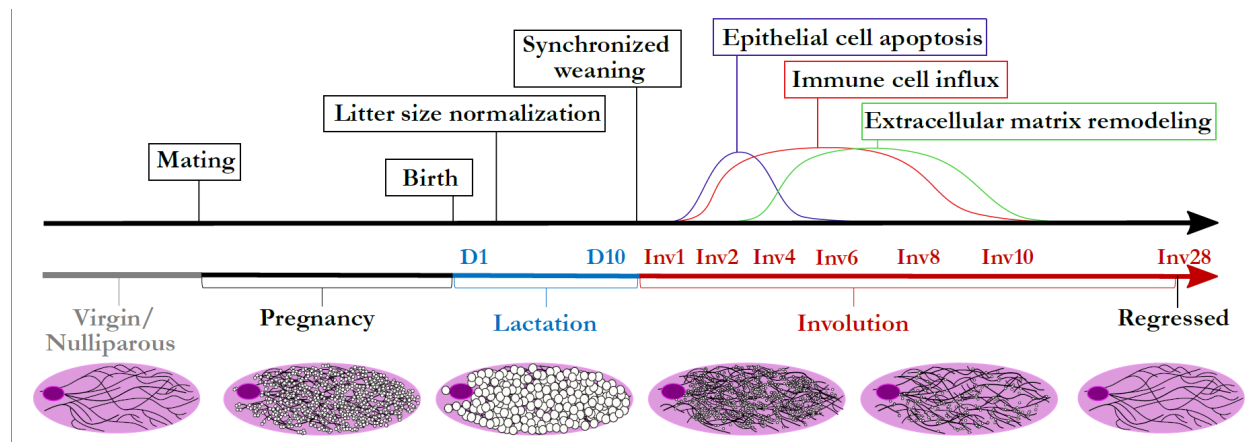


Figure 1- 5. Rodent model of synchronized weaning-induced mammary gland involution. Male and female rodents are mated for 3-5 days. After pup birth, litter size is normalized to ensure equal lactation load per dam, and weaning initiated during peak lactation (9-13 days) by pup removal. The kinetics of three major cellular events during involution are shown above the timeline: epithelial cell apoptosis, immune cell infiltration, and extracellular matrix remodeling. Days since the start of lactation are indicated by “D” followed by a number, and days since synchronized weaning by “Inv”. Whole gland representation of mammary epithelial cells (small black circles) as well as milk accumulation (white fill) is displayed below the corresponding developmental stages in the timeline. Figure from (Guo Q, Betts C, Pennock N, Mitchell E, Schedin P. Mammary Gland Involution Provides a Unique Model to Study the TGF- β Cancer Paradox. *J Clin Med.* 2017 Jan 13;6(1).)

Weaning-induced mammary gland involution can be separated into two distinct phases [22]. The first phase is the initiation of epithelial cell apoptosis, which lasts for approximately 48 hours. This is a reversible phase, as return of pups to the mother within 48 hours results in commencement of lactation [22]. During this initial cell-death phase, the majority of epithelial cells undergo cathepsin and caspase-mediated cell death [30, 31]. Multiple signaling pathways are involved in initiating epithelial cell death during involution, including JAK1 (Janus Kinase 1), LIF (Leukemia inhibitory factor), Dock1 (Dedicator of cytokinesis 1), NF κ B/TNF and TGF β . Impairment in any of these

pathways can result in delayed involution [32-36]. Apoptotic cell clearance also occurs simultaneously. During the first phase of involution, the clearance of apoptotic cells is largely accomplished by epithelial cells that do not initiate early cell death, but rather become phagocytic [37]. Recently, TGF β 3 has been shown to be sufficient to induce a phagocytic phenotype in mature mammary epithelial cells cultured under conditions that mimic epithelium tight junction closure unique to the lactating gland [38], suggesting a critical function of TGF β 3 in facilitating apoptotic cell clearing during the early phase of involution.

Following the first wave of mammary epithelial cell (MEC) apoptosis, involution progresses into a non-reversible, protease-dependent phase, primarily characterized by lobuloalveolar collapse and adipocyte repopulation. The main events during the second phase of weaning-induced involution are additional intensive epithelial cell apoptosis and stromal remodeling [22, 39, 40] consisting of ECM deposition and turnover, and immune cell infiltration [24, 28, 41, 42]. The similarities between the stromal remodeling of involution and wound healing, a process known to be tumor promotional, has provided rationale for investigating mammary gland involution as a window of risk for metastasis. The detailed stromal remodeling of weaning-induced involution is described below.

- **ECM Remodeling.**

As stated above, ECM components are dynamically regulated by reproductive state and during weaning-induced involution share similarities with wound healing microenvironments. For example, fibrillar collagen, fibronectin (FN) and tenascin-C all increased during involution, as shown by western blot [14, 28, 29, 43-45]. What's more, fragmentation of fibrillar collagens and FN have been shown to dramatically increase during involution, which is consistent with proteolysis and remodeling of ECM during this window [46]. Consistent with ECM proteolysis,

upregulation of several matrix metalloproteinases occurs post weaning, including increases in MMP2, MMP3, and MMP9 [46].

ECM isolated from the involuting mammary gland is tumor promotion in numerous models of breast cancer. For example, rat mammary matrix isolated from involuting glands supports MDA-MB-435 cell invasion, whereas, matrix isolated from nulliparous rat mammary glands suppressed motility and invasion of this highly metastatic cell line [47]. The mechanisms by which ECM isolated from different reproductive states can influence tumor progression has been investigated. In one study, MDA-MB-231 human breast tumor cells or murine mammary tumor cells cultured on ECM isolated from involuting rat mammary glands led to disruption of e-cadherin and occluding based cell adhesion junctions, resulting in the formation of more invasive cells as compared to tumor cells cultured on matrix isolated from nulliparous rat mammary glands [43, 48]. Changes in cell adhesion junctions upon ECM engagement is potentially mediated by integrins. It has been shown that tumor cells cultured on fibrillar collagen have decreased cell membrane integrin $\beta 1$ and increased subcellular integrin $\beta 1$ distribution with a more invasive morphology compared with tumor cells cultured in the non-fibrillar collagen, and that blocking endocytic trafficking reverted tumors to a more indolent morphology [49]. These data suggest that endocytic trafficking of integrins mediates the response of cells to their ECM microenvironment. The ability of involution ECM to support tumor cell invasion also was tested directly in an orthotopic xenograft model. In this study, MDA-MB-231 cells were mixed with ECM matrix isolated from nulliparous or involuting rat mammary glands and then injected into the inguinal fat pads of female nude mice. Increased lung, liver, and kidney metastases were observed when tumor cells were mixed with involution matrix, data supporting increased tumor cell invasion by involution matrix [43]. More ECM protein changes of the involuting mammary gland have been

revealed by proteomics analysis, including increases in collagen I, IV, V, VI, and XVIII [29, 50]. Cumulatively, the data indicate dynamic changes of the mammary ECM composition and support a tumor promotional microenvironment during involution, and also serve as strong evidence of the critical role of ECM in regulating mammary epithelial cell behavior, as originally proposed by Mina Bissell [51].

- **Immune Modulation.**

Immune cells have critical functions during weaning-induced involution. Efficiently clearance of dying cells in the tissue is a crucial biological requirement to achieve desire structure/organization and avoid inflammation [52]. Defects in the clearance of apoptotic cells have been attributed to the onset of persistent inflammatory disorders [53]. Immune cell infiltration into the mammary gland has been found during weaning-induced involution [19]. Immunohistochemistry (IHC) staining of CD68, a macrophage marker, shows a dramatic increase of macrophage during involution, consistent with the increased demand for apoptotic cell clearance [28]. Rather surprisingly, macrophages are also found to be necessary for epithelial cell death during involution, suggesting additional critical functions of macrophages during involution. A macrophage depletion mouse model has been used to investigate macrophages during weaning-induced involution. In this model, CSF1R positive cells express a modified FAS transgene that dimerizes upon treatment with the drug AP20187. FAS dimerization induces apoptosis in the CSF1R+ macrophages. Depletion of CSF1R+ macrophages in this mouse model blocked MECs death in the first phase of weaning-induced involution, regardless of STAT3 upregulation, a primary mediator of MEC apoptosis. Lack of MECs apoptosis leads to delayed involution as evidenced by delayed alveolar regression and adipocyte repopulation. Involution can be rescued by injection of

bone marrow-derived macrophages (BMDMs) into the mammary gland [54]. These data suggest a critical role for macrophages during the normal weaning-induced mammary gland involution.

Considering the importance of the immune cells during weaning-induced involution and their roles in cancer promotion, a lot of effort has been focused on characterizing the immune cells present in the gland during involution. In the post-weaning mammary gland, we and others have reported dramatic temporal changes in the abundance and types of immune cells [19, 24, 28, 55]. During involution, we have observed an increase in number and population of regulatory T cells, immature myeloid cells, and M2 macrophages (Figure 1-6). Consistent with these observations, we also noted increases in the immunosuppressive cytokines, IL-4, IL-13, IL-10, and TGF β during involution [28, 38], suggesting immunosuppression during the clearance of apoptotic cells. Cumulatively, these immune profiling data are consistent with expected roles in developmental tissue reconstruction and promoting immune tolerance, as described below.

In the normal weaning-induced mammary gland involution, the link between the coordinated epithelial cell death and immune suppression likely exists to minimize self-antigen exposure to tissue resident and local lymphatic immune cells. This is important for maintaining tissue homeostasis and preventing inflammation. However, in the presence of tumor cells, this microenvironment will favor tumor cell escape from immune surveillance and tumor promotion from the M2 skewed myeloid cells [56]. In fact, the immune phenotypes characterized during involution carried forward into the tumor microenvironment. In the involuting mammary gland, there are increased numbers of immature myeloid cells, M2 macrophages, and IL-10 expressing T cells; an immune signature associated with pro-tumor immunity. Moreover, IL-10 blockage through antibody administration reduced the observed growth advantage in post-weaning hosts compared to genetically identical tumors implanted into nulliparous hosts [19], suggesting the

presence of tumor promotional immune response in the involuting mammary gland and its potential role in tumor progression in this window.

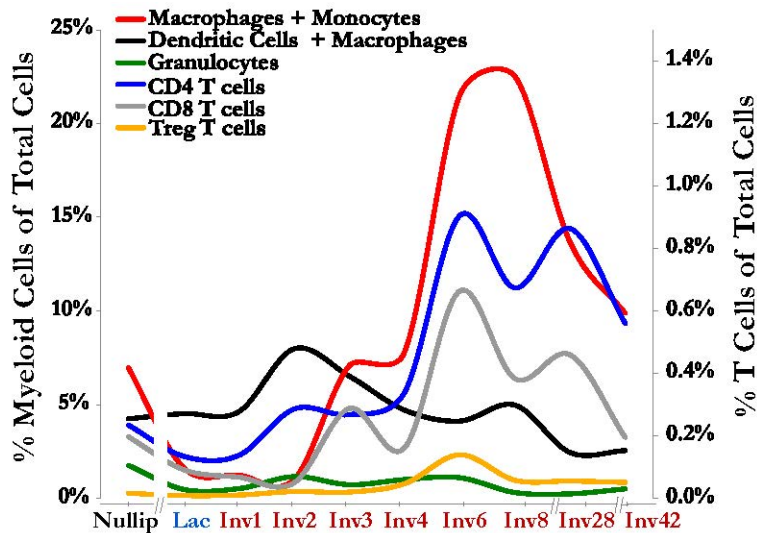


Figure 1- 6. Immune cells increase in the mammary gland during involution.

An influx of immune cells consistent with classic wound healing is observed during mammary gland involution including various myeloid cell populations (left axis): Macrophages and monocytes (CD45+ Gr1int/lo F480+ CD11b+, red line), Dendritic cells and macrophages (CD45+ CD11c+ MHCII+, black line), and Granulocytes (CD45+ Gr1hi F480- CD11b+, green line). T cells are also increased in the mammary gland during involution (right axis): CD4 T cells (CD45+ CD3+ CD4+, blue line), CD8 T cells (CD45+ CD3+ CD8+, gray line) and the immunosuppressive Treg T cells (CD45+ CD3+ CD4+ FoxP3+ CD25+, orange line). The involution window is labeled in red, as “Inv” followed by a number for the day post weaning. Both axes represent frequencies of indicated cell populations as a fraction of total cells from the gland, as determined by single cell suspensions analyzed by flow cytometry. Figure from (Guo Q, Betts C, Pennock N, Mitchell E, Schedin P. Mammary Gland Involution Provides a Unique Model to Study the TGF- β Cancer Paradox. *J Clin Med.* 2017 Jan 13;6(1).)

○ **NSAIDs Decrease Tumor Promotional Attributes of Involution.**

Studies in sections above support the conclusion that ECM remodeling, immune suppression and M2-skewed myeloid cells during weaning-induced involution support mammary tumor promotion during weaning-induced mammary gland involution. Thus, targeting the involution stromal microenvironment might benefit postpartum breast cancer prevention and treatment efforts. In support of this hypothesis, the Schedin lab has reported that nonsteroidal anti-inflammatory drugs (NSAIDs) decrease tumor growth and dissemination to nulliparous levels in both

immunocompromised and immunocompetent PPBC mouse models [14, 20] (and Martinson unpublished data).

NSAIDs are cyclooxygenase (COX) inhibitors and include the COX2 specific inhibitor, such as celecoxib, and COX1 and COX2 nonspecific inhibitors, such as aspirin and ibuprofen. COX1 and COX2 are key enzymes in the synthesis of homeostatic and pro-inflammatory prostanoids [57]. The major difference between COX1 and COX2 is that COX1 is constitutively produced by many different epithelium, whereas, COX2 is predominantly found to be induced on epithelium in the case of chronic inflammation and cancer [58] (Figure 1-7).

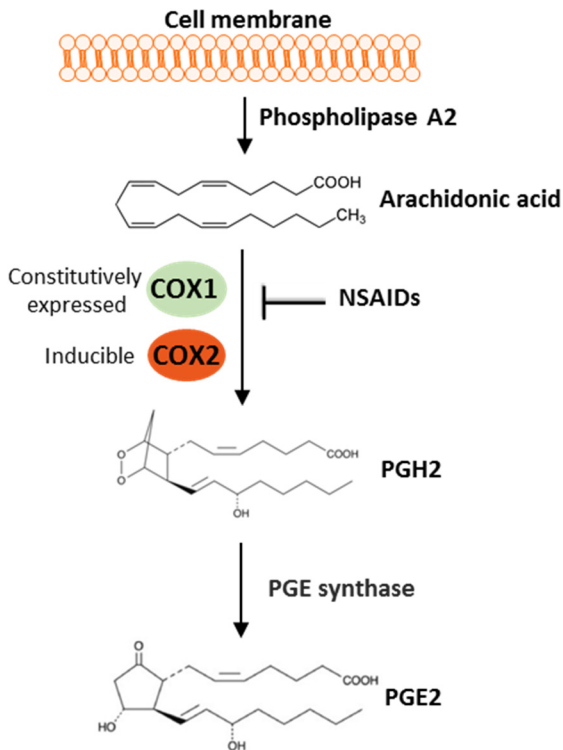


Figure 1- 7. The COX/PGE2 pathway.

Arachidonic acid is released from the plasma membrane by phospholipase A2, then converted into PGH2 by COX1 or COX2. With the function of PGE synthase, PGH2 is converted to PGE2. The function of NSAIDs is to inhibit the COX enzymes.

The first clinical evidence that NSAIDs can prevent cancer is the observation that patients with familial colorectal polyposis treated with NSAIDs displayed a reduction in adenoma number [59]. Epidemiological studies carried by Thun et al, reports that regular intake of the COX1 and COX2 dual inhibitor aspirin, or low dose COX2 specific inhibitor celecoxib, reduces the risk of colorectal

cancer [60, 61]. These reports provide strong links between prostaglandins, their synthetic enzymes, and cancer, with a focus on COX2. COX2 has been shown to be upregulated in many types of cancer, including oral [62], colorectal [63] and breast [58]. Clinical data show overexpression of COX2 in ductal carcinoma in situ correlates with an increased nuclear grade and Ki67 [64], and high COX2 level in breast cancer is associated with poor outcomes as measured by decreased disease-free and overall survival [65, 66]. Additionally, regular use of NSAIDs associates with a modest reduction in overall breast cancer risk [67, 68]. These studies indicate a critical role of COX2 in cancer overall, and further suggest NSAIDs as potential prevention and therapeutic drug for breast cancer.

The mechanisms by which COX2 promotes cancer is likely associated with its enzyme products, the prostanoids, such as prostaglandin E2 (PGE2), prostaglandin D2 (PGD2), prostaglandin I2 (PGI2), and thromboxane (TXA2). PGE2 is one of the best characterized products of the COX pathway, and is closely associated with pain, inflammation and cancer. PGE2 is a bioactive lipid that elicits a wide range of biological functions, both pro- and anti-inflammatory. In a cutaneous wound, damaged tissue releases PGE2, which acts as a vasodilator to facilitate the influx of neutrophils, macrophages and mast cells, leading to swelling and edema at early stages of wound resolution. Furthermore, PGE2 stimulates sensory nerves to increase the pain response and acts on neurons in the preoptic area to promote pyrogenic effects. However, PGE2 also has anti-inflammatory functions to resolve inflammation and facilitate tissue repair. The immunosuppressive functions of PGE2 include suppressing IL-12 and enhance IL-10 production in monocytes and dendritic cells. These effects of PGE2 will lead to the shift from Th1 to Th2 in CD4 T cells [69, 70], and blocking the ability of dendritic cells to attract naïve T cells [71]. What's more, PGE2 also can directly suppress the interactions between CD8 T cells and pathogens or

tumor cell [71]. This evidence indicates the critical functions of COX2/PGE2 in immune suppression, which, in the context of a tumor, is thought to lead to escape from immune surveillance and cancer progression.

The COX2/PGE2 pathway is also involved in tumor angiogenesis. In the process of solid tumor growth, the high metabolic demand of the tumor needs to be fulfilled by an increased blood supply, thus, tumor-induced angiogenesis is critical for tumor progression. It has been reported that overexpression of COX2 in tumor cells induces the production of angiogenesis factors, such as vascular endothelial growth factor (VEGF), which can stimulate endothelial cell growth and formation of new blood vessels. Treatment with NSAIDs can inhibit endothelial cell proliferation and tube formation *in vitro*, which can be rescued by adding PGE2, indicating the important function of PGE2 in COX2 induced angiogenesis.

In addition to tumor microenvironment modification, COX2/PGE2 also act as tumor intrinsic factor that stimulates tumor progression. Tumor cells that are COX2 positive display increased proliferation, migration and invasion abilities. Further studies have demonstrated that PGE2 promotes cytoskeletal reorganization and increases cancer cell migration and invasion via PI3K signaling [72].

COX2 upregulation is not only found in pathological conditions such as cancer, it is also increased during weaning-induced involution [73], providing a potential mechanism for the increased aggressiveness of PPBC, and justifying the use of NSAIDs as putative prevention and therapeutic drugs in PPBC. In rodent models of PPBC, NSAIDs reduce tumor burden and progression during involution in part by targeting the microenvironment. ECM isolated from ibuprofen-treated involuting rat mammary glands suppresses D2.OR mouse mammary tumor cells growth and invasion in an *in vitro* 3D culture model [48]. NSAID treatment also decreases lymphangiogenesis

and metastasis in a PPBC mouse model [20]. Interestingly, analysis of the normal involuting mouse mammary glands shows that NSAIDs treatment decreases collagen in the involuting mammary gland [14]. Considering the strong links between collagen and breast cancer, the finding that NSAIDs inhibit collagen deposition provides another potential mechanism by which NSAIDs suppress tumor development during involution; a topic discussed in more depth in the next section.

- **Collagen and Breast Cancer.**

- The Role of Collagen in Promoting Breast Cancer.

Collagen I, a fibrillar forming collagen, is the most abundant extracellular matrix protein in the breast. Fibrillar collagen is not only closely associated with breast cancer risk by contributing breast density, but high collagen I also contributes to breast cancer progression. The *Coll1a1^{tmJae}* transgenic mouse model that mimics a high collagen mammary environment has been used to directly study the effect of collagen I in the initiation and progression of breast cancer. *Coll1a1^{tmJae}* mice carry mutations near the highly-conserved matrix metalloproteinase (MMP) cleavage site for type I collagen (between Gly₇₇₅ and Ile₇₇₆ of the $\alpha 1(I)$ chain), which makes collagen I resistant to MMP digestion. Although collagen can still be digested by other enzymes, the enzymatic digestion is not sufficient to maintain the balance between collagen production and degradation. This results in increased collagen accumulation in skin, uterus, and bone in the mouse model as well as a more than 2.5-fold increased stromal collagen in the mammary glands. The crossing of the spontaneous mouse mammary tumor model MMTV-PyMT with the *Coll1a1^{tmJae}* model induced an approximately 3-fold increase in primary mammary tumor formation concurrent with increased lung metastasis [74]. These *in vivo* data are supported by *in vitro* culture model studies. Compared to low-density collagen, mammary epithelial cells cultured in high-density collagen have increased cell proliferation and form invasive organoids with disrupted e-cadherin junctions [14, 74]. Further, it has been reported that tumor cells upregulated COX2 when attached to high density

fibrillar collagen, which serves as an additional potential mechanism for how dense collagen induces tumor cell proliferation and invasive behaviors.

Collagen structure is another critical parameter in breast cancer progression. Collagen surrounding tumors has been characterized and classified into three tumor-associated collagen signatures (TACSs) based on collagen organization. In early stage tumors, tumors are usually surrounded by high abundance of collagen, which shows wavy fibers (TACS-1) that are thought to be at low tension. With the increased tumor size, straight collagen fibers that are parallel to the tumor border can be found at the tumor border (TACS-2). During tumor progression, straight collagen fibers are rearranged to be perpendicular to the tumor border, which is termed as TACS-3. In breast cancer patients TACS-3 have been shown to be an independent poor prognosis indicator of metastasis [75]. Further, intravital imaging studies show tumor cells migrate on perpendicular collagen fibers to gain access to vasculature, an early requisite of metastasis [76, 77]. Taken together, these data support a strong link between collagen density and organization in both breast cancer initiation and progression, suggesting collagen as a potential preventative and therapeutic target for breast cancer.

- **Main Types of Collagen In the Mammary Gland.**

Collagens are the most abundant extracellular proteins in all animals and humans, comprising about one-third of total protein. So far, 28 types of collagen have been identified. The defining feature of collagen is an elegant structural motif in which three parallel polypeptide strands in a left-handed, polypro-line II-type helical conformation coil about each other with a one-residue stagger to form a right-handed triple helix. The defining protein sequence in all types of collagen is a repeating Xaa-Yaa-Gly, where the most common Xaa and Yaa are (2S)-Proline (28%) and (2S,4R)-4-hydroxyproline (38%) respectively. Collagens can be divided into two main groups,

fibrillar and non-fibrillar collagens. Fibrillar collagen molecules consist of an uninterrupted triple helix approximately 300 nm in length and 1.5 nm in diameter flanked by N- and C-terminal telopeptides that assemble into large fibrils. In contrast, non-fibrillar collagens lack the ability to assemble into large fibrils, but serve as collagen fiber stabilizers and can have other unique functions, such as supporting cell adhesion and providing an interface between cells and fibrillar collagen. Non-fibrillar collagens can be subcategorized into network, fibril-associated collagen with interrupted triple helices (FACIT), membrane-associated collagen with triple helices (MACIT), and multiple triple helix domains and interruptions (MULTIPLEXIN) and anchoring fibrils (Figure 1-8).




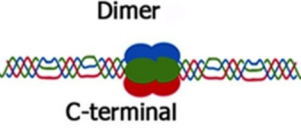
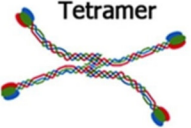
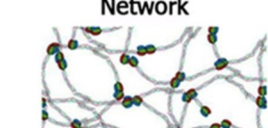

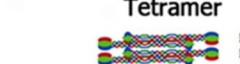



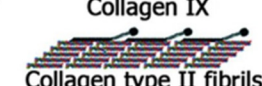

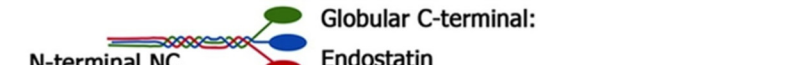

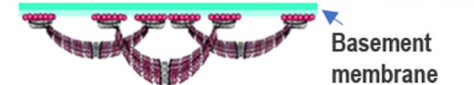
| | | | | |
|--------------------------|--|---|--|--|
| Fibril forming | Microfibrils  | Collagen fibrils  | Collagen fibers  | Collagen types: I, II, III, V, XI, XXIV, XXVII |
| Network forming | Dimer  | Tetramer  | Network  | Collagen types: IV, VI, VIII, X |
| | Dimer  | Tetramer  | Beaded filament  | |
| FACITs | Monomer  | Collagen XII or XIV  | Collagen IX  | Collagen types: IX, XII, XIV, XVI, XIX, XX, XXI, XXII, XXVI |
| MACITs | Cytoplasm  | | | Collagen types: XIII, XVII, XXIII, XXV |
| Multiplexin | N-terminal NC  | | | Collagen types: XV, XVIII |
| Anchoring fibrils | Dimer  |  | | Collagen types: VII |

Figure 1- 8. Structures and functions of different types of collagens.

FACIT: Fibril Associated Collagens with Interrupted Triple helices. MACIT: Membrane Associated Collagens with Interrupted Triple Helices. Multiplexin: Multiple Triple Helix domains with Interruptions. Reprinted with permission: (Soro, L., Bartus, C., and Purcell, S. *Recessive dystrophic epidermolysis bullosa: a review of disease pathogenesis and update on future therapies*. J Clin Aesthet Dermatol, 2015.) and

(Singh, B., et al., *Human pathogens utilize host extracellular matrix proteins laminin and collagen for adhesion and invasion of the host*. FEMS Microbiol Rev, 2012.)

In collaboration with proteomics expert Dr. Kirk Hansen (University of Colorado Anschutz Medical Campus, Aurora, CO), the Schedin lab has identified the primary collagen types present in the rat mammary gland by whole tissue proteomics. In nulliparous rat mammary glands, the main types of collagens are the fibrillar collagens, including collagen I, III, and V and the non-fibrillar collagens, including the networking collagen VI, and the FACIT collagen XIV (Figure 1-9). More detailed information of these types of collagen is described below.

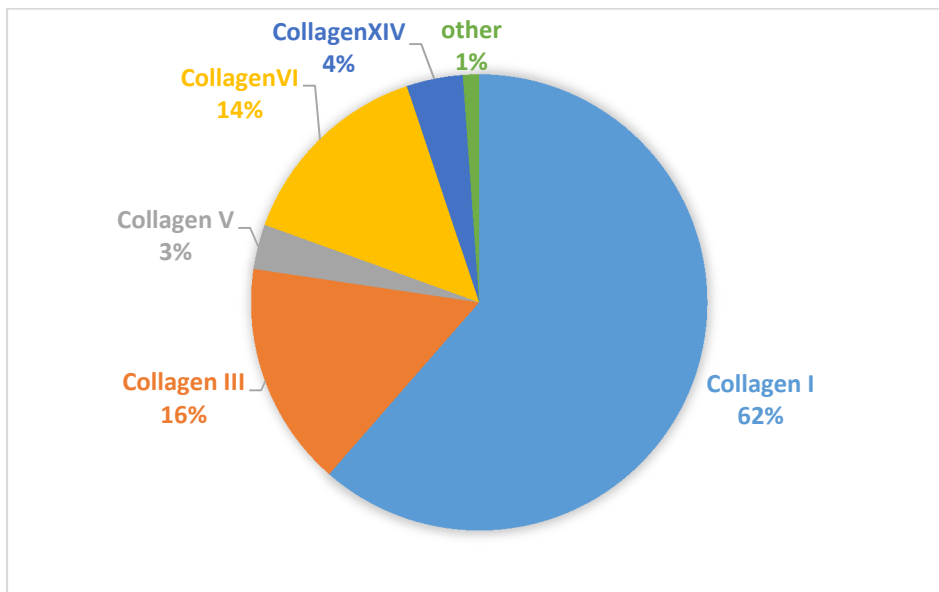


Figure 1- 9. Main types of collagen in the nulliparous rat mammary glands by ECM proteomics.

Fibrillar collagens - Type I, III and V:

The top three types of fibrillar collagen in the nulliparous rat mammary gland, making up ~80% of collagen protein, are collagens I, III and V. Among these three types of collagen, collagen I is the most abundant collagen in the rat mammary gland, which potentially functions in providing tensile stiffness. Collagen I contains three chains: two $\alpha 1$ chains and one $\alpha 2$ chain, which are coded by *Colla1* and *Colla2* genes respectively. Mutations of collagen I genes can lead to diseases such

as type 1 Ehlers–Danlos syndrome, with symptoms from loose joints to lethal complications, like aortic dissection.

Collagen III is the second most abundant collagen in the human body, and closely associated with collagen I in terms of location and function. It has been suggested that collagen fibers in the skin are hybrids of type I and III collagen, and by immunolabeling of fibrils, it has been found that collagen III is located at the periphery or within the collagen I fibrils [78, 79]. Collagen III regulates collagen fibril diameter. Both in vitro and in vivo studies have shown that collagen fibers formed by collagen III and collagen I generate thinner fibers with smaller fiber diameters compared with fibers generated by collagen I alone or with mutated collagen III [80, 81]. Collagen III plays a role in cutaneous wound healing. Collagen III level increases significantly at 10 hours with wounding and returns to normal skin levels of 20% of total collagen by 24 hours. This acute increase in collagen III may function in providing initial wound structure and support for the subsequent healing processes [82]. Using a Col3 knockdown mouse model, it has been found that collagen III deficiency accelerated wound closure in aged mice, potentially caused by increased myofibroblast density and wound contraction. However, significantly decreased neoeppithelium formation was found in the scar tissue of the Col3 knockdown mouse model, suggesting the important role of collagen III in supporting new epithelium in the wound [83].

Type V collagen typically forms heterofibrils with collagen I and III in bone, skin and other organs [84]. Collagen V controls collagen fibrillogenesis through its conserved $\alpha 1(V)$ -N-propeptide domain. Collagen V regulates fibril diameter and is required for collagen fibril nucleation. Col5a1-/- animals die in early embryogenesis due to cardiovascular failure and a virtual lack of fibril formation in the embryonic mesenchyme [85]. Yet Collagen 5a1+/- animals are viable; the reduced type V collagen content is associated with a 50% reduction in fibril number and dermal collagen

content. Collagen fibrils in adult +/- animals have enlarged fiber diameter and irregular contours [85, 86]. Overall data suggests that type V collagen may function as a core structure of the fibrils with type I and III collagens polymerizing around it [85, 86].

Common methods for detecting fibrillar collagens are Trichrome, Picro-Sirius red, and second harmonic generation imaging (SHG). SHG is a sensitive method for imaging only fibrillar collagen. In SHG, when photons interact with noncentrosymmetric media, new photons with half the wavelength are formed and can be detected. Since the common structure of fibrillar collagen is three left-handed procollagens join and twist into a right-handed triple helix, collagen is a highly noncentrosymmetric material and in tissue, and is highly abundant. When high intense laser light passes through collagen, the emerged second-harmonic light is exactly half the wavelength (frequency doubled) of the light entering collagen, which can be separated and detected. The major advantages of this technology are that SHG can detect fibrillar collagen without any staining procedure, and it can detect the fine structures of collagen fibers. SHG gives access to more accurate structural information than allowed with Picro-Sirius staining or trichrome staining, which are traditionally used special stains for fibrillar collagen [87]. However, none of these methods can definitively separate different collagen types. Antibody-based IHC must be used to study different types of collagen in tissue. However, robust collagen type specific antibodies are poorly developed, in part due to the similarities between the collagen types.

Anti-type I collagen IHC staining of rat mammary glands reveals thick fibers covering the mammary ducts. Collagen I is also found within the mammary lobules but with lower amount compared to the ductal collagen (Figure 1-10). Similar localization is observed for collagen III, which is expected, as in general, large fibrillar collagen bundles are composed of different types of collagens. Type V collagen antibody has not been optimized for IHC staining in the rat.

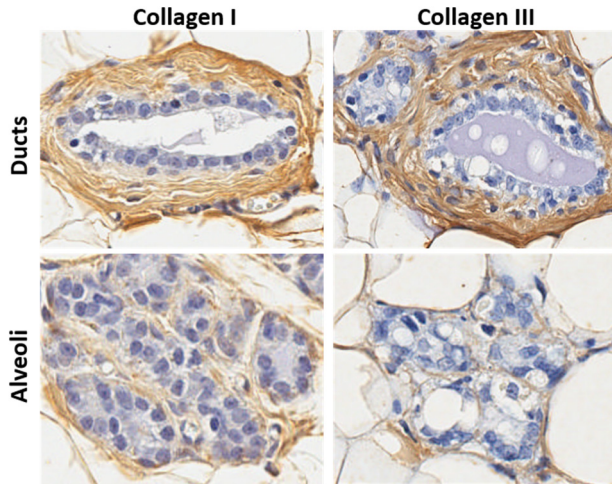


Figure 1- 10. Type I collagen and type III collagen have similar location pattern in the mammary gland.

Left panel: IHC staining of Collagen I. Right Panel: IHC staining of collagen III. Top panel: rat mammary ductal structures. Bottom panel: rat mammary alveoli structures.

Non-fibrillar collagens: collagen VI, XIV:

By proteomics, we found collagen VI is highly represented in the mammary gland, accounting for ~14% of the total collagen protein detected in the nulliparous mammary gland (Figure 1-8).

Collagen VI is essentially a collagenous glycoprotein that is assembled into extensive and highly flexible microfibrils to form filamentous networks interwoven among the major interstitial structures such as collagen fibrils, blood vessels, and nerves in the surrounding extracellular matrix [88]. Collagen VI is present as 100nm periodic beaded micro-filaments and is widely distributed in several tissues, including skeletal muscle, skin, lung, blood vessels, and cornea, as well as peripheral nerves, brain and myocardium. Collagen VI can bind to the basement membrane and serve as a link between muscle cells and ECM [89]. Furthermore, in the lung, collagen VI is a component of the basement membrane and provides elasticity and mechanical support [90]. Collagen VI is expressed by fibroblasts. Interestingly, collagen VI also can be expressed by adipocytes. Lack of collagen VI in adipose tissue results in a loose and disorganized tissue. Additionally, collagen VI is highly expressed in a variety of tumors. In breast cancer, collagen VI protein has been found in the tumor invasive front [91]. Several studies have demonstrated that

collagen VI is an anti-apoptotic factor for different cell types, including fibroblasts, muscle fibers, neurons and endothelial cells [92]. Moreover, collagen VI has been found to promote breast cancer cells growth and metastasis in the MMTV-PyMT transgenic mouse background [93].

Another highly enriched non-fibrillar collagen in the rat mammary gland is collagen XIV. Collagen XIV is highly expressed in development in a variety of connective tissues with high mechanical demand, such as tendon [94], suggesting a potential function of collagen XIV on collagen fiber strength. Collagen XIV decorates the surface of fibrillar collagen fibrils and its NC3 domain projects into the interfibrillar space. The NC3 domain has been implicated in the regulation of fibril packing, Collagen XIV-fibrillar collagen interactions are expected to inhibit lateral fibril growth. This is consistent with the characterization of collagen XIV-deficient mouse tendons, which showed a shift toward larger-diameter fibrils. Maximum load, stiffness, and modulus were all significantly reduced in the *Col14a1(-/-)* mouse tendons compared with wild-type tendons [95]. The function of collagen XIV in mammary gland is not clear so far, but a supported role of collagen fiber stabilizing is proposed. The structural role of fibrillar collagen during mammary ductal elongation and side branching refers to its relatively stiff properties, and act as a physical barrier to branching epithelium [96]. Interestingly we have observed that *coll14a1-/-* mouse mammary glands have increased ductal branching compared to WT mouse (data not shown), indicating fibrillar collagen is weak and easy to break down in the *coll14a1-/-* mouse; further supportive of collagen fiber stabilization of collagen XIV.

- NSAIDs decrease collagen during weaning-induced mammary gland involution.

Increased fibrillar collagen abundance has been found in the mammary gland during weaning-induced involution as measured by Picro-Sirius red staining and proteomics [28, 50]. Based on tissue proteomics, major fibrillar collagens, such as collagen I, III and V, and non-fibrillar

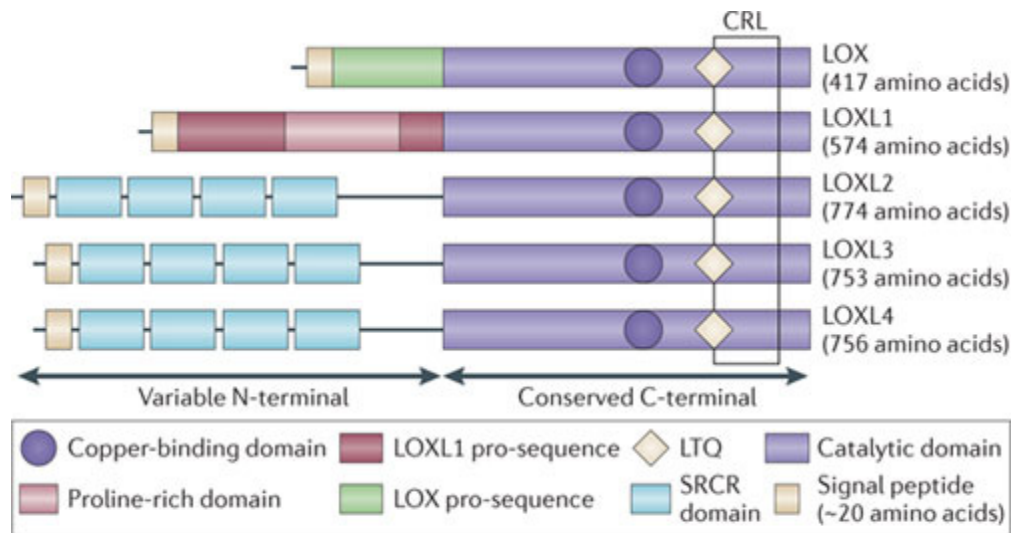
collagens, such as collagen VI, XIV, and XVIII are increased during weaning-induced involution compared to lactating mammary glands [50]. Increased collagen during involution is consistent with increased tumor growth and invasion in this microenvironment. As mentioned above, NSAIDs treatment during involution suppresses the tumor promotional capacity of the involution-microenvironment. Remarkably, analysis of the normal involuting mammary gland with NSAIDs treatment reveals that the NSAID-induced tumor protection was accompanied by decreases in mammary fibrillar collagen accumulation [14]. In this study, ductal collagen abundance was measured by SHG in mouse mammary gland at 6 days post-weaning with/without celecoxib or ibuprofen treatment. Quantification of collagen abundance indicated that both celecoxib and ibuprofen treatment decreased collagen abundance surrounding the mammary ducts to nulliparous levels [14]. More recently in the *Colla1^{mjae}* mouse model of breast density (described in chapter “The Role Of Collagen In Promoting Breast Cancer”), where a mutation in the collagen I collagenase cleavage site leads to increased collagen accumulation and subsequent mammary tumor promotion, celecoxib was found to suppress collagen abundance and tumor growth [97]. The observation that NSAIDs reduce collagen has also been shown during wound healing in animal models, such as in rat and rabbit [98, 99], where Celecoxib treatment for 3 weeks significantly lower the percentage of type I collagen during tendon healing in rabbits [98]. These studies indicate that collagen can be targeted by NSAIDs and suggests a potential mechanism of the tumor suppression function of NSAIDs in the involution microenvironment, i.e. by decreasing collagen abundance. However, the cellular and molecular mechanisms associated with how NSAIDs inhibit collagen remain to be elucidated.

- **Introduction of fibroblast.**
 - Fibroblast definition and function.

Fibroblasts were first described in the late 19th century, based on their location and microscopic appearance [100, 101]. Fibroblasts, elongated spindle-like shape cells that are non-epithelial, non-immune, and non-vascular cells, are found within the connective tissue and are responsible for producing ECM [102]. Fibroblasts are widely distributed in all types of tissue and are easy to culture in vitro, which makes them the most common contaminant in primary tissue cultures. The definition of a fibroblast is still largely limited to morphology and major functions, such as deposition of ECM. The molecular markers of fibroblasts are poorly defined. Many of the markers used for identifying fibroblasts, such as platelet-derived growth factor receptor (PDGFR), fibroblast specific protein 1 (FSP1), vimentin and alpha-smooth muscle actin (α SMA) can be found in other cell types. For example, FSP1 can be expressed by an inflammatory subpopulation of macrophages in the liver [103], and also can be found in invasive carcinoma cells [104].

To date, the main function of fibroblasts in normal tissue is thought to be deposition of ECM proteins maintain the structural integrity of connective tissues. Fibroblasts are responsible for many types of collagen synthesis, including collagens I, III, IV, V, and VI [105-109]. They also function in organization of collagen fibrils. Fibroblasts crawl over their secreted collagen, exerting force on the fibers, which compacts collagen fibers into sheets or stretches it out into cables, thus fibroblast-collagen interactions dramatically influence the organization and alignment of collagen fibers [110, 111]. Fibroblast also produces collagen remodeling proteins, such as MMPs (including MMP1, MMP13), lysyl hydroxylase, and members of the lysyl oxidase (LOX) family, LOX and LOX-like enzymes [112-115]. Among those collagen enzymes, LOX is the well-known collagen cross-linking enzyme that controls a critical step in collagen fiber formation. The main catalytic function of LOX is to catalyze the formation of reactive aldehydes from lysine residues [116].

Covalent aldol cross-links can form between two lysine or hydroxylysine residues, which are rich at the C-terminus of the collagen molecule. This cross-linking stabilizes collagen microfibrils and generates a strong fibril [117]. Four other LOX family members have been described, LOXL1-4, which have a conserved catalytic C-terminal domain, and similar amine oxidase activity, but are genetically distinct from LOX [118] (Figure 1-11).



Nature Reviews | Cancer

Figure 1- 11. Comparison of LOX family members [119]

Reprinted with permission from Nature Publishing Group. (Cox, T.R. and J.T. Erler, *Lysyl oxidase in colorectal cancer*. *Am J Physiol Gastrointest Liver Physiol*, 2013. **305**(10): p. G659-66.)

Fibroblasts in tissue under homeostatic conditions are generally quiescent with negligible metabolic activity and low production of ECM proteins necessary to maintain tissue integrity. Quiescent fibroblasts are poised to become activated when the need arises. Many factors are involved in fibroblast activation, such as mechanical tension, fibroblast growth factors (e.g. TGF β), and cytokines. Activated fibroblasts are proliferative, have increased migration abilities and

produce a large amount of ECM proteins, growth factors, and cytokines, which are involved in ECM remodeling, re-epithelialization and immune modulation to fulfill the needs of the microenvironmental challenge. The major difference between quiescent fibroblasts and activated fibroblasts, called myofibroblasts, are enlarged cell size, highly active endoplasmic reticulum and elevated transcriptomic activity, and the presence of stress fibers. α SMA is incorporated into the stress fibers in myofibroblasts and generates more contractile force than normal stress fibers. Thus, α SMA is widely used as a marker of myofibroblasts.

- [Fibroblast in wound healing.](#)

Wound healing is an essential process in response to a pathological insult that maintains tissue integrity and restores homeostasis [120]. Wound healing in the skin has been well studied and includes four main steps: hemostasis, inflammation, proliferation and remodeling or resolution [121]. Fibroblasts have a critical function in the proliferation and remodeling phases of wound healing. The macrophage related inflammation phase produces large amounts of cytokines and growth factors including TGF β and PDGF, which activate and recruit fibroblasts to the wound site [122, 123]. Fibroblasts within the wound site proliferate profusely and produce matrix proteins to replace the fibrin clot [124, 125] that is formed by the platelets during the initial wound healing response [126]. The ECM produced at the wound site by fibroblasts include hyaluronan, fibronectin, collagen I, and collagen III [127, 128]. New ECM deposition by fibroblasts impacts the integrity and strength of the tissue and is important for the proliferation and remodeling phase of epithelial repair. Another important function of fibroblasts is to provide contractile forces necessary to close the wound prior to re-epithelialization [129]. Fibroblasts in wounds usually gain myofibroblast phenotypes. They develop thick actin bundles below the plasma membrane and actively extend pseudopodia, attaching to fibronectin and collagen. They also contract and

organize the ECM protein in order to close the wound [123]. The activated fibroblasts in wounds also produce growth factors and cytokines to stimulate the proliferation and migration of keratinocytes to promote re-epithelialization [130, 131]. At the late stages of wound healing, unnecessary fibroblasts are eliminated by apoptosis, and the dense ECM is remodeled to restore the normal architecture by collagen synthesis, bundling, and degradation [132, 133]. Under chronic irritation from physical, toxic, or other insults, the remodeling and resolution phase of wound healing persists, leading to fibrosis or scarring. Thus, tissue scarring can be considered as a wound that never completed the healing process.

- **Fibroblasts in Cancer.**

Cancers are considered to be wounds that do not heal [134]. Tumors share similarities with a persistent wound healing process, including cell proliferation, immune cell infiltration, angiogenesis, and sustained fibrosis. In support of this concept, fibroblasts in the cancer stroma or cancer associated fibroblasts (CAFs) share similarities with wound healing fibroblasts, including increased proliferation, extensive ECM production, growth factor and cytokine production.

CAFs are closely associated with cancer initiation and progression. The linkage between CAFs and cancer initiation has been shown in a prostate model of cancer [135]. In this model, the simian virus 40 (SV40) transformed normal prostate epithelial cells were used to compare the functional difference between normal fibroblasts and CAFs. SV40 is a non-tumorigenic cell line and when SV40-prostate epithelial cells are grafted beneath the renal capsule of rodent hosts, no tumor growth can be detected even up to one year post engraftment. However, dramatic tumor growth can be found when SV40-prostate epithelial cells are grafted together with CAFs but not with normal fibroblasts [135]. Assessment of the tissue reveals tumor growth, with high proliferation and low cell death. The histological appearance of the tumors resembled poorly differentiated

adenocarcinomas [135]. CAFs are also involved in progression of overt tumor cells, as multiple studies have demonstrated that co-injection of CAFs and established tumor cells promotes tumor growth compared with co-injection of normal fibroblasts [136-138]. The promotional function of CAFs in tumor initiation and progression can be mediated by factors released from CAFs, such as TGF β , hepatocyte growth factor (HGF), insulin-like growth factor (IGF) and epidermal growth factor (EGF), which stimulate proliferation in adjacent epithelial cells or tumor cells [139].

CAFs also remodel the tumor promotional microenvironment by deposition large amount of collagen [101] and collagen cross-linking enzymes, such as LOX [140]. More recently, numerous studies have shown a strong positive correlation between expression of LOX family members and tumor metastasis in multiple types of tumors including head and neck squamous cell carcinoma, breast, colorectal, and prostate cancers [119, 141-143]. CAFs also produce MMPs, which can assist tumor cells in breaking through the basement membrane and invading into the local stroma. MMP3, which is highly expressed by CAFs, can increase tumor cell motility through cleavage of the extracellular domain of E-cadherin and induce tumor cell Epithelial–mesenchymal transition [144].

CAFs can also promote cancer progression through secretion of cytokines and chemokines which modulate the immune microenvironment. Generally, CAFs are considered to be promotional of an immunosuppressive tumor microenvironment. Studies have shown that CAFs can release cytokines such as IL-4, IL-6, IL-8, TGF β , which can induce immunosuppressive myeloid cell differentiation [145, 146]. CXCL12, 14 and 16 released by the CAFs are chemoattractants for monocytes and macrophages and can induce macrophages M2 polarization and IL-10 production [147-151]. Programmed cell death protein 1 (PD1) and its ligand (PDL1) have been studied intensively in the interactions between tumor cells and immune cells in terms of immune

suppression and tumor progression [152, 153]. Interestingly, subpopulations of CAFs also have been shown to express PDL1 and may convey an immune suppression function to suppress cytotoxic T cells directly in the tumor, leading to tumor cell escape from immune surveillance [154]. In summary, CAFs are tightly associated with tumor progression in part by directly stimulating tumor cells, depositing and remodeling the tumor stroma, with emerging roles in immunosuppression. Targeting CAFs as a therapeutic strategy against tumors has become a new avenue of intense research. In my thesis studies, I used knowledge gained from wound-associated and CAF studies to inform my work on mammary fibroblasts, as described in Chapter III.

CHAPTER II. COLLAGEN CHARACTERIZATION DURING WEANING-INDUCED INVOLUTION.

Qiuchen Guo, Sonali Jindal, Matthew Conklin, Patricia Keely, Virginia Borges, Pepper Schedin

Author contributions

Q. Guo and P. Schedin developed the hypothesis, conceptual and experimental designs, and are responsible for data analysis and interpretation. Q. Guo performed all experiments using rat tissue, including RT-qPCR for fibrillar and non-fibrillar collagen expression analysis, SHG based collagen density and structural analysis. S. Jindal and V. Borges performed human collagen abundance analysis. M. Conklin and P. Keely performed human collagen structural analysis.

- **Abstract.**

Fibrillar collagen is a major contributor to breast density and has been shown to impact aggressiveness of cancer cells *in vitro* and in rodent models. Fibrillar collagen density increases in the mammary gland during weaning, correlates with tumor progression in rodent models of postpartum breast cancer, and in women, has potential links with the poor outcomes of breast cancers diagnosed within 5-10 years postpartum. We hypothesized that regulation of mammary collagen during wean-induced involution shares similarities with poor prognostic tumor associated collagen, including increased abundance, and structural alterations consistent with tumor cell motility. Here, using the Sprague Dawley rat, we analyzed mammary collagen gene expression, density and structure regulation in nulliparous, lactating and post-weaning rats. I focused on known rat mammary collagens previously identified by proteomic analyses: fibrillar collagens type I, III and V, and the non-fibrillar collagens type VI, VII, XIV, XV, and XVII and the key modifying enzyme lysyl oxidase. Mammary collagen gene expression was decreased during lactation and increased during involution when compared to the nulliparous host, with evidence for concordant changes in protein levels confirmed by second harmonic generation imaging (SHG). Increased fibrillar collagen density, as observed during involution, may implicate fibrillar collagen in tumor promotion during involution. Collagen structure, another important parameter that influences cancer cell invasiveness, was evaluated using SHG imaging. Gap area between collagen fibers, a measure of collagen packing and tension, was decreased during involution in both rat and human mammary tissue, consistent with increased collagen abundance and increased tension. Further, an increased ratio of collagen fibers perpendicular to the mammary ducts were found during involution in the rat mammary gland, an organization previously associated with poor prognostic

breast cancer in women. Increased expression of the primary collagen cross-linking enzyme lysyl oxidase, which is known to increase fiber strength and tension, was also found during weaning-induced involution. In summary, we found active collagen gene expression, increased fibrillar collagen protein and structural reorganization during the involution window, suggesting collagen deposition and ultimately breast density might be modified by the reproductive history, and in a manner consistent with tumor promotion, implicating collagen in the poor prognosis of postpartum breast cancer.

- **Introduction.**

A strong link between breast density and breast cancer risk has been proposed by multiple epidemiological studies [155-159]. Breast density is measured by mammography, which assesses the relative contribution of dense tissue to the total breast area [160]. The non-dense area is mainly comprised of fat tissue, as fat is radiologically lucent [160]. The dense area, referred to as fibroglandular tissue, is composed of epithelial and fibrous stromal tissue, however, radiographic imaging alone cannot resolve epithelium from fibrous stroma [160]. Extreme breast density, observed in ~20% of women, confers a 4 to 6-fold increase in breast cancer risk compared with low dense breast [156]. For example, a recent large epidemiological study, with 58146 premenopausal and 144600 postmenopausal women, concluded that breast density is the most prevalent risk factor for both premenopausal and postmenopausal women, being more predictive of risk than family history, body mass index (BMI), age at first live birth and history of benign breast biopsy [161]. Further, many of the breast cancer risk factors listed above influence breast density. Age is one of the main factors that influences breast density; 74% of women between 40 to 49 years old have dense breasts, and for women in their 70s, the ratio drops to 36% [162]. Decreased breast density is not in conflict with the increased breast cancer incidence observed with older age, as the increased incidence with age is thought to be attributed to increased acquired

mutation load [163]. Breast density is also heritable, and the inherited factors explain 63% of the density variance, and might account partially for the association between family history and breast cancer risk [156, 164-166]. Other factors, such as vitamin D intake, can also influence breast density [167]. In sum, these data suggest multiple factors can influence breast density, including genetics, age, and dietary exposures.

Collagen is the major contributor of breast density. Histological analysis of breast biopsies shows that radiographic breast density is positively correlated with total nuclear area, nuclear area of both epithelial and nonepithelial cells, collagen and area of glandular structures [168]. Of these tissue components, collagen is the most abundant, and associates most strongly with breast density [169, 170]. Analysis has shown that collagen accounts for 29% of the variance in percent mammographic density, versus, nuclear area, which accounts for only 4% [170]. This observation suggests that targeting collagen deposition within the breast may be highly effective at reducing overall breast density and its associated risk for increased breast cancer incidence and progression.

Fibrillar collagens are the major stromal proteins in the extracellular matrix in the mammary gland, and have critical roles in breast cancer [29, 117]. Mouse models have confirmed that high fibrillar collagen content in the mammary gland promotes the initiation of tumors in the MMTV-PyMT background and lung metastasis [74]. Further, tumor cells acquire proliferative and motile phenotypes when cultured on high-density collagen pads [74]. In addition to collagen density, collagen structure predicts breast cancer progression. The structural features of collagen surrounding tumors have been classified into a series of tumor-associated collagen signatures (TACS) [76]. In early stage tumors, increased collagen abundance with similar structural organization found around normal ducts has been found surrounding the tumor, i.e., wavy collagen bundles arranged horizontal to the axis of the duct (TACS-1). Collagen fibers can also be found

with increased linearity (straightness) and arranged parallel to the tumor border (TACS-2). Further, radially aligned collagen fibers that are perpendicular to the tumor border (TACS-3) negatively correlate with breast cancer patient survival and are thought to facilitate tumor cell motility. In model systems, evidence that fibrillar collagen directly impacts tumor cell motility and invasion have been obtained from intravital imaging studies that show tumor cells migrating on TACS-3-like collagen fibers and invading the vasculature [76]. In contrast, collagen fibers organized randomly or non-linearly has been shown to associate with low stromal stiffness and tumor suppression in tumor transplant models [49]. Together, these data demonstrate the important role of fibrillar collagen abundance and organization in rodent models of breast cancer risk and progression.

Pregnancy has been correlated to breast density and breast cancer risk. It has been shown that pregnancy is associated with a decreased postmenopausal breast density, which is consistent with the long-term protective effect of pregnancy to breast cancer [171]. However, and somewhat paradoxically, women have an increased risk of breast cancer during the postpartum window following pregnancy, and these postpartum breast cancer patients have significantly decreased survival rates compared with nulliparous patients regardless of their age, breast cancer subtype, tumor stage, and year of diagnosis [4, 172]. In contrast, breast cancers diagnosed during pregnancy do not show significantly decreased survival rate compared with nulliparous patients [9-11]. Together, these data strongly suggest unique biological events in the postpartum window that contributes to the breast cancer risk and poor prognosis. In rodents, we had previously reported an increase in total collagen abundance in the involuting mammary gland [28], suggesting collagen as a potential contributor of the poor outcome of the postpartum breast cancer patients.

Here using rat mammary glands and human tissue, we describe the alteration of collagen abundance and structure during the postpartum window, to shed light into physiologic regulation of collagen density that may impact breast cancer risk and progression. We characterized the main types of stromal collagen found in mammary glands of nulliparous, lactating and weaning-induced involution hosts, and report dynamic regulation of collagen gene expression – low collagen during lactation and intensive collagen deposition during weaning-induced involution. The collagen crosslinking enzyme lysyl oxidase was also dynamically regulated; data consistent with the structural reorganization during involution and consistent with a tumor promotional collagen signature. Potential relevance of collagen remodeling during involution is also assessed in human breast tissue. Together, our data provide evidence of physiologic regulation of fibrillar collagen in the adult mammary gland; data which may provide insight into breast density variation observed between women, as well as provide novel avenues for breast cancer prevention and therapeutics.

- **Results.**

- **De novo collagen synthesis during rodent mammary gland involution.**

Based on published rat mammary gland ECM proteomics data [29, 50], we assessed gene expression by RT-qPCR for the abundant fibrillar collagens type I, III and V, whose main function is assembling fibrillar collagen bundles, and the expressed non-fibrillar collagens, including type VI – the network forming collagen, type VII – the anchoring fibers collagen, type XIV – FACIT collagen (Fibril Associated Collagens with Interrupted Triple helices), type XV – the Multiplexin collagen (Multiple Triple Helix domains with Interruptions), and type XVII – the MACIT collagen (Membrane Associated Collagens with Interrupted Triple Helices). While the specific functions of most of the non-fibrillar collagens in the mammary glands have not been reported, collagen VI and XIV have reported functions in collagen fibrillogenesis in other organs [173, 174]. It also has

been shown that adipocyte-derived collagen VI has growth-stimulatory and pro-survival effects on mammary tumor cells [93]. Further, collagen VII and XV are associated with the connection between basement membrane and fibrillar collagens, and potentially stabilized the epithelium and underlying stroma [175, 176]. Collagen XVII is a transmembrane protein shown to maintain linkage between the keratinocytes and the underlying stroma [177].

Compared to mammary glands from nulliparous mice, gene expression of almost all types of collagen fell to low or undetectable levels during lactation (Figure 2-1A). The three types of fibrillar collagen had increased gene expression during involution compared to lactation (Figure 2-1A). Of note, collagen I, as the most abundant fibrillar collagen, also had significantly increased levels in 8 and 10 days post weaning compared with nulliparous stage (Figure 2-1A). The gene expression of non-fibrillar collagen VI, XIV and XV had a slight trend of increase during early involution – 2 and 4 days post-weaning, compared with lactation, and further increased during late involution – 6, 8, and 10 days post-weaning (Figure 2-1A). On the other hand, gene expression of collagen VII and XVII were low through the early involution stages and only increased at 8 and 10 days post-weaning. The sum of the eight types of collagen gene expression showed a suppression of collagen gene expression during lactation with increases during the lobular regression phase of involution, returning to baseline levels by 28 days post weaning (regressed) (Figure 2-1B).

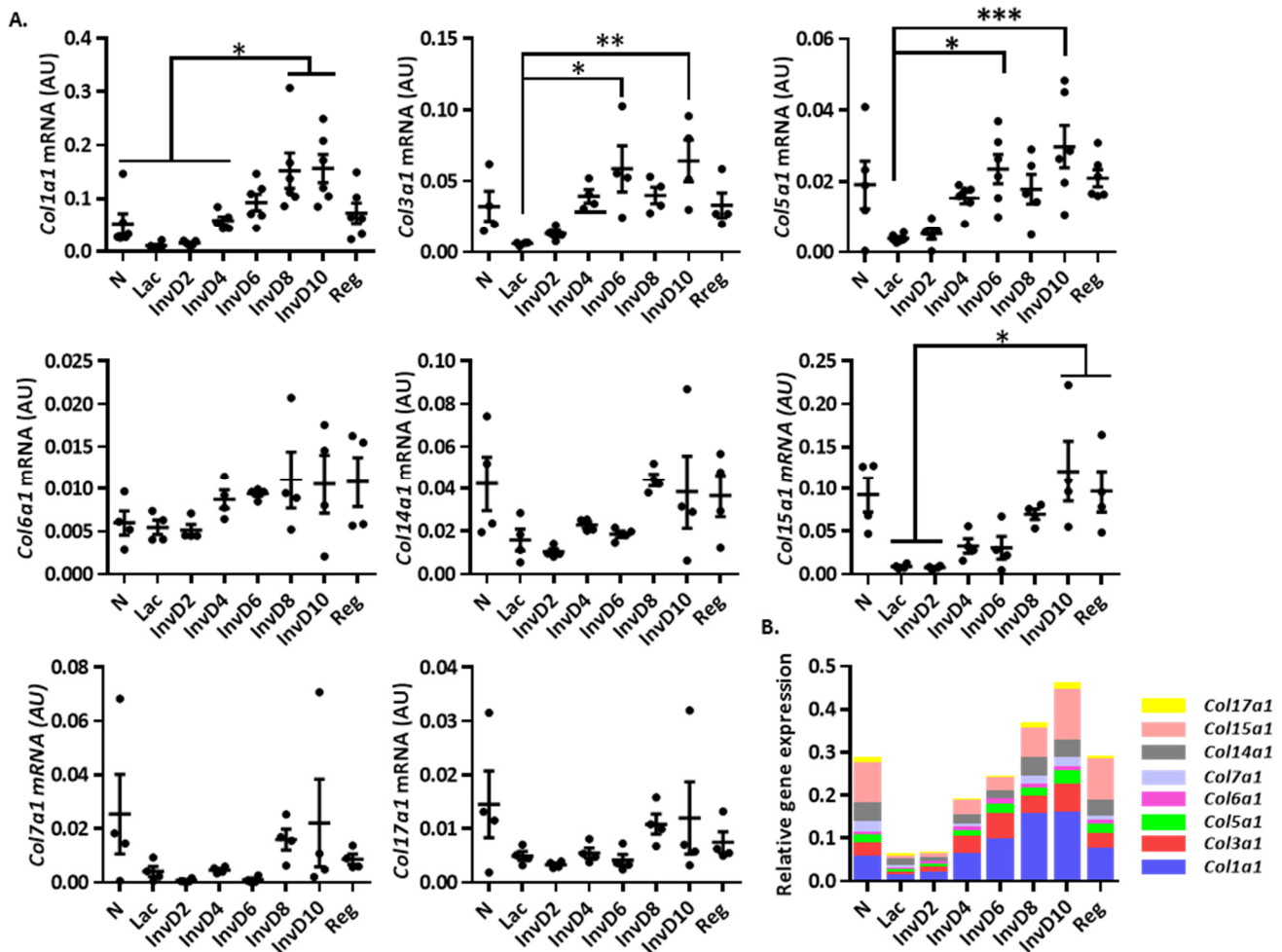


Figure 2- 1. De novo collagen synthesis during rat mammary gland involution.

(A) RT-qPCR analysis of three types of main mammary fibrillar collagen, Col1a1, 3a1 and 5a1 and five types of the main mammary non-fibrillar collagen, Col6a1, 14a1, 15a1, 7a1 and 17a1 in nulliparous (N), lactation (Lac), 2, 4, 6, 8, 10, and 28 days post-weaning (InvD2, InvD4, InvD6, InvD8, InvD10, Reg). n=4-6 per stage. (B) Summarized view of eight types of collagen gene expression. *P<0.05, **P<0.01, ***P<0.001. One-way ANOVA with Tukey correction.

Fibrillar collagen protein level increased during weaning-induced involution. The protein levels of mammary fibrillar collagens were measured by SHG, a microscopy technique based method that is more sensitive for imaging fibrillar collagen compared with the conventional ways, such as Picro-Sirius red staining. Recently the acinus, rather than the individual epithelial cell, has been identified as the unit of lobular loss during involution [178], thus, we investigated these highly

dynamic epithelial structures for collagen abundance changes as a function of reproductive state. The dramatic morphological changes that occur in the mammary lobules between lactation and weaning are shown by H&E staining (Figure 2-2A). By SHG, collagen abundance is relatively high in the mammary lobules of nulliparous hosts (Figure 2-2B, 2-2C). In contrast, collagen is almost undetectable around mammary lobules during lactation (Figure 2-2B, 2-2C), potentially to not compromise mammary lobule expansion and contraction required to secrete and transport milk. After lactation, with the beginning of weaning-induced involution, collagen abundance in the lobular area increases gradually back to the nulliparous level at day 10 post-weaning (InvD10) (Figure 2-2B, 2-2C). Cumulatively, these collagen gene expression and protein data demonstrate orchestrated collagen deposition in the mammary gland during involution that is dependent on reproductive state.

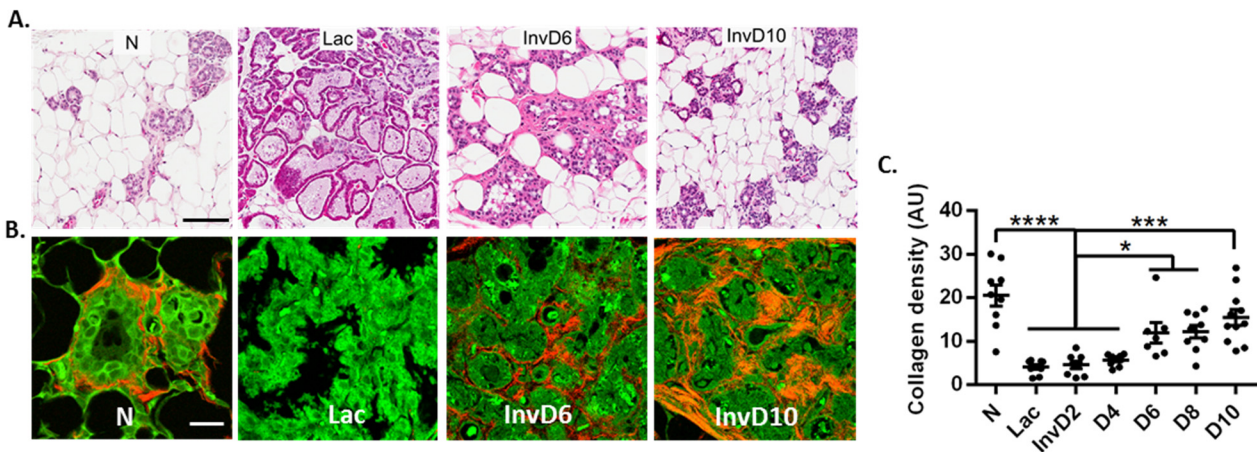


Figure 2- 2. Fibrillar collagen abundance in rat mammary lobules in nulliparous and involuting hosts. (A) H&E stain of rat mammary gland during reproductive stages. Scale bar: 100 μ m. (B) Second harmonic generation (SHG) image for rat mammary lobules in the reproductive stages matching in (A). For SHG pictures, cellular structure: green. Fibrillar collagen: red. Scale bar: 20 μ m. (C) Quantification of collagen signal in lobules from lactation and involution rat mammary gland. 3-4 animals per condition, 1-4 lobules were analyzed per animal. *P<0.05, ***P<0.001, ****P<0.0001. One-way ANOVA with Tukey correction

○ Rat mammary collagen structural reorganization during weaning-induced involution. Collagen organization, independent of abundance, strongly influences epithelial cell behavior, including tumor cells [49, 74]. To analyze collagen structural alteration, we evaluated further our SHG images to assess collagen bundle organization. For these analyses, we first assessed mammary ductal collagen, which unlike mammary acinar structures, retain collagen bundles across the entire reproductive cycle. Thus, mammary ducts are relevant structures to look for global changes in collagen re-organization with reproductive state. We found the collagen fiber bundles in nulliparous mammary glands to be optically discreet, wavy and oriented largely along the length of the ducts, i.e., in a parallel orientation (Figure 2-3A left panels), whereas collagen fibers were straighter, less wavy during involution, a phenotype most evident at 6 days post weaning (Figure 2-3A right panels). Further, per unit area, there were fewer areas devoid of collagen at InvD6 (i.e. fewer gaps in the optical signal) compared to nulliparous, InvD8 and InvD10 glands (Fig 2-3B). Linearized collagen with fewer optical gaps by SHG has been suggestive of collagen bundles under high tension [179].

In tumors, an additional parameter of assessing collagen structure is the angle of collagen fibers in relation to the leading edge of the tumor, as fibers radially (i.e. perpendicular) aligned to the tumor edge an independent indicator of breast cancer metastasis [76]. Collagen alignment in relation to the mammary duct was quantified from SHG images using CurveAlign V2.2 software. In nulliparous mammary glands, collagen fibers were aligned primarily parallel to the ductal epithelium, like a sheath covering a tube (Figure 2-3C). Further, while parallel aligned fibers were the dominant fiber type in both nulliparous and involuting mammary glands, both reproductive stages displayed a wide range of fiber orientations (Figure 2-3D). However, compared to glands in nulliparous hosts, day 6 involuting glands had a significantly increased percentage of radially aligned fibers at an angle greater than 75 degrees to the epithelium (Figure 2-3E), as well as “hot

spots” of radially aligned collagen fibers (Figure 2-3F). LOX is an enzyme which crosslinks collagen fibers [33] and thus is a key contributor to collagen architecture [34], tension [35], and tumor cell invasiveness [36, 37]. Compared with nulliparous glands, extremely low *Lox* gene expression was found during lactation, and increased rapidly with weaning (Figure 2-3G). By Western blot, the level of active form of LOX enzyme (~35 kD [38]) was analyzed. Regardless of high gene expression of *Lox* in nulliparous gland, the active LOX was low in nulliparous. Low levels of LOX were also found in lactation gland, and high levels of active LOX enzyme were found throughout the involution stages (Figure 2-3H and 2-3I), suggesting intensive collagen crosslinking during involution.

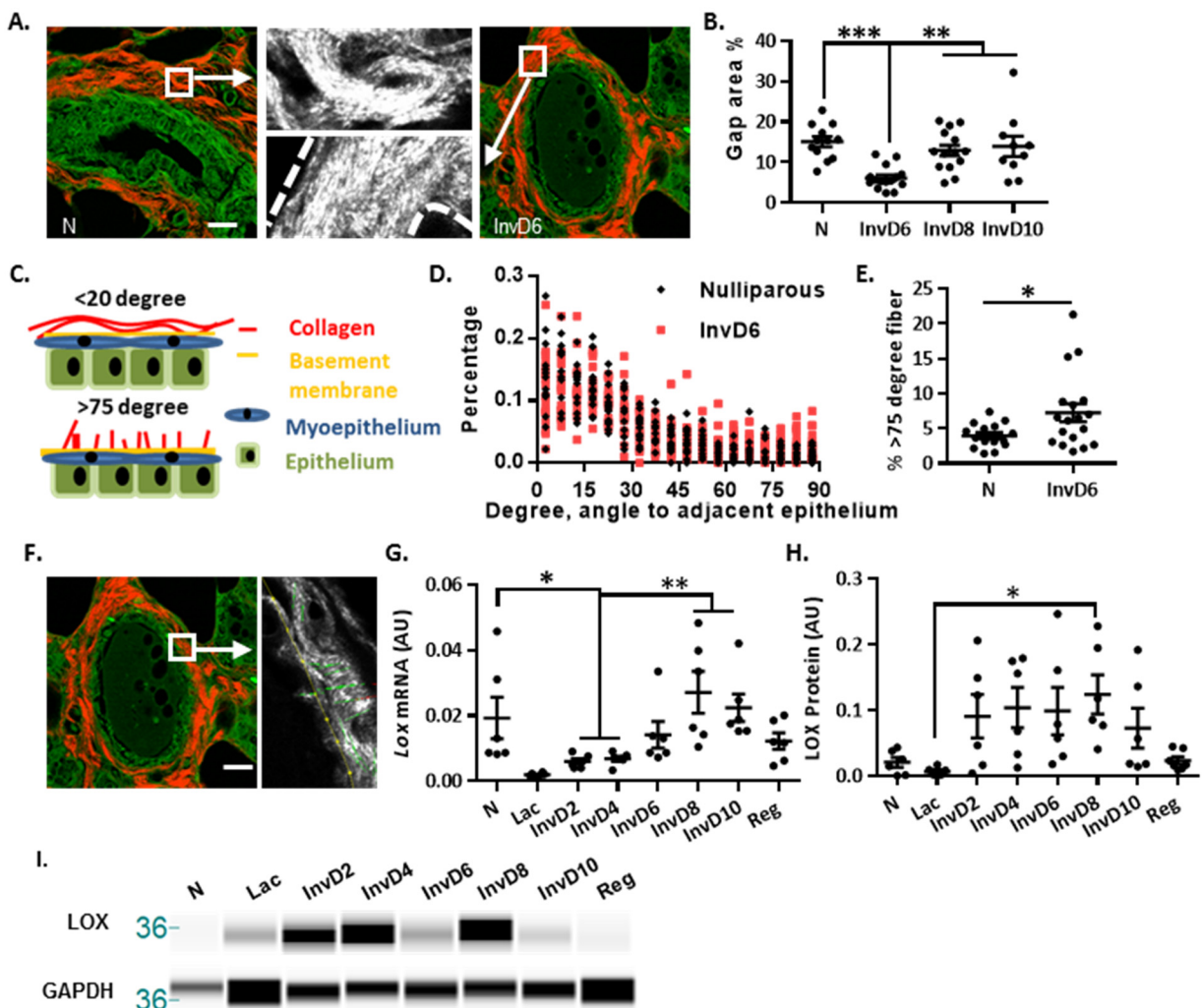


Figure 2- 3. Rat mammary collagen structural remodeling during weaning-induced involution.

(A) SHG imaging of rat mammary ductal structure in nulliparous and InvD6. Zoomed in areas in black and white. Dash line marks collagen region surrounding mammary duct. Scale bar: 20 μ m. (B) Quantification of percentage of gaps area between collagen fiber bundles surrounding ductal structure for nulliparous, InvD6, InvD8 and InvD10 mammary glands. 4 animals each condition and 3-5 ducts were analyzed per animal. (C) Model of collagen fibers parallel (top panel) or perpendicular (bottom panel) to mammary epithelium. (D) Collagen fiber angle to mammary epithelium distribution. (E) Percentage of collagen fibers being more than 75 degree to mammary epithelium. 4 animals each condition and 3-5 ducts were analyzed per animal. (F) Representative images of hot spot of radially aligned collagen fiber in ductal structure of 6 days post weaning rat mammary gland. Yellow line shows the epithelium boarder, green lines show the calculated direction of collagen fibers. Scale bar: 20 μ m. (G) RT-qPCR of LOX in rat mammary glands. N=4-9/stage. Gene expression data are normalized to Actb. (H) Quantification of western blot of lysyl oxidase in mammary gland tissue lysis. N=6-8/stages. LOX protein was normalized to GAPDH. *P<0.05, **P<0.01, ***P<0.001. t test and One-way ANOVA with Tukey correction.

o Collagen abundance and structural change in human breast tissue during postpartum involution.

Breast lobular collagen abundance shows similar pattern with the rat mammary gland, with low collagen in the lactating gland and increased collagen during involution, compared with nulliparous gland. Breast specimens were obtained from premenopausal women between the ages of 20 to 45 years, who were either healthy volunteer or underwent clinically indicated surgical treatment. The patients were grouped based on their reproductive status of never-been-pregnant (NBP), pregnant, lactating, and postpartum stages. Collagen abundance in the breast lobule was assessed by trichrome staining not SHG, as trichrome gives better histological view to define the histologically adjacent normal region within the background of cancer. Similar to the rat, changes in collagen abundance with reproductive state were observed in the human breast. Breast collagen levels in nulliparous patients varied widely (Figure 2-4A, 2-4B), consistent with the high variation of breast density observed in women. There were almost non-detectable collagen levels in lobules obtained from lactating women (Figure 2-4A, 2-4B), and in later post-weaning breast samples, collagen levels increased and were similar to nulliparous levels on average, however, inter-case variation was less pronounced (Figure 2-4A, 2-4B).

The structure of human breast collagen is altered during postpartum involution. We assessed collagen structure surrounding breast ducts from the same patient cohort with addition of early involution cases. Tissues were separated into three groups based on patients' reproductive history: nulliparous, early involution (1-4 weeks after weaning) and parous (more than 4 years postpartum). Lobular, ductal and interlobular collagen structures were analyzed for evidence of collagen reorganization with weaning, as observed in the rat. In the ductal structures, we found increased collagen fiber width, but not length, straightness or TACS-3 signatures in the early involution group compared with the nulliparous and parous groups (Table 1, and supplemental table 1, 2 and 3).

| | TDLU | Duct | Bulk |
|---|--------------------------------|---------------------------------|--------------------------------|
| Nulliparous (n= 30 images from 6 slides) | 2.02 ± 0.05 N vs. E p= 0.29 | 1.78 ± 0.11 N vs. E p= 0.05* | 2.05 ± 0.03 N vs. E p= 0.14 |
| Early Involution (n= 25 images from 5 slides) | 2.06 ± 0.06 E vs. P p= 0.06 | 1.92 ± 0.09 E vs. P p= 0.05* | 2.10 ± 0.08 E vs. P p= 0.11 |
| Parous (n= 30 images from 6 slides) | 1.98 ± 0.06 N vs. P p= 0.20 | 1.77 ± 0.11 N vs. P p= 0.97 | 2.04 ± 0.03 N vs. P p= 0.69 |

Table 3. The width of collagen fibers.

The width of collagen fibers were extracted from SHG images via the ctFIRE algorithm was measured. Values are $\mu\text{m} \pm \text{S.D.}$ *denotes statistical significance between stages. TDLU: collagen in the terminal duct lobular unit. Duct: collagen surround breast ducts. Bulk: The rest of collagen, mainly collagen within the stroma.

We also quantified gap area between ductal collagen fibers and found significantly decreased gap area in the early involution group compared with nulliparous and parous groups, which is consistent with the rodent model and suggests increased collagen tension during weaning-induced involution (Figure 2-4A top panel: H&E staining, bottom panel: SHG imaging and quantification

in 2-4B). Combined, these data demonstrate that collagen within the involuting gland is organized into straight and tight fibers in comparisons to the nulliparous gland, and suggest transient collagen fiber attributes consistent with a tumor promotional microenvironment.

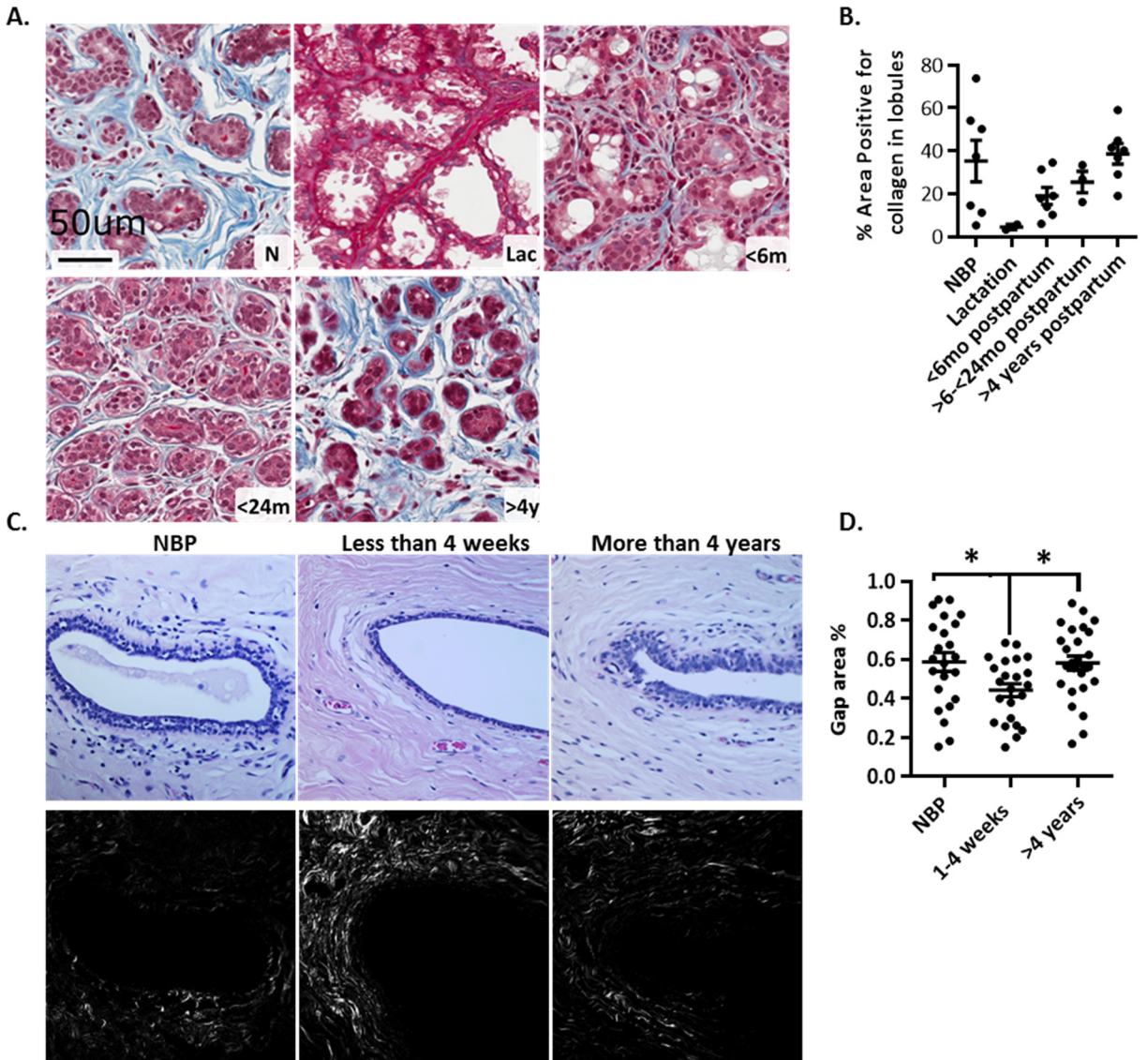


Figure 2- 4. Breast collagen abundance and structural change during postpartum involution.

(A) Trichrome staining for fibrillar collagen abundance in breast lobules in nulliparous (NBP), lactation, less than 6 months postpartum (<6mon postpartum), 6-24 months postpartum (>6-<24mo postpartum) and more than 4 years postpartum (>4 years postpartum) patients. Collagen abundance quantified in (B) n=2-7 patients per stage. (C) Top panel: H&E images of breast ducts in nulliparous, less than 4 weeks post-weaning (1-4 weeks), and more than 4 years postpartum (>4 years) patients. Bottom panel: SHG images of the same sections with the H&E images. (D) Gap area quantified in the three reproductive stages. 5-6

patients per stage and 3-5 ducts per patients were analyzed. * $p < 0.05$, One-way ANOVA with Tukey correction.

- **Discussion.**

The links between breast density and breast cancer has been studied intensively, and demonstrate breast density as a dominant determinate of breast cancer risk, and more recently of outcome [14, 74, 161]. Further, fibrillar collagen has been identified as the primary glandular constituent of breast density [168]. However, little is known about the physiologic regulation of collagen. Here we focused on collagen regulation between lactation and weaning-induced involution, which represent low and high collagen expression states, respectively. Using rat and human breast tissue, we find dynamic regulation of collagen expression, deposition and structural organization, with weaning-induced involution being a ‘hot-spot’ of fibrillar collagen regulation. These data provide evidence that, like family history and age, postpartum involution is also a potential factor that influences breast density. The high collagen abundance could potentially contribute to increased breast density during weaning-induced involution, which may explain the increased breast cancer risk and aggressiveness during postpartum window.

By SHG imaging of rat mammary gland, we found that ductal collagen fibers in the involuting gland were aligned more straightly with fewer gaps area between collagen fibers. More gaps between collagen fibers have been suggested by other studies to be associated with decreased collagen tension, but not directly tested. What’s more, the type and function of the materials that fill the gap areas are unknown, which warrants further investigation. We also found increased presence of collagen fibers that are “radially aligned” to mammary ductal epithelial cells in the involuting rat mammary gland. These findings are consistent with the tumor promotional attributes of the microenvironment during involution, as if tumor cells are present during involution, they are more likely to invade the stroma via movement along radially aligned collagen fibers.

However, the increased radially aligned fibers is not found in human breast tissue during involution. By only choosing to study the early involution stage (less than 4 week postweaning), it is possible that we missed the window of detecting the radially aligned fibers, so further characterization with more involution stage categories and higher number per stage is warranted.

Collagen structural reorganization during weaning-induced involution is potentially due to the increased abundance and activity of the collagen fiber cross-linking enzyme LOX. LOX controls the last step of collagen microfiber assembling and degree of collagen crosslinking at this step can alter collagen fiber structure [116, 117]. Breast cancer patient data show that high LOX levels in the tumor is associate with increased metastasis [180, 181]. The function of LOX in promote breast cancer metastasis can potentially be mediated by modeling collagen fiber organization to favor cancer cell invasion. Collagen fiber organization is not just controlled by LOX. Other collagen associated enzymes, such as lysyl hydroxylase [117] and MMPs [182], also play a critical role in collagen structural reorganization during involution. Stromal and immune cells also have critical roles in reorganize collagen. For example, it has been shown that fibroblasts in the wound can sense the tension to reorganize their actin skeleton and actively extend pseudopodia, attaching to collagen to contract and organize the ECM protein [123]. Moreover, macrophages have been shown to promote collagen fibrillogenesis around terminal end buds of the developing mammary gland to direct the shape of terminal end buds [183]. These data suggest the possibility of involvement of fibroblasts and macrophages in the collagen remodeling observed during involution, which should be further explored.

In summary, we have demonstrated physiologic regulation of collagen remodeling in the mammary gland during weaning-induced involution, which potentially serves as another factor that influences breast density. The features of collagen remodeling, including increased deposition

and structural remodeling during weaning-induced involution, are consistent with a tumor promotional microenvironment. It provides a potential explanation of the aggressiveness of the breast cancer diagnosed in the postpartum window and also brings insight into targeting collagen during the involution window to better prevent and treat postpartum breast cancer. To explore the mechanism of collagen remodeling during involution, the collagen producing cells, fibroblasts, are investigated for their functional changes during weaning-induced involution in the next chapter.

- **Method.**

Rat breeding, reproductive staging, and histology. Seven to ten week-old Sprague-Dawley rats from Taconic Farms (Germantown NY) were housed, bred and pup number normalized as described [28], with age-matched litter mate nulliparous as controls. Pups were weaned between 9-13 days of age to initiate synchronized involution. Rats were euthanized by CO₂ asphyxiation and mammary glands were collected. For histological based analysis, the region of the gland with associated lymph node was dissected and fixed in 10% neutral buffered formalin (Anatech Ltd) for 48 hours and then processed, embedded in paraffin and sectioned at 4 μm. The confirmation of normal histology was performed by hematoxylin and eosin staining. The lymph node free mammary tissue was snap-frozen in liquid nitrogen and stored in -80°C for RNA and protein analysis.

Human tissue acquisition. Formalin-fixed, paraffin embedded breast tissue obtained from 26 premenopausal women aged 20 to 45 years who were either healthy volunteer (Komen tissue bank biorepository, IN) or underwent clinically indicated surgical treatment (University of Denver, CO) were included in the study. All patient information was de-identified and cases were approved by Oregon Health & Science University IRB for research. 2 cases were obtained from Komen tissue Bank biorepository at Indianapolis (<http://komentissuebank.iu.edu/>). Donors provided written informed consent, and were recruited under a protocol approved by the Indiana University

Institutional Review Board. 24 cases were included with approval of the Colorado Multiple Institution Review Board under two protocols. One protocol was a retrospective chart review and tissue collection-only study deemed exempt from subject consent and Health Insurance Portability and Accountability Act (HIPPA) authorization, whereas the other protocol included informed written patient consent.

Second harmonic generation imaging and analysis for rat mammary glands. SHG imaging was performed as described previously [49]. In general, mammary gland tissues were sectioned at 10 μ m in thickness, and 135 μ m x135 μ m images were captured via ZEN2009 software using 60x, 1.4 NA Plan-Apochromat oil-immersion objective (Carl Zeiss Inc.). Alveoli structures were imaged by selecting lobules with more than three alveoli. Ductal structures with similar sizes were selected in the nulliparous and involuting glands. Gaps between collagen fibers were analyzed by image J software (version 1.48V) by measuring the ratio between area devoid of collagen and the entire ductal collagen area. For collagen fiber directionality analysis, a border was drawn in every image align the ductal epithelial cells, and then the angle of collagen fibers to this border was calculated by CurveAlign software developed by the Laboratory for Optical and Computational Instrumentation (LOCI, University of Wisconsin, Madison, WI, USA).

Trichrome staining and quantification. Formalin-fixed human breast tissue was sectioned at 4 μ m. Slides were baked at 60 °C for 1 hour followed by deparaffinization and rehydration. Trichrome staining was performed using MasterTech special stain kit (catalog number: KTMTR). Tissue sections were fixed in Bouin's Fluid for 1 hour at 60 °C and rinsed in distilled water. Slides were then treated with Weigert's Hematoxylin for 10 minutes, Biebrich Scarlet-Acid Fuschin for 15 minutes, phosphomolybdic/phosphotungstic acid for 10 minutes, aniline blue for 10 minutes.

After staining, slides were scanned by Aperio ScanScope AT, and slides analysis was done by Aperio ImageScope v12.1.0.5029 as described previously [14].

RT-qPCR analysis of gene expression. RNA was isolated from 50 mg whole rat mammary gland tissue using Trizol reagent (Invitrogen 15596-018). Concentration and purity were determined by 260 nm, 230 nm, and 280 nm absorbance. RNA quality was determined by Agilent 2100 Bioanalyzer. cDNA was synthesized using Bio-Rad cDNA synthesis kit and qPCR was performed using Bio-Rad SYBR Green supermix. Primer sequences: reference gene β -actin (*Actb*): forward: TTGCTGACAGGATGCAGAAGGAGA, reverse: ACTCCTGCTTGCTGATCCACATCT. *Col1a1*: forward: TGGCCAAGAAGACATCCCTGAAGT, reverse: ACATCAGGTTTCCACGTCTCACCA. *Col3a1*: forward: ATGAGCTTTGTGCAATGTGGGACC, reverse: ACTGACCAAGGTAGTTGCATCCCA. *Col5a1*: forward: ATAAGGCTATCCGCTTCTTGGGCT, reverse: TGCTCAACTTTGGGCGTGTCAATC. *Col6a1*: forward: TGCGGCTCAGACATTCAGGTAGTT, reverse: AAGCCTTGCCAGGAAATGACGTTG. *Col7a1*: forward: GATGTTTCGAGCCGGGATTAG, reverse: CCTGCAGTCCTGGGATAATAA. *Col14a1*: forward: TATGTTGTTGAAGGCCTGGACCCT, reverse: TACAGTTGTGGGTGCTTCAGTCCA. *Col15a1*: forward: GACATAGCTCCCTCCCTAAGA, reverse: GCTCTCTTTCTCTGGCTGTAT. *Col17a1*: forward: GTCTATACTGGGAGGAGGAAG, reverse: GGATGGTGACTCTTGGACATA. Decorin: forward: GGTGGCAAATACCCGGATTA, reverse: GCCAGAAGGAATAAGACGAGAG. Lysyl Oxidase: forward: TGAATTCAGCCACTACGACCTGCT, reverse: TGTGTGTGCAGTACAGGCAAATCG.

Western blot. 50 mg rat mammary tissue was lysed in 500 μ l lysis buffer (10 mM Tris pH 7.4, 150 mM NaCl, 0.1% SDS, 1% Na-Deoxycholate, 1% Triton X-100) supplemented with 1x proteinase inhibitor (Sigma) and 200 μ g/ml PMSF (Sigma), and then homogenized for 8 seconds. Protein concentration was determined by Bio-rad protein assay (Bio-rad 5000006). Equal amounts of protein (4 μ g) were loaded. Western blot was performed by Wes instrument (Proteinsimple), with 25 minutes of separation time at 375 volts, 10 minutes of blocking, 60 minutes of primary antibody incubation (anti-LOX, Abcam, ab174316, 1:20 dilution), 30 minutes secondary antibody incubation (Proteinsimple, PS-MK14), and 5 seconds of exposure time.

Collagen fiber width, length, straightness and curvelet angle analysis. Five areas per slides were imaged from nulliparous (n=6), early involution (n=5) and parous (n=6) slides with one slide per case, where over 10,000 collagen fibers from each group were analyzed. All samples in this study were imaged with a custom-built integrated SHG/brightfield imaging system¹. A MIRA 900 Ti:Sapphire laser tuned to 780 nm, with a pulse length of approximately 100 fs, was directed through a Pockel's cell (ConOptics, Danbury, CT), half and quarter waveplates (ThorLabs, Newton, NJ), beam expander (ThorLabs), a 3mm galvanometer driven mirror pair (Cambridge, Bedford, MA), a scan/tube lens pair (ThorLabs), through a dichroic beam splitter (Semrock, Rochester, NY) and focused by a 20X/0.75 N.A. objective lens (Nikon, Melville, NY). SHG light was collected in the forward direction with a 0.54 NA condenser lens (ThorLabs) and 390/22 nm bandpass filter (Semrock). The back aperture of the condenser lens was imaged onto the 5 mm aperture of a 7422-40P photomultiplier tube (Hamamatsu, Hamamatsu, Japan) the signal from which was amplified with a C7319 integrating amplifier (Hamamatsu) and sampled with an A/D converter (Innovative Integration, Simi Valley, CA). Timing between the galvanometer scanners, signal acquisition, and motorized stage positioning was achieved using our custom software. The Rapid Automated

Modular Microscope system (Applied Scientific Instrumentation, Eugene, OR) served as our microscope base and we used ASI motorized translation stages for x, y and z motion control. The SHG light source was verified to be circularly polarized at the sample using the protocol of Chen et. al.². Brightfield images were captured with the same system using a MCWHL2 white LED lamp (ThorLabs) set up for Kohler illumination. White light from this lamp was separated from SHG light traveling through the condenser assembly using a short pass dichroic mirror with a cutoff at 670 nm (Semrock). An RGB camera (QImaging, Surrey, BC, Canada) was used to capture bright field images through WiscScan to allow for acquisition within a single application. SHG images were captured as a stack of 3 images spaced 3 μm apart, then z-projected to improve field flatness. Individual images of 1024 x 1024 pixels were captured at an image size of 410 μm^2 . Five images per slide were captured from n= 6 nulliparous, n= 5 early involution and n= 6 parous slides, respectively.

Computer-based quantitation of collagen features via ctFIRE and CurveAlign:

Two different custom-written open source software packages (ctFIRE and CurveAlign) were used to analyze SHG images, and are available for free download at (<http://loci.wisc.edu/software/home>). Both programs execute a curvelet transform of the SHG image, which is a multiscale, orientation-sensitive version of the wavelet transform where edges in image features are identified, making it ideal for fiber analysis³. Following the transform, many individual curvelets are identified as a result of the high contrast fibrous nature of the SHG image of the collagen matrix. Each curvelet has an x-y location in the image, as well as an orientation. The program then uses the FIRE algorithm to merge the unitary curvelets into single extracted fibers which recapitulates the collagen fiber. The program then calculates the length, width, and straightness of each individual fiber in our SHG image (for hundreds of fibers per image), and then

summarizes the raw data into summary statistics for each slide. In addition, a boundary separating the collagen matrix from breast epithelial cells was drawn in the CurveAlign program. CurveAlign then measured the angle of extracted fibers with respect to that boundary for each fiber, and tabulated the results. The TACS-3 % was calculated as the percentage of pixels within a 100 mm radius from the boundary that were associated with fibers oriented at ≥ 60 degrees with respect to that boundary.

Study Approval. Animal procedures were approved with ethical consideration by the University of Colorado Anschutz Medical Campus and Oregon Health & Science University Institutional Animal Care and Use Committees.

- **Supplemental tables.**

| | TDLU | Duct | Bulk |
|---|-----------------------------------|-----------------------------------|-----------------------------------|
| Nulliparous (n= 30 images from 6 slides) | 22.1 \pm 1.0 N vs. E p= 0.61 | 21.7 \pm 0.9 N vs. E p= 0.29 | 22.6 \pm 0.9 N vs. E p= 0.50 |
| Early Involution (n= 25 images from 5 slides) | 21.8 \pm 0.9 E vs. P p= 0.71 | 22.2 \pm 0.8 E vs. P p= 0.52 | 23.0 \pm 1.2 E vs. P p= 0.21 |
| Parous (n= 30 images from 6 slides) | 21.6 \pm 1.3 N vs. P p= 0.41 | 21.7 \pm 1.6 N vs. P p= 0.97 | 22.0 \pm 1.2 N vs. P p= 0.39 |

Supplemental table 1. Length of collagen fibers

The length of collagen fibers extracted from SHG images via the ctFIRE algorithm was measured. Values are $\mu\text{m} \pm$ S.D. TDLU: collagen in the terminal duct lobular unit. Duct: collagen surround breast ducts. Bulk: The rest of collagen, mainly collagen within the stroma.

| | TDLU | Duct | Bulk |
|---|---|----------------------------------|----------------------------------|
| Nulliparous (n= 30 images from 6 slides) | 0.929 ± 0.001 N vs. E p= 0.12 | 0.925 ± 0.006 N vs. E p= 0.10 | 0.927 ± 0.002 N vs. E p= 0.39 |
| Early Involution (n= 25 images from 5 slides) | 0.927 ± 0.002 E vs. P p= 0.97 | 0.920 ± 0.002 E vs. P p= 0.16 | 0.928 ± 0.002 E vs. P p= 0.29 |
| Parous (n= 30 images from 6 slides) | 0.927 ± 0.005 N vs. P p= 0.49 ¹ | 0.926 ± 0.009 N vs. P p= 0.80 | 0.926 ± 0.004 N vs. P p= 0.57 |

Supplemental table 2. Straightness of Collagen Fibers

The straightness of collagen fibers extracted from SHG images via the ctFIRE algorithm was measured. Values are $\mu\text{m} \pm$ S.D. TDLU: collagen in the terminal duct lobular unit. Duct: collagen surround breast ducts. Bulk: The rest of collagen, mainly collagen within the stroma.

| | Mean Curvelet Angle | TACS-3 percentage(%) |
|---|--------------------------------|-------------------------------|
| Nulliparous (n= 30 images from 6 slides) | 34.5 ± 4.9 N vs. E p= 0.301 | 2.2 ± 1.3 N vs. E p= 0.145 |
| Early Involution (n= 25 images from 5 slides) | 31.7 ± 3.4 E vs. P p= 0.758 | 1.2 ± 0.5 E vs. P p= 0.101 |
| Parous (n= 30 images from 6 slides) | 32.4 ± 4.2 N vs. P p= 0.444 | 1.9 ± 0.7 N vs. P p= 0.628 |

Supplemental table 3. Properties of Collagen Fibers

The mean curvelet angle and the TACS-3 percentage of fibers were calculated using CurveAlign software. Values are angle degree \pm S.D. TDLU: collagen in the terminal duct lobular unit. Duct: collagen surround breast ducts. Bulk: The rest of collagen, mainly collagen within the stroma.

CHAPTER III. PHYSIOLOGICALLY ACTIVATED MAMMARY FIBROBLASTS PROMOTE POSTPARTUM MAMMARY CANCER.¹

Qiuchen Guo, Jessica Minnier, Julja Burchard, Kami Chiotti, Paul Spellman, Pepper Schedin

Author contributions

Q. Guo and P. Schedin developed the hypothesis, conceptual and experimental designs, and are responsible for data analysis and interpretation. Q. Guo performed all experiments and P. Schedin is responsible for data integrity. For the RNA sequencing study, P. Spellman assisted with experimental design, K. Chiotti processed the raw RNA sequencing data, J. Burchard performed data normalization and J. Minnier performed statistical analysis. Q. Guo and P. Schedin wrote the manuscript with the help of J. Minnier and J. Burchard for the RNA seq method section.

¹Most of the chapter III was re-printed with permission from the JCI Insight. (Qiuchen Guo, Jessica Minnier, Julja Burchard, Kami Chiotti, Paul Spellman, Pepper Schedin. Physiologically activated mammary fibroblasts promote postpartum mammary cancer. Accepted 2/2017)

- **Abstract.**

Women diagnosed with breast cancer within 5 years of childbirth have poorer prognosis than nulliparous or pregnant women. Weaning-induced breast involution is implicated, as the collagen rich, immune suppressive microenvironment of the involuting mammary gland is tumor promotional in mice. To investigate the role of mammary fibroblasts, isolated mammary PDGFR α ⁺ cells from nulliparous and post-weaning mice were assessed for activation phenotype and pro-tumorigenic function. Fibroblast activation during involution was evident by increased expression of the fibrillar *collagens*, *lysyl oxidase*, *Tgfb1*, and *Cxcl12* genes. The ability of mammary tumors to grow in an isogenic, orthotopic transplant model was increased when tumor cells were co-injected with involution- compared to nulliparous-derived mammary fibroblasts. Mammary tumors in the involution-fibroblast group had increased Ly6C⁺ monocytes at the tumor border, and decreased CD8 T cell infiltration and tumor cell death. Ibuprofen treatment suppressed involution-fibroblast activation and tumor promotional capacity, concurrent with decreases in tumor Ly6C⁺ monocytes, and increases in intratumoral CD8 T cell infiltration, granzyme levels, and tumor cell death. In total, our data identify a COX-PGE2 dependent activated mammary fibroblast within the involuting mammary gland that displays pro-tumorigenic, immune suppressive activity, identifying fibroblasts as potential targets for the prevention and treatment of postpartum breast cancer.

- **Introduction.**

A diagnosis of breast cancer within 5-10 years of childbirth is an independent predictor of poor prognosis due to increased risk of metastasis [4, 9, 10, 184]. Further, an estimated 40% to 50% of all young women's breast cancers are associated with a recent pregnancy, identifying postpartum breast cancer as a significant unmet clinical need [4]. Unexpectedly, the poor outcomes of postpartum breast cancer do not appear to be due to pregnancy per se, as the prognosis of breast cancers diagnosed during pregnancy is not significantly worse than breast cancers diagnosed in nulliparous women [9, 10]. Rather, data implicate a unique biology of the postpartum breast in the promotion of postpartum breast cancer. Specifically, weaning-induced mammary gland involution is implicated because, in rodents, the tissue microenvironment of the involuting mammary gland enhances tumor growth, local tumor cell dissemination and distant metastasis [14, 19, 20].

Weaning-induced mammary gland involution is a biologically normal process, whereby milk stasis induces gland regression to a non-lactational state. Mammary gland involution is well characterized in rodents [22, 24, 25, 28, 46] and recently described in women [28, 178]. Involution can be separated broadly into an initial phase of secretory epithelial cell death followed by a stromal remodeling phase that re-establishes the adipocytes and connective tissue as dominant constituents of the non-lactating gland [22, 40]. The stromal remodeling phase of involution shares numerous attributes with wound healing [185-187], including lymphangiogenesis [20], orchestrated immune cell infiltration, immune suppression [19, 28], and deposition of a fibrotic-like ECM, mainly the fibrillar collagens [28, 46]. The mechanistic links between wound healing, and cancer [134, 188] and the known role of fibroblasts in these processes [101, 129, 189, 190] identify the mammary fibroblast as a potential mediator of postpartum breast cancer progression.

Fibrillar collagen deposition, which is increased during mammary gland involution, is one mechanism by which mammary fibroblasts might promote breast cancer in the postpartum window [28]. Fibrillar collagens are the most abundant ECM proteins in the breast and contribute to breast density, a dominant risk factor for breast cancer in women [191, 192]. Fibrillar collagens are also implicated in human breast cancer progression, as the presence of straight collagen fibers arranged perpendicular to the tumor border, an orientation referred to as radial alignment, is an independent predictor of breast cancer metastasis [75]. Further, in preclinical models of breast cancer, collagen density and tension regulate progression of pre-existing tumor cells [74, 193, 194]. Intravital imaging studies provide additional support for collagen mediating tumor cell dissemination, as tumor cells migrate on mammary collagen fibers to gain access to vasculature [76, 77]. We have reported that targeting the window of postpartum involution with NSAIDs reduces the levels of the COX2 enzymatic product PGE2 during mammary gland involution [48] and is sufficient to reduce mammary tumor growth and metastasis to levels observed in nulliparous mice [14, 20]. The tested NSAIDs in those studies include COX2 non-specific inhibitors ibuprofen and aspirin and the COX2 specific inhibitor Celecoxib. Surprisingly, NSAID-induced tumor protection was accompanied by decreases in mammary fibrillar collagen accumulation during involution [14], implicating collagen as a potential driver of postpartum breast cancers. Cumulatively these studies raise the possibility that fibroblasts mediate the collagen-rich, pro-tumorigenic microenvironment of the involuting mammary gland through a COX2/PGE2 dependent mechanism.

Immune suppression, which also is increased during normal weaning-induced mammary gland involution [19], is another mechanism by which mammary fibroblasts may contribute to breast cancer progression in the postpartum window. Immune suppression is implicated in breast cancer progression overall [195-197], and analyses of breast cancer patient cohorts show that low CD8 T

cell tumor infiltration, the dominant anti-tumor cytotoxic T cell [198, 199], is associated with decreased patient survival rate [199-201]. In addition to direct suppression by tumor cells, CD8 T cells can be inhibited by other immune cells within the tumor microenvironment, including immune suppressive monocytes, tumor associated macrophages (TAMs) and dendritic cells [202-204], resulting in tumor cell escape from immune surveillance. Of potential relevance, cancer associated fibroblasts (CAFs) have been reported to regulate immune cell infiltration and immunosuppression via secretion of IL-6, TGF β and CXCL12 [190, 205, 206]. These CAF studies raise the provocative question of whether fibroblasts under physiologic conditions, such as weaning-induced mammary gland involution, contribute to breast cancer by regulating immune cell recruitment and/or immune cell suppression.

In this report, we provide evidence that normal PDGFR α ⁺ cells isolated from involuting mammary glands, referred to as involution-fibroblasts, have a unique activation state, including increased fibrillar collagen, matrix remodeling, and immune modulatory gene expression patterns. Further, we demonstrate that in comparison to mammary PDGFR α ⁺ cells isolated from nulliparous mice (nulliparous-fibroblasts), involution-fibroblasts promote tumor growth, produce CXCL12, induce monocyte recruitment and associate with blockade of CD8 T cell tumor infiltration, identifying a role for fibroblasts in inhibiting intratumoral CD8 T cell infiltration and tumor cell death. Importantly, we find that the NSAID ibuprofen suppresses these tumor promotional fibroblast attributes. In summary, our studies identify the involution-fibroblast as a unique mediator of murine mammary cancer progression in the postpartum setting, as well as a direct therapeutic target of NSAIDs. These data suggest that further investigation into fibroblast-based strategies for the prevention and treatment of postpartum breast cancer is warranted.

- **Results.**

- **Involution mammary fibroblasts are uniquely activated.**

In rodents, mammary stromal remodeling is most active between 4 and 8 days post weaning [22, 28] and previous studies have shown fibrillar collagen protein abundance increases during this window of involution [14, 28]. However, the cell type responsible for mammary collagen production has not been definitively described. To this end, we utilized a transgenic, collagen 1a1 reporter mouse where green fluorescent protein (GFP) is driven by the *Coll1a1* promoter [207]. Using dual-immunofluorescence, we found GFP⁺ (Red) *Coll1a1* producing cells co-localized with cells expressing the established fibroblast marker PDGFR α (Figure 3-1A, arrows) [208]. These dual positive cells were found in high abundance surrounding the mammary ducts, but did not co-localize with calponin positive (purple) myoepithelial cells (Figure 3-1A) [209], ruling out the myoepithelial cell as a dominant cellular source of mammary collagen. IHC analysis demonstrated ~85% of PDGFR α ⁺ cells were located around the mammary ductal and alveolar structures with ~15% of staining around the less prevalent blood vessels (Supplemental figure 3-1A-C). We next isolated PDGFR α ⁺ cells by positive selection using FACS (Figure 3-1B). Isolated PDGFR α ⁺ cells were found to express the fibrillar collagen genes *Coll1a1*, *Col3a1* and *Col5a1*, which are the most abundant fibrillar collagens in the rodent mammary gland [29, 55], with low level or no expression of markers for leukocytes (*Cd45*), macrophages (*F4/80*), endothelial cells (*Cd31*), epithelial cells (*E-cadherin*) or adipocytes (*Adipoq*) (Figure 3-1C). These PDGFR α ⁺ cells were also PDGFR β ⁺ (Supplemental figure 1D). Further, the PDGFR α ⁻ cell population expressed low levels of fibrillar collagens and lysyl oxidase (*Lox*) compared to the PDGFR α ⁺ cells (Supplemental figure 1E). Together, these data suggest that PDGFR α ⁺ selection results in a highly enriched mammary fibroblast population.

To determine if mammary fibroblasts from nulliparous mice differed phenotypically from those isolated from actively involuting mammary glands, we performed global gene expression analyses by RNA-Seq on FACS isolated PDGFR α ⁺ fibroblasts from nulliparous and involution day 6 (InvD6-fibroblasts) mammary glands. We selected InvD6-fibroblasts because the ECM remodeling phase of involution, a putative fibroblast function, peaks at InvD6 [22]. Moreover, InvD6 is the peak of immune cell infiltration, and we anticipated that interactions between immune cells and fibroblasts may contribute to fibroblast activation. Over 850 differentially regulated genes were detected between nulliparous and InvD6-fibroblasts (Figure 3-1D). Pathway analysis confirmed that ECM protein associated pathways, especially fibrillar collagen production and ECM remodeling, were upregulated in PDGFR α ⁺ fibroblasts isolated from InvD6 mammary glands compared to mammary fibroblasts isolated from nulliparous hosts (Figure 3-1E).

To investigate the time course of fibroblast activation during weaning-induced mammary gland involution, we FACS isolated PDGFR α ⁺ mammary fibroblasts from nulliparous and 4, 6, and 8 days post-weaning (InvD4, InvD6, InvD8) mice and assessed for fibroblast density and activation markers. The number of PDGFR α ⁺ cells per gram of mammary gland tissue, as determined by FACS analysis, was low in nulliparous mice and at InvD4, but doubled at InvD6 and InvD8 (Figure 3-1F). Further, on a per cell basis, *Coll1a1* and *Col3a1* expression levels measured by RT-qPCR, were increased across all three involution time points compared to nulliparous-fibroblasts, and *Col5a1* was increased at InvD4 (Figure 3-1G). Gene expression for the collagen cross-linking enzyme *Lox* was highly increased in fibroblasts at InvD4 and InvD6 (Figure 3-1G), data consistent with elevated fibrillar collagen production. Further, *Mmp2*, *Mmp3* and *Tgfb1* expression levels were increased at InvD6 (Figure 3-1H). These gene expression patterns are consistent with classical fibroblast activation, so we co-stained mammary tissue for PDGFR α and α -smooth

muscle actin (α SMA-red), a fibroblast activation marker under pathologic conditions [210]. α SMA was undetectable in mammary fibroblasts at all reproductive stages (Figure 3-1I and data not shown).

Another pro-tumorigenic hallmark of mammary gland involution is macrophage and monocyte infiltration, with the peak influx occurring during mid (InvD4 & 6) to late (InvD8 & 10) involution [28, 55]. We assessed for immune regulatory pathways in involution-fibroblasts, and in comparison to nulliparous-fibroblasts, InvD6 fibroblasts had increased gene expression of several immune pathways including rheumatoid arthritis and cytokine-receptor interaction (Figure 3-1J). A subset analysis of chemokine RNA expression profiles revealed *Cxcl12* as the most highly expressed chemokine in these mammary fibroblasts (Figure 3-1K). CXCL12 is a lymphocyte chemoattractant and immune suppressive chemokine that induces macrophage M2 polarization and IL-10 production [149-151]. Further, CAF secreted CXCL12 stimulates cancer cell proliferation via paracrine signaling [211]. By RT-qPCR, we confirmed that *Cxcl12* gene expression was increased in InvD6- compared to nulliparous-fibroblasts (Figure 3-1L). In summary, the lack of α SMA concurrent with high expression of fibrillar collagens, *Lox*, *Tgfb1*, *Mmps*, and *Cxcl12* indicates that involution-fibroblasts are not “classically” activated as occurs during wound-healing, but rather are alternatively activated through a developmentally regulated process. Further, phenotypic characterization of involution-fibroblast suggests these cells are capable of modulating two key aspects of the tumor microenvironment, fibrillar collagen

deposition and the immune milieu.

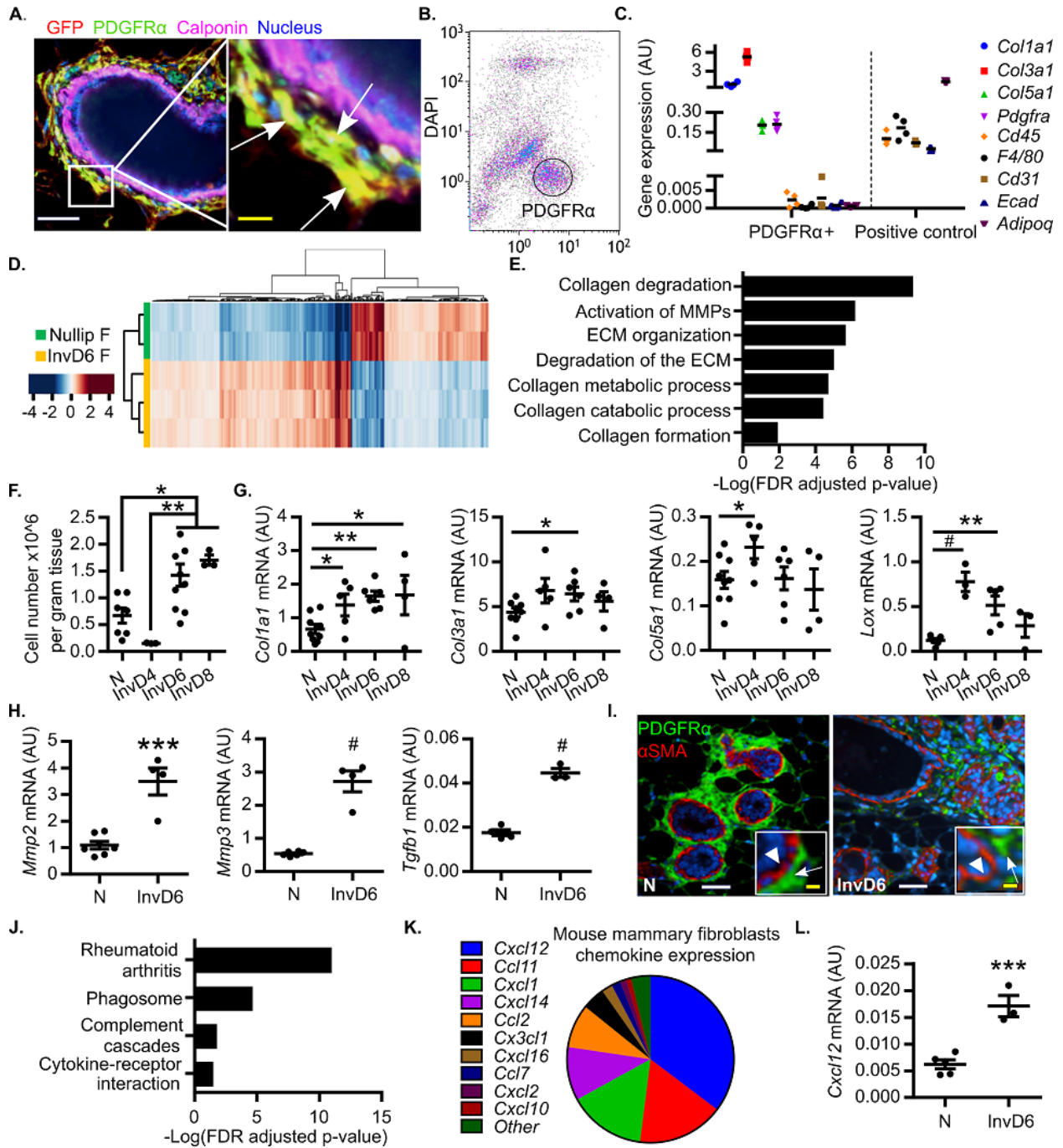


Figure 3- 1. Mammary fibroblasts are activated during weaning-induced gland involution.

(A) Mammary gland thin sections from the *Col1a1*-GFP reporter mouse immunofluorescence stained for GFP⁺ collagen 1 expressing cells (red), fibroblast PDGFR α (green), and myoepithelial cell calponin (purple), show colocalization of GFP and PDGFR α (yellow), but not calponin. Nuclei stained with DAPI (blue). White scale bar: 50 μ m. Yellow scale bar: 10 μ m. Arrows show PDGFR α ⁺ GFP⁺ Calponin⁻ cells. (B) Flow gate for isolating murine mammary PDGFR α ⁺ cells. (C) RT-qPCR on flow sorted PDGFR α ⁺ cells for fibroblast markers (*Col1a1*, *Col3a1*, *Col5a1*, and *PDGFR α*) and markers of potential contaminating

cell populations: *Cd45* (lymphocyte common antigen), *F4/80* (mature macrophage), *Cd31* (endothelial cell), *Adipoq* (adipocyte), and *Ecad* (epithelial cell). Sorted PDGFR α negative cells were used as positive controls for *Cd45*, *F4/80*, *Cd31*, *Adipoq*, and mammary epithelial EpH4 cells were used as the *Ecad* positive control. n=3-4 per group. **(D)** RNA-seq heat map illustrates 870 significantly differentially expressed genes (>1.3-fold changes) between fibroblasts isolated from nulliparous and InvD6 mammary glands. Red: relative high expression. Blue: relative low expression. **(E)** Pathway analysis of RNA-seq data set showing ECM regulation related pathways that are upregulated in InvD6 fibroblasts. **(F)** PDGFR α ⁺ fibroblasts reported as number per gram of mammary tissue observed in nulliparous, 4, 6, and 8 days post weaning mice, n=3-10 per group. **(G)** Fibrillar collagens and *Lox* gene expression analysis by RT-qPCR in sorted PDGFR α ⁺ mammary fibroblasts in nulliparous, 4, 6, and 8 days post weaning mice, n=3-10 per group. **(H)** *Mmp2*, *Mmp3* and *Tgfb1* gene expression analysis by RT-qPCR in nulliparous and InvD6 fibroblasts, n=6-9 per group. **(I)** Immunofluorescence staining shows non-colocalization of α -smooth muscle actin (red) and PDGFR α (green) in mammary glands of nulliparous and InvD6 mice. Box: images at high magnification. Arrow: PDGFR α ⁺ cells. Arrowhead: α SMA⁺ cells. White scale bar: 50 μ m. Yellow scale bar: 10 μ m. **(J)** Pathway analysis of RNA-seq data described in (D) showing immune regulation related pathways that are upregulated in InvD6 fibroblasts. **(K)** RNA seq data show chemokine expression pattern of fibroblasts isolated from nulliparous mammary glands. **(L)** RT-qPCR gene expression for *Cxcl12* in sorted PDGFR α ⁺ fibroblasts from nulliparous and InvD6 mammary glands, n=3-5 per group. Gene expression data are normalized to *Actb*. Gene expression data were from 2-6 independent studies. RNA seq data are archived at Gene Expression Omnibus (GEO GSE94761). *P<0.05, **P<0.01, ***P<0.001, #P<0.0001. Unpaired two-tailed *t*-test. Data represent mean \pm SEM.

- **Ibuprofen inhibits involution fibroblast activation in vivo.**

In rodent models, systemic NSAIDs treatment after weaning inhibits fibrillar collagen accumulation in the involuting mammary gland through an unknown mechanism [14, 97]. To determine if systemic NSAID treatment inhibits collagen gene expression in mammary fibroblasts, we treated mice with control diet or Ibuprofen at two different doses (equivalent to 117 mg and 234 mg per day for humans) [212], starting at weaning through InvD6 (Figure 3-2A). Based on histologic examination, we found that ibuprofen treatment did not delay normal, post-weaning lobule regression (Figure 3-2B), data consistent with previous studies [14, 20, 48]. Ibuprofen treatment also did not influence the number of fibroblasts per gram tissue in the involuting mammary gland (Supplemental figure 2A). However, assessing FACS isolated fibroblasts revealed that both doses of Ibuprofen decreased fibroblast expression of *Colla1* (Figure 3-2C left panel), but not *Col3a1*, *Col5a1* or *Lox* (Supplemental figure 2B). To determine if this decrease in type I collagen gene expression correlated with decreased protein levels within the mammary

gland, type I collagen protein levels were quantitated by IHC. This analysis demonstrated decreased type I collagen protein levels after ibuprofen treatment (Figure 3-2C right panel). Ibuprofen treatment also reduced fibroblast *Mmp3* gene expression (Figure 3-2D), but not *Mmp2* expression (Supplemental figure 2B). Additionally, *Tgfb1* and *Cxcl12* expression were decreased by ibuprofen treatment (Figure 3-2D). Cumulatively, these data demonstrate that ibuprofen treatment suppresses key aspects of fibroblast activation including type I collagen production and *Mmp2*, *Tgfb1* and *Cxcl12* gene expression.

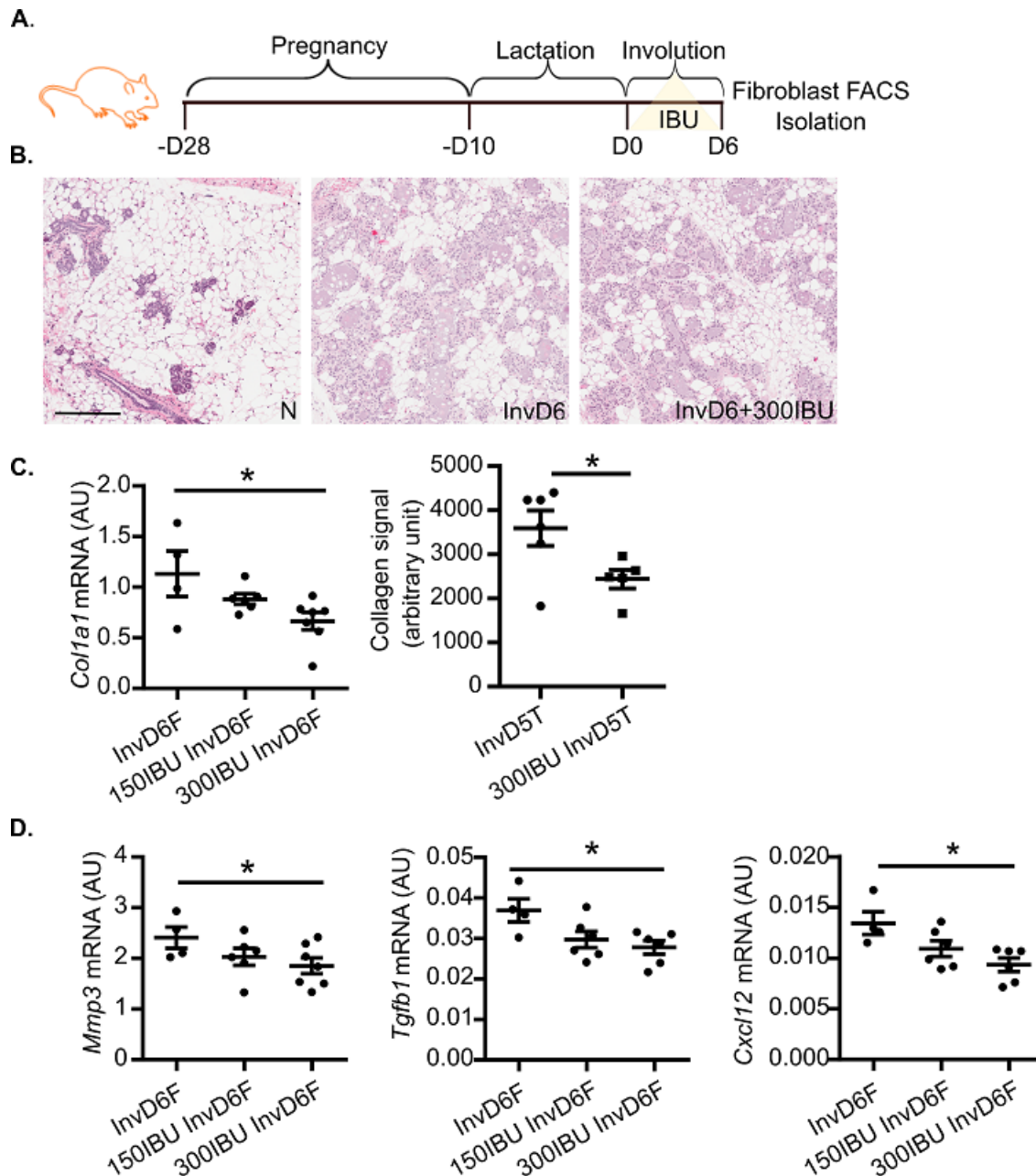


Figure 3- 2. Systemic in vivo ibuprofen treatment during weaning-induced mammary gland involution decreases mammary fibroblast activation.

(A) Schematic shows breeding and weaning-induced mammary gland involution timeline with 0 mg/kg (control), 150 mg/kg (150IBU) and 300 mg/kg (300IBU) Ibuprofen provided in chow for 6 days following weaning, with mammary fibroblasts FACS isolated on InvD6. (B) Representative H&E images of Nulliparous, InvD6 and 300IBU mammary glands depicting normal nulliparous and InvD6 gland morphology in the absence and presence of ibuprofen treatment. Scale bar: 200 μ m. (C) Left panel: RT-qPCR of *Colla1* gene expression in isolated fibroblasts, n=4-7 per group. Right Panel: Type I collagen IHC quantification around InvD5 mammary lobules (InvD5T) with and without 300IBU treatment for 5 days, n=5-6 per group. (D) RT-qPCR analysis of targeted genes in isolated fibroblasts, n=4-7 per group. Gene expression data are normalized to *Actb*. Ibuprofen intervention data were from 2 independent studies

breeding studies. *P<0.05. One-way ANOVA with Tukey correction and unpaired two-tailed *t*-test. Data represent mean ± SEM.

- **Ibuprofen inhibits fibroblast activation in vitro.**

While the above studies demonstrate that systemic ibuprofen treatment reduces mammary fibroblast activation in vivo, these studies do not address whether Ibuprofen directly suppresses fibroblast collagen production. To address this question, we isolated mammary fibroblasts from nulliparous mice [213], expanded them in culture, and evaluated their function in an adapted fibroblast contraction model whereby fibroblasts are cultured within a floating collagen pad [214]. In comparison to mammary fibroblasts cultured on tissue-culture plastic, fibroblasts in the floating collagen pads had a compacted phenotype (Figure 3-3A) and expressed low level α SMA, similar to the level observed in freshly FACS isolated mammary fibroblasts (Figure 3-3B). We next modeled the involution microenvironment by treating the fibroblast impregnated collagen floating pads with TGF β 1, a key mediator of mammary gland involution [35, 215] with established roles in fibroblast activation [216-218]. TGF β 1 treated fibroblasts had an elongated phenotype (Figure 3-3C), increased *Colla1* and *COX2* gene expression (Figure 3-3D), and contracted the collagen pads in a TGF β 1 dose-dependent manner (Figure 3-3E upper panel). Importantly, under these culture conditions, TGF β 1 treatment did not increase fibroblast α SMA expression (Supplemental figure 3), modeling numerous aspects of the activated fibroblast phenotype observed in the involuting gland. Ibuprofen, added to the cultures at levels detected in the plasma of humans with regular Ibuprofen intake [219], inhibited the ability of fibroblasts to contract the collagen pad (Figure 3-3E lower panel and quantification in 3-3F), elongate (Figure 3-3G), or induce *Colla1* and *COX2* expression (Figure 3-3H).

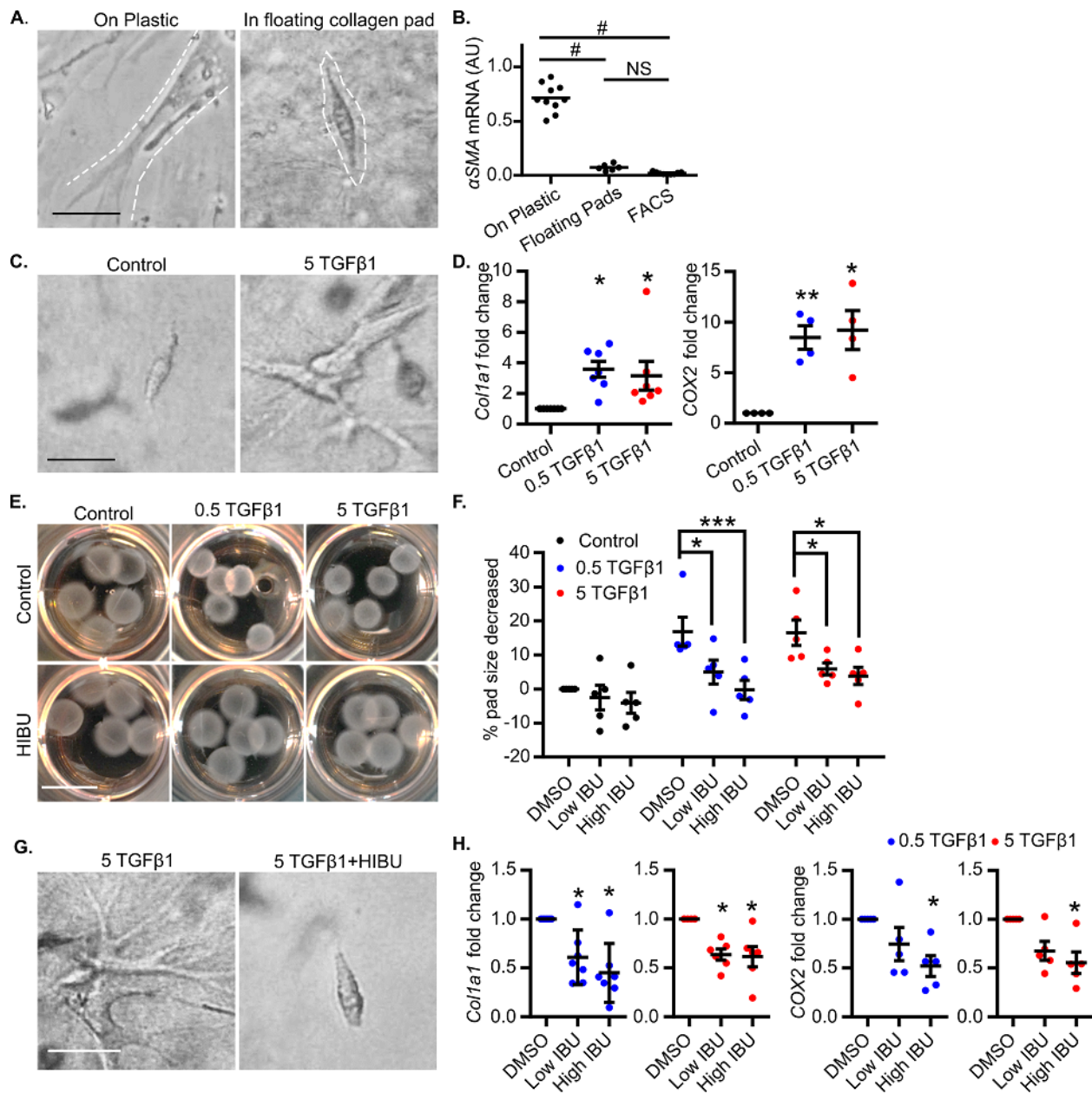


Figure 3-3. In vitro mammary fibroblast activation by TGF β 1 is directly inhibited by ibuprofen.

Treatment conditions are: 0.5 TGF- β 1 = 0.5 ng/ml TGF- β 1, 5 TGF- β 1 = 5 ng/ml TGF- β 1, Low IBU = 10 μ g/ml ibuprofen, High IBU = 30 μ g/ml ibuprofen (HIBU). (A) Mammary fibroblast morphology when cultured on plastic (left panel) or within floating collagen pads (right panel). Dashed lines show the outline of the cells. (B) α -Smooth muscle actin gene expression (α SMA) in primary mammary fibroblasts cultured on plastic, within floating collagen pads, or from freshly sorted mammary PDGFR α + fibroblasts, n = 6–10 per condition. (C) Morphologic evidence of TGF- β 1–induced fibroblast activation in the floating collagen pad culture model. (D) Increased *Colla1* and *Cox2* gene expression in fibroblasts treated with TGF- β 1, n = 4–7 per condition. (E) The ability of TGF- β 1–treated fibroblasts to contract collagen pads (top) is suppressed by ibuprofen (bottom) and (F) data quantification, n = 5 per condition. (G) Fibroblast morphology with TGF- β 1 treatment in the presence or absence of ibuprofen. (H) *Colla1* and *Cox2* gene expression in fibroblasts with TGF- β 1 treatment in the presence or absence of ibuprofen, n = 5 per condition.

Scale bars: 100 μm (A, C, and G) and 1 cm (E). All gene expression data are normalized to *Actb* and then normalized to the control groups in each experiment. TGF- β 1 and ibuprofen combination treatment studies were repeated 5 times. *P < 0.5, **P < 0.01, ***P < 0.001, #P < 0.0001 by 1-way ANOVA with Tukey correction. For data normalized to control, statistics were performed using matched 1-way ANOVA with Tukey correction on the raw data that are not normalized to control. Data represent mean \pm SEM. NS, not significant.

The ability of NSAIDs to inhibit these fibroblast activation phenotypes suggests that activation is partially dependent on COX2 pathway metabolites. Thus, we treated fibroblasts with a COX2 enzymatic product PGE2, which is abundant in the involuting mammary gland [48], and found PGE2 induced fibroblast *Colla1*, *MMP3* and *Cxcl12* expression, but not cellular elongation or pad contraction (Figure 3-4A, B).

- Fibroblasts recruit monocytes in a COX-PGE2 dependent manner in vitro.

The induction of *Cxcl12* in PGE2 treated fibroblasts (Figure 3-4A) supports the hypothesis that PGE2-activated fibroblasts may mediate chemotaxis of monocyte-derived cells, an immune cell abundantly present in the involuting mammary gland [19]. To begin to test this hypothesis, we utilized a modified cell migration assay, where collagen pads containing fibroblasts were separated from fluorescently labeled bone marrow derived monocytes by a membrane with 5 μm pores. Fibroblasts were then treated with vehicle (Control), PGE2, or PGE2 with CXCL12 neutralizing antibody, and impact on monocyte-derived cell recruitment into the collagen pad quantified (Figure 3-4C). We found that PGE2 treatment of fibroblasts induced monocyte-derived cell migration and further, found that the addition of CXCL12 neutralizing antibody completely reversed this phenotype (Figure 3-4D left panel and 3-4E). In the absence of fibroblasts, monocyte-derived cells failed to migrate in response to PGE2, demonstrating the requirement of fibroblasts for monocyte-derived cell migration in this assay (Figure 3-4D right panel and 3-4E).

Collectively, our cell culture studies demonstrate a role for PGE2 in fibroblast activation and subsequent monocyte-derived cell recruitment via CXCL12.

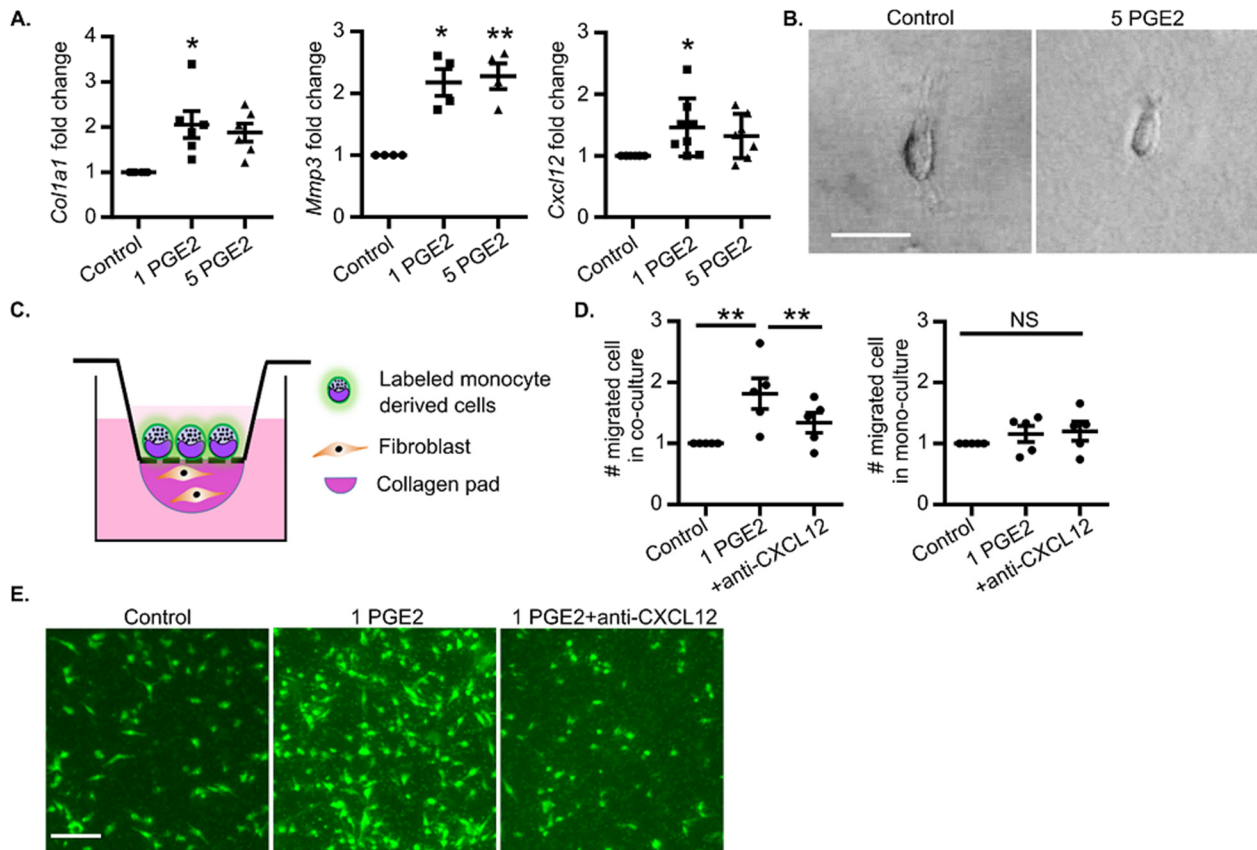


Figure 3- 4. PGE2 directly stimulates fibroblast collagen and cytokine expression but not cell elongation.

(A) *Col1a1*, *Mmp3* and *Cxcl12* gene expression induced by 1 ng/ml PGE2 (1 PGE2) or 5 ng/ml PGE2 (5 PGE2) treatment, n=4-8 per group. All gene expression data are normalized to *Actb* and then normalized to the control groups in each experiment. Gene expression data obtained from 4-8 independent experiments. (B) Mammary fibroblast morphology when cultured within floating collagen pads in the absence (right panel) and presence of 5 ng/ml PGE2. Scale bar: 100 μ m. (C) Model of fibroblast induced monocyte derived cell migration assay set-up. (D) Quantification of the number of monocyte derived cell that migrated into collagen pads in Control (1 μ g/ml mouse IgG1 isotype control), 1 PGE2 (1 ng/ml PGE2 with 1 μ g/ml mouse IgG1 isotype control), and +anti-CXCL12 (1 ng/ml PGE2 with 1 μ g/ml CXCL12 neutralizing antibody) conditions, with data normalized to control, n=5/condition. Monocyte derived cell migration assay was repeated 5 times. (E) Representative images of migrated monocyte derived cells labeled with green fluorescence dye in Control, 1 PGE2 and 1 PGE2+anti-CXCL12" conditions as described in D. Scale bar: 200 μ m. *P<0.05, **P<0.01. Matched One-way ANOVA with Tukey correction on the raw data that are not normalized to control. Data represent mean \pm SEM.

- **Ibuprofen inhibits tumor promotional capacity of involution fibroblasts.**

To determine the functional significance of mammary fibroblast activation state on mammary cancer promotion, we orthotopically injected BALB/c mice with D2A1 mammary tumor cells mixed 1:1 with mammary fibroblasts FACS isolated from mice that were nulliparous, InvD6, or InvD6 treated with ibuprofen at weaning through InvD6 (IBU-InvD6-fibroblasts) (Figure 3-5A). Sorted fibroblasts, plated in culture, confirmed uniform cell viability across groups (Supplemental figure 4). Compared to nulliparous-fibroblasts, D2A1 mammary tumor cells co-injected with InvD6-fibroblasts formed larger tumors (Figure 3-5B). Tumors that developed from co-injection with IBU-InvD6-fibroblasts were smaller, similar in size to the nulliparous-fibroblast group tumors (Figure 3-5B). At study end we found no significant difference in intratumoral collagen deposition between nulliparous- and InvD6-fibroblast group tumors (Figure 3-5C, 3-5E). However, we did find evidence supportive of involution-fibroblasts mediating a pro-tumorigenic, immune suppressive milieu, as tumors in the InvD6-fibroblast group had increased Ly6C⁺ Ly6G⁻ monocyte density at the tumor border (Figure 3-5D, 3-5E and Supplemental figure 5A), and decreased intratumoral CD8 T cell and granzyme A⁺ and granzyme B⁺ cell infiltrates (Figure 3-5D, 5E and Supplemental figure 5D, 5E). In contrast, tumors in the IBU-InvD6-fibroblast group had decreased Ly6C⁺ monocytes at the tumor border, increased intratumoral CD8 T cell, and increased granzyme A⁺ and granzyme B⁺ cell infiltrates (Figure 3-5D, 3-5E, and Supplemental figure 5D, 5E). Co-staining of CD8 and granzyme B demonstrated a subset of granzyme B⁺ CD8 T cells, consistent with presence of activated, intratumoral CD8 T cells in the IBU-InvD6-fibroblast group tumors (Supplemental figure 5B, 5C). However, the identity of the immune cells producing granzyme A remains unknown. By IHC we found these granzyme A⁺ cells to be CD45⁺CD3⁻CD8⁻CD4⁻NCR1⁻, suggesting they are not T cells, NKT cells, or NK cells (Supplemental figure 5F). No differences in Foxp3⁺ T regulatory cells were observed between

groups (Supplemental figure 6A, 6B). Further, in spite of significant tumor size variation between groups, we did not observe differences in tumor cell proliferation (Supplemental figure 6C). However, we did observe differences in tumor cell death, with InvD6 fibroblasts associated with decreased death and IBU-InvD6 fibroblasts with increased death (Figure 3-5C, 3-5D).

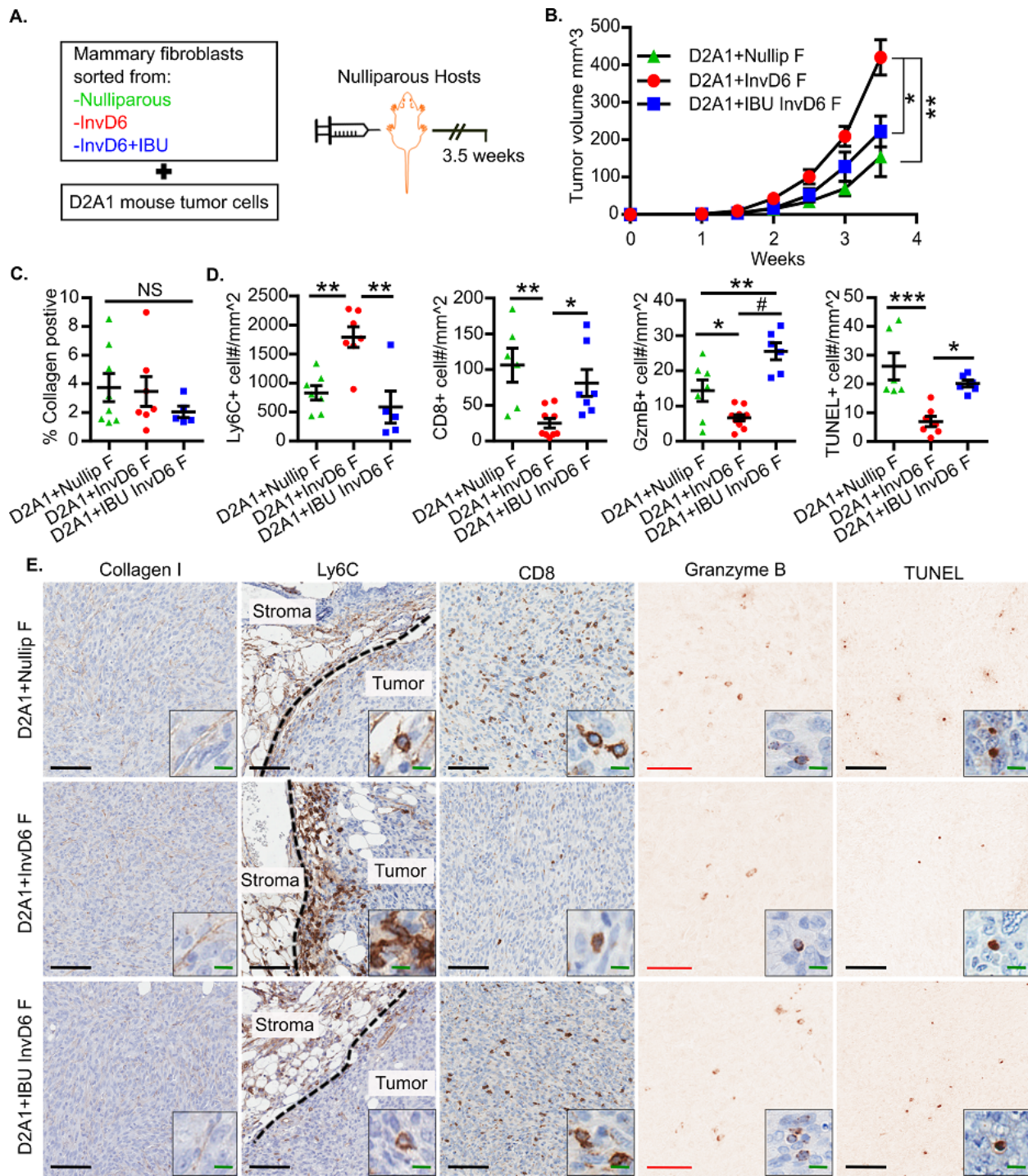


Figure 3- 5. Mammary involution-fibroblasts are tumor promotional via a COX2 dependent mechanism that suggests immune modulation.

(A) Schematic design for mammary fibroblast treatment, isolation and use in an orthotopic mammary tumor model. 20,000 FACS isolated mammary fibroblasts isolated from nulliparous, InvD6, or InvD6 hosts treated during involution with 300 mg/kg ibuprofen in chow (IBU InvD6 F), were mixed with D2A1 tumor cells at 1:1 ratio, injected into mammary fat pads of nulliparous Balb/c mice and tumor tissue collected 3.5 weeks post tumor cell injection. (B) Tumor growth curve of D2A1 cells co-injected with sorted fibroblasts

from nulliparous (D2A1+Nullip F), InvD6 (D2A1+InvD6 F) and InvD6 with ibuprofen treatment (D2A1+IBU InvD6 F) mice. n=7-10 tumors per group. **(C)** IHC quantification of intratumoral type I collagen, n=5-8 tumors per group. **(D)** IHC quantification of tumor border Ly6C, intratumoral CD8, granzyme B, and TUNEL. n=5-10 tumors per group. **(E)** Representative IHC images of markers quantified in (D). From left to right: intratumoral collagen I, tumor border Ly6C (dashed lines show tumor border), intratumoral CD8, granzyme B and TUNEL. Black scale bar: 20 μ m. Red scale bar: 10 μ m. Counterstaining (blue) is not shown in granzyme B and TUNEL stained images to enhance visualization of the positive cells. All tumor data were obtained from 2 independent breeding studies. NS (not significant), *P<0.05, **P<0.01, ***P<0.001, #P<0.0001. One-way ANOVA with Tukey correction. Data represent mean \pm SEM.

Cumulatively our combined studies suggest fibroblast activation during mammary gland involution that is mediated through a COX dependent-mechanism. These activated fibroblasts recruit Ly6C⁺ monocytes via CXCL12 secretion, which in the presence of tumor, inhibit CD8 T cell tumor infiltration and tumor cell death, resulting in enhanced tumor size (Figure 3-6).

Weaning-Induced mammary gland involution

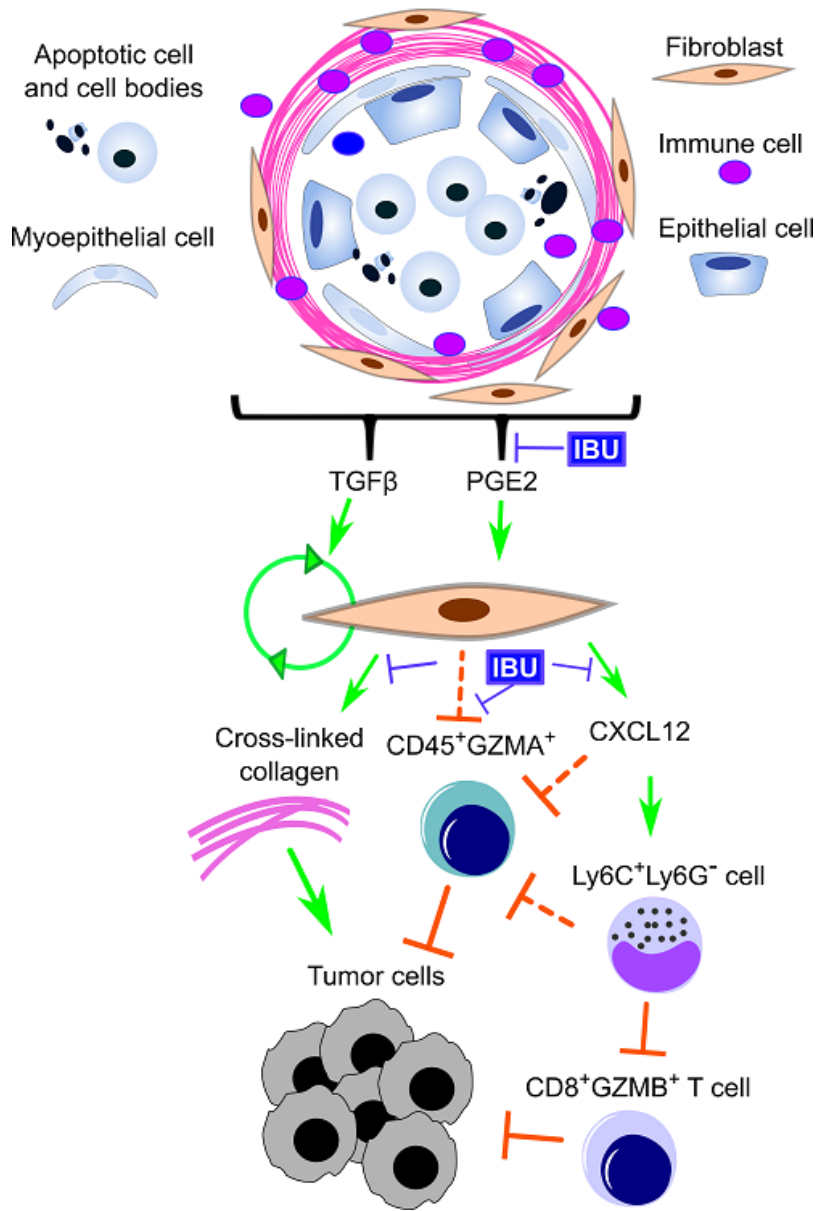


Figure 3- 6. Schematic overview of the potential tumor promotional contributions of mammary involution-fibroblasts.

Activation of involution-fibroblasts by TGFβ and PGE2 in the involution microenvironment leads to increased fibrillar collagen expression, which is tumor promotional. Involution-fibroblasts also have increased CXCL12 expression, which recruits Ly6C⁺Ly6G⁻ monocytes, blocking CD8 T cell tumor infiltration and tumor cell death. Involution-fibroblasts also block CD45⁺GZMA⁺ cell infiltration into tumor by an unknown mechanism (dashed block arrows). These tumor promotional attributes of the involution-fibroblasts can be blocked by ibuprofen.

- **Discussion.**

We identify, for the first time, a developmentally activated PDGFR α ⁺ fibroblast population in the post-weaning rodent mammary gland that shares numerous attributes with myofibroblasts activated under wound healing and cancer pathologies. These PDGFR α ⁺ fibroblasts are characterized by increased gene expression for the fibrillar collagens *Colla1*, *Col3a1* and *Col5a1*, and the stromal remodeling factors *Tgfb1*, *Lox*, *Mmp2*, *Mmp3* and *Cxcl12*. Unlike fibroblasts activated under pathological conditions, mammary involution-fibroblasts have low α SMA expression, suggesting a previously unrecognized activation state. Further, we find involution-fibroblasts to be tumor promotional, as they increase mammary tumor growth in an immune competent, orthotopic tumor transplant model. These rodent studies are consistent with the concept that breast cancers can misappropriate normal developmentally regulated programs to their advantage, such as physiologic fibroblast activation during mammary gland involution. Young women's breast cancer may be especially responsive to such developmentally regulated programs due to the remarkable, physiologic breast remodeling that accompanies gland regression in the postpartum setting [28, 178].

The links between NSAIDs, COX2, mammary gland collagen density, and breast cancer progression were first reported in a model of postpartum breast cancer [14]. More recently in the *Colla1*^{tm1jae} mouse model of high breast density, where a mutation in the collagen I collagenase cleavage site leads to increased collagen accumulation and subsequent mammary tumor promotion, celecoxib was found to suppress both phenotypes [97]. Here, for the first time, we identify a potential mechanism by which NSAIDs inhibit collagen deposition by demonstrating that the COX2 metabolite PGE2 induces, and ibuprofen suppresses, *Colla1*, *MMP3* and *CXCL12* production in normal mammary fibroblasts. Given the paucity of data pertaining to physiologic

collagen regulation in the breast, we propose that weaning-induced mammary gland involution may be a useful model to study the role of fibroblast activation and collagen production under normal physiological conditions. Such studies may provide insight into the regulation of breast density, a dominant risk factor for breast cancer [220], as well as breast cancer progression [74].

One unanswered question pertains to the source of COX2 metabolites in the involuting mammary gland. Surprisingly, mammary epithelial cells (MECs) express high levels of COX2 during weaning-induced involution and MECs may be the dominant source of PGE2 in the mammary gland [73]. Supportive roles for mammary epithelial cells in fibroblast activation and collagen production have been previously reported. For example, overexpression of p190B RhoGAP (GTPase activating protein) in mammary epithelial cells has been shown to increase TGF β secretion and subsequent fibroblast activation [221]. Additionally, epithelial cell derived pappalysin-1, which is upregulated during weaning-induced involution, releases bound IGF through cleavage of the IGF binding proteins 4 and 5. The resulting elevated IGF signaling stimulates collagen production in mammary fibroblasts [222, 223]. It remains to be determined whether the COX2/PGE2 pathway we describe here for mammary fibroblast activation integrates with either the p190B RhoGAP or pappalysin-1 pathways during weaning-induced involution.

Having demonstrated that involution-fibroblasts upregulate fibrillar collagen expression, it was surprising that there were no observable increases in collagen abundance in mammary tumors that developed after co-injection with InvD6-fibroblasts. One limitation of our tumor study is that we did not determine the fate of the injected primary fibroblasts over time, which are non-transformed and likely do not survive to study end. Early loss of fibroblasts in our transplant model may explain the unchanged collagen levels across groups. However, tumor sizes did differ between fibroblasts groups, raising the question of whether early collagen exposure contributes to differences in tumor

size across groups. One possible explanation, consistent with an early role for collagen in tumor expansion, is that transient exposure to fibroblast collagen durably influences tumor cell behavior. In support of this possibility, in an orthotropic model, compared to ECM isolated from nulliparous mammary glands, collagen-rich ECM isolated from involuting mammary glands promoted mammary tumor development for several weeks, even at ECM volumes that limited direct tumor cell-ECM interactions to only a few days post tumor cell injection [43, 48]. In further support of a durable pro-tumor effect resulting from transient exposure to the involuting microenvironment, mammary tumor cells that evolved for 2-weeks within the involuting gland retained elevated expression of COX2 and pro-metastatic attributes ex-vivo [20]. Of potential relevance, durable, pro-tumorigenic effects have been reported after transient activation of the Src oncoprotein in immortalized breast MCF10A cells [224]. In this report, stable cellular transformation was maintained in the absence of the initiating oncogenic signal due to establishment of a positive feedback loop involving NF- κ B, IL6 and STAT3 [224]. Such feed-forward loops may explain, in part, how fibroblast collagen gene expression at time of tumor cell injection might impact tumor size, even in the absence of differences in tumor collagen abundance at study end. However, additional studies are required to test this hypothesis.

We also found that mammary fibroblasts isolated from involuting mammary glands had immune modulatory function consistent with immune suppression. Immune modulatory activity of CAFs has been previously reported [101, 190], and shown to be mediated in part by cytokine and chemokine secretion. Additional indirect evidence for immune regulatory functions of CAFs is suggested by the positive correlations between the high extracellular matrix deposition by CAFs, tumor immune cell infiltration, and breast cancer progression in women [169, 225]. Here, we show for the first time that physiologically activated fibroblasts, weaning-induced involution

fibroblasts, characterized by high ECM production and chemokine secretion, also have immune modulation functions. Previous studies of the involuting mammary microenvironment have identified increased M2 polarized macrophages (Arginase 1 positive), immature monocytes that suppress T cell CD25, CD69 and IFN- γ production, and increased levels of immune suppressive cytokines, including IL-4, IL-13 and IL-10 [19, 24, 28, 226]. Here, we extend these studies to show that the chemokine CXCL12, a powerful monocyte lineage chemoattractant [149], is produced by fibroblasts during mammary involution, potentially in response to increased PGE2 signaling, as in vitro, PGE2 treatment induced fibroblast *Cxcl12* expression and monocyte-derived cell recruitment. Further, we show that fibroblast *Cxcl12* expression levels correlate with the presence of tumor associated monocytes at the tumor border, and inversely with tumor infiltrating CD8 T cells, two critical immune cell populations controlling tumor cell death [227]. How fibroblasts influence CD8 T cell infiltration and tumor cell death in this transplant model of postpartum breast cancer remains to be determined.

One limitation of our study is that by using PDGFR α positively selected mammary fibroblasts, we may be evaluating a subset of mammary fibroblasts, as other PDGFR α ⁻ fibroblasts have been reported, such as in bone marrow [228]. Further, while we confirmed these PDGFR α ⁺ cells to be largely devoid of epithelial, immune, and endothelial cell type markers, this population likely includes pericytes and perivascular fibroblasts [229, 230]. Another limitation is that we restricted our functional analyses to nulliparous and InvD6 mammary fibroblasts, which does not fully capture the dynamic nature of fibroblasts in the involution window, nor the duration of fibroblast activation. Further, we have not evaluated the phenotype of mammary fibroblasts during pregnancy, another dynamic tissue remodeling window, due to our focus on postpartum breast cancer [9, 10].

With respect to postpartum breast cancer in women, an unanswered question is how the transient event of weaning-induced involution contributes to the poor prognosis of breast cancers diagnosed a full 5-10 years after childbirth. As discussed above, one possible mechanism is the establishment of positive feed-forward loops that persist in the primary tumor microenvironment after completion of postpartum breast involution. An additional unexplored mechanism is that the involution microenvironment stimulates existing indolent tumor cells to disseminate at early stages. The indolent primary tumor and the disseminated tumor cells might then require additional years of evolution to become clinically detectable. Postpartum models that encompass clinically relevant early stage breast disease are required to address these important questions.

Our data suggest the fibroblast as a potential therapeutic target for postpartum breast cancer patients. However, the balance of fibroblast function needs to be carefully considered as it is becoming increasingly clear that fibroblasts exhibit a range of activities from tumor promotional to tumor suppressive, similar to that observed for immune cells [231]. On one side of this functional spectrum, numerous robust studies report the ability of pathologically-activated fibroblasts to support cancer progression [135, 232, 233]. Further, our observation that normal mammary fibroblasts can be tumor promotional, combined with published data showing that senescent fibroblasts associated with natural aging promote breast cancer [234], demonstrate how physiologic states might contribute to pro-tumorigenic fibroblasts. In sum, these pro-tumorigenic fibroblast studies suggest that fibroblast ablation in the tumor microenvironment might have therapeutic merit. However, a recent, paradigm-shifting study showed that depletion of murine pancreatic cancer fibroblasts increased tumor metastasis and decreased survival [235]. Thus, therapies directed at fibroblasts need to be focused on modulating the balance towards tumor suppressive activity rather than ablation, as recently proposed [101].

In summary, we describe a physiologically activated fibroblast with tumor promotional attributes that is present within the involuting mammary gland following weaning. Systemic treatment with Ibuprofen post-weaning reverts this activated and tumor promotional phenotype to baseline, nulliparous levels, identifying fibroblast activation as a target of NSAIDs for the first time. Further, our finding of fibroblast NSAID responsivity raises the interesting hypothesis that the ability of NSAIDs to inhibit breast cancer [67, 236] may comprise targeting the mammary stroma, including fibroblast mediated collagen deposition and immune suppression. Finally, postpartum breast cancer may be uniquely driven by a collagen rich and immune suppressed microenvironment [14, 19, 28], and thus particularly responsive to NSAID intervention; identifying NSAIDs as a treatment strategy warranting further investigation.

- **Method.**

Mouse breeding, reproductive staging and histology. 8-week old female BALB/c mice (Jackson Laboratory) were housed, bred and pup number normalized as described [28], with age matched littermate nulliparous mice for controls. To initiate involution, pups were weaned between 9-13 days of age. Mice were euthanized on designated day of involution and left and right inguinal mammary glands harvested. For histological-based assays, the region of the gland with associated lymph nodes was dissected, fixed in 10% Neutral buffered formalin (Anatech Ltd) for 48h and then processed, paraffin embedded and sectioned at 4 μ m. The confirmation of normal histology was performed by hematoxylin and eosin staining. The lymph node free mammary tissue was either stored in cold Hank's Balanced Salt Solution for flow analysis or snap-frozen in liquid nitrogen and stored at -80°C for RNA and protein analyses. For mice receiving ibuprofen, treatment was initiated at the day of weaning and continued for 6 days of treatment, at which time tissues were harvested. Ibuprofen (Sigma, I7905) was delivered at 150 mg/kg or 300 mg/kg of chow with mice fed ad libitum.

Tissue processing, fluorescence activated cell sorting and tumor model. Mammary glands from Balb/c mice were harvested and processed as previously described [208]. PDGFR α antibody (BioLegend, 135910) was used at 1:25 to stain fibroblasts for FACS. The purity of isolated fibroblasts was >90% as evaluated by flow cytometry using PDGFR α . Sorted fibroblasts were either frozen at -80°C for gene expression analysis or mixed with 20,000 D2A1 cells at a 1:1 ratio in 10 μ l PBS and injected into the left and right fourth mammary glands of Balb/c nulliparous mice (12 weeks old), under isoflurane (Terrell) anesthesia. Tumor length (L) and width (W) were measured twice a week using an electronic caliper. Tumor size was calculated as $L*W*W/2$. Mice were sacrificed at 3.5 weeks post-injection for tissue collection with tumors fixed in 10% Neutral buffered formalin (Anatech Ltd) for 48 hours and then processed, paraffin embedded and sectioned at 4 μ m for staining.

RNA isolation and RT-qPCR analysis. RNA was isolated from sorted fibroblasts (Macherey-Nagel 740955), or floating collagen pads (Invitrogen 10296-028, QIAshredder 79656, Invitrogen 12183-016). To ensure adequate RNA yield, more than 0.1 million FACS isolated PDGFR α ⁺ cells were used for RNA isolation and hence mammary glands were pooled from 5-6 nulliparous mice and 2-3 involution mice (InvD4, 6, 8). RNA concentration and purity were determined by 260 nm, 230 nm and 280 nm absorbance. RNA quality was determined by Agilent 2100 Bioanalyzer. cDNA was synthesized using Bio-Rad cDNA synthesis kit and qPCR was performed using Bio-Rad SYBR Green supermix with MyiQ Single Color Real-Time PCR Detection System. Mouse primer sequences: reference gene β -actin (*Actb*): forward: GCAACGAGCGGTTCCG, reverse: CCCAAGAAGGAAGGCTGGA. *Coll1a1*: forward: TTCTCCTGGCAAAGACGGACT, reverse: AGGAAGCTGAAGTCATAACCG. *Col3a1*:

forward: AGCTTTGTGCAAAGTGGAACC, reverse: CAAGGTGGCTGCATCCCAATT.

Col5a1: forward: TCTCTGTGTGTGTGCCAAGAT, reverse:

AGCCAGAGTCCATCCCACATT. Lysyl oxidase: forward:

CAAGGGACATCGGACTTCTTAC, reverse: TGGCATCAAGCAGGTCATAG. α SMA

(*Acta1*): forward: CCATCATGCGTCTGGACTT, reverse:

GGCAGTAGTCACGAAGGAATAG. *Tgfb1*: forward:

TACGTCAGACATTCGGGAAGCAGT, reverse: AAAGACAGCCACTCAGGCGTATCA.

Mmp2: forward: AGTGGTCCGCGTAAAGTATGGGAA, reverse:

ATTGCCACCCATGGTAAACAAGGC. *Mmp3*: forward:

TGGAACAGTCTTGGCTCATGCCTA, reverse: TGGGTACATCAGAGCTTCAGCCTT.

COX2: forward: GCATTCTTTGCCCAGCACTTCACT, reverse:

TTTAAGTCCACTCCATGGCCCAGT. All primers were purchased from Integrated DNA

Technologies. RT-qPCR conditions were as follows (except for *COX2*): 95 °C for 3 minutes,

then 40 cycles of 95 °C for 15 seconds, 60 °C for 30 seconds and 72 °C for 30 seconds. For

COX2 qPCR, QuantiTect SYBR Green (Qiagen, 204243) was used. The conditions for *COX2*

qPCR were 95 °C for 15 minutes, then 40 cycles of 94 °C for 15 seconds, 55 °C for 30 seconds

and 72 °C for 30 seconds.

RNA-Seq analysis. Total RNA was purified as described above. mRNA isolation and library preparation were performed by the Massively Parallel Sequencing Shared Resource at Oregon Health & Science University, using TruSeq RNA Sample Preparation V2 kit. Four samples were pooled per lane and sequenced on an Illumina HiSeq 2500 with 100 base single-ended reads. The resulting data were converted to FASTQ format using Bcl2Fastq software (Illumina). Reads were

aligned to the mouse reference genome, build GRCm38 using STAR 2.4.2a. STAR performed counting of reads per gene as defined in Ensembl build 81 (GENCODE version m6). Read counts were adjusted to a common non-zero minimum via addition of uniform minor background counts. Read count distributions were normalized across samples using cyclic Loess normalization by R software. Normalized read counts were log₂-transformed for further analysis. Differential expression was determined by fitting linear regression models for each log₂ normalized gene expression level with InvD6 as the independent variable. A Wald test was performed to test the null hypothesis of no association of involution with expression for each gene. Multiple hypothesis-testing was accounted for by controlling the False Discovery Rate (FDR) at 5% with the q-value approach [237]. The final set of significant genes was further filtered to include only genes with absolute value of log₂-fold change greater than 0.4 (1.3-fold). Power analyses were performed via simulations based on the variability of expression and magnitude of fold changes observed in the current data. The analysis methods were assumed to be identical to the methods above. Power analyses were performed under the alternative hypothesis of 500 truly differentially expressed genes with absolute value log₂ fold changes greater than 0.7. Unsupervised clustering was performed on the set of differentially expressed genes to generate a heatmap of normalized expression values, centered and scaled within each gene. Pathway analyses were also performed, and the Hypergeometric Test was performed with Holm adjustment for multiple testing to control the family-wise error rate within an annotation source. This commonly used competitive test examines the odds of finding at least the observed number of significant genes in the pathway while the remainders not in the pathway are greater than expected by chance. The upper tail of the Hypergeometric Test was used to determine whether the number of selected genes also present in a pathway-based gene set is greater than expected by chance. The sets of pathways annotation

sources queried were KEGG, The Broad Institute's Molecular Signatures Database v5, Gene Ontology Biological Process, Gene Ontology Molecular Function, Gene Ontology Cellular Component, Pathway Commons, BioCarta, and Reactome. Analyses and annotations were performed using custom R scripts and Bioconductor the R packages "data.table", "AnnotationDbi", "XML" and "GOdb".

Immunofluorescence. Formalin fixed tissue was paraffin embedded (FFPE) and sectioned at 4 μm . Slides were pre-treated in Target Retrieval Solution, pH 9 (Dako, S2367) at 125°C under pressure for 5 minutes. Tissues were blocked with 0.6% H₂O₂ (diluted in PBS) for 10 minutes, and then treated with protein block (Dako, X0909) for 10 minutes. The staining was performed using Opal™ 3-Plex kit (PerkinElmer). Primary antibodies used: anti-PDGFR α (R&D, AF1062): 1:50 for 2 hours in room temperature (RT), anti-GFP (Vector, BA0702): 1:1000 for 1 hour in RT, anti-calponin (Abcam, ab46794): 1:600 for 16 hours in 4°C, anti- α SMA (Dako, M0851): 1:400 for 30 minutes in RT. Secondary antibodies used: anti-goat (Santa Cruz, SC-2922): 1:100, streptavidin-HRP (DAKO, P0397), anti-rabbit (Thermo, 31461): 1:500, anti-mouse (Dako, K4001). All secondary antibody incubations were for 1 hour at RT.

Immunohistochemistry. Four- μm sections of formalin-fixed, paraffin-embedded mouse mammary glands were used for IHC. Pretreatment: For collagen I, slides were pretreated with Citra buffer (BioGenex HK086) in microwave at 1100 W for 2 minutes. For Ly6C, CD8, and granzyme B, slides were pretreated with Target Retrieval Solution (Dako S1699) at 125 °C under pressure for 5 minutes. Pre-treated slides were then treated with 0.6% H₂O₂ in Methanol (for CD8) or 3% H₂O₂ in methanol (for all other targets) for 10 minutes and then blocked with protein

block (Dako, X0909) for 1 hour. Primary and secondary antibodies used: anti-Collagen I (Abcam ab34710, 1:100), followed by DAKO EnVision+ Peroxidase Rabbit (DAKO, K4003); anti-Ly6C (Abcam, ab15627, 1:1500), followed by Rat-on-Mouse HRP-Polymer (Biocare RT517); anti-CD8 (eBioscience 14-0808-82, 1:50) followed by Histofine Simple Stain anti-Rat; and anti-granzyme B (Abcam, ab4059, 1:300) followed by Histofine Simple Stain anti-Rabbit. All primary antibodies were incubated for 1 hour and secondary antibodies were incubated for 30 minutes, followed by incubation with the chromogen 3,3'-diaminobenzidine (Dako, K346811) for 10 minutes and counterstained in hematoxylin for 6 minutes. For TUNEL staining, the TACS 2 TdT-DAB In Situ Apoptosis Detection Kit (from Trevigen) was used with Mn^{2+} cation at a final concentration of 1x as per the manufacturer's instructions. Protocol and antibody information for data in supplemental figures are in supplemental methods section. After staining, slides were scanned by Aperio ScanScope AT, and IHC signal quantification performed by Aperio ImageScope v12.1.0.5029 as described previously [14]. Tumor border was defined as 100 μm from the tumor edge for Ly6C quantification study.

Cell culture: The mouse tumor cell line D2A1, a gift from Ann Chambers (London Regional Cancer Program, London Health Sciences Centre), was obtained from Jeffrey E. Green (Laboratory of Cell Biology and Genetics, National Cancer Institute). D2A1 cells were cultured on tissue culture plastic in DMEM medium (HyClone, SH30022.01) supplemented with 10% FBS (HyClone, SH30071.03) and 1x Penicillin-Streptomycin Solution (Corning, 30-002-CI). D2A1 cells were cultured for 48 hours before mammary fat pad injection. Primary mouse mammary fibroblasts were acquired by first plating nulliparous mouse mammary gland digest (2.5 mg/ml collagenase II and IV Worthington, 37 °C for 30 minutes) on tissue culture plastic or on

Polydimethylsiloxane (SYLGARD, 184 SILICONE ELASTOMER KIT) coated plastic, and supplied with DMEM-F12 medium (HyClone, SH30023.01) and 10% FBS [213]. Under long term culture, after 9 days, fibroblasts were highly enriched. These fibroblasts were passaged three times to expand the population before freezing in liquid nitrogen. For fibroblast collagen floating pad cultures, frozen fibroblasts were thawed and plated on Polydimethylsiloxane coated plates supplied with DMEM-F12 medium and 10% FBS for 48 hours, and then changed to DMEM-F12 medium with 1% FBS and 200uM ascorbic acid (Sigma, A0278) and 1x Penicillin-Streptomycin (fibroblast base medium) for 4-6 days until cells reached 80% confluency. Fibroblasts were then mixed with 2 mg/ml collagen I (Corning, 354249) and plated in a 96-well plate, at a concentration of 20,000 cells per 50 μ l collagen pad. Collagen pads were supplied with fibroblast base medium with the following additives: 0.5 ng/ml or 5 ng/ml TGF β 1 (eBioscience, 14-8342-62), 10 μ g/ml or 30 μ g/ml Ibuprofen (Sigma, I7905), 1 ng/ml or 5 ng/ml PGE2 (Sigma, P6532). After 18 hours in culture, collagen pads were disassociated from the 96-well plate and put in a 12-well plate. After another 30 hours, pictures were taken and pad diameter measured by Aperio ImageScope and then 3-5 pads of the same condition were pooled for RNA isolation.

Monocyte derived cells. Monocyte derived cells were generated according to previous publications [238, 239]. Briefly, bone marrow cells were isolated from femurs and tibias of 10 week old female Balb/c mice, plated in 6 cm petri dish at 10 million cells/plate and cultured in RPMI medium (HyClone, SH30096.01) supplied with 5% FBS (HyClone, SH30071.03), 1x Penicillin/streptomycin (Corning, 30-002-CI) and 30% conditioned medium from the supernatants of M-CSF-secreting L929 fibroblasts [240], a gift from Peter Henson (National Jewish Health). After 48 hours of cell-plating and the plates washed gently twice with PBS to eliminate dead cells,

and then fresh medium with 10ng/ml of mouse recombinant IL4 (PeproTech, 214-14) was added. After 24 hours, monocyte derived cells were harvested by gently pipetting to collect only the loosely adhered cells, as previously described [238]. Using this protocol and as determined by flow analysis (Supplemental figure 7) we obtained a mixture of Ly6C⁺ monocytes (30%), macrophages (25%) and immature precursors (45%) [241]. We refer this cell population as monocyte derived cells. Detailed methods are provided in the supplemental methods section.

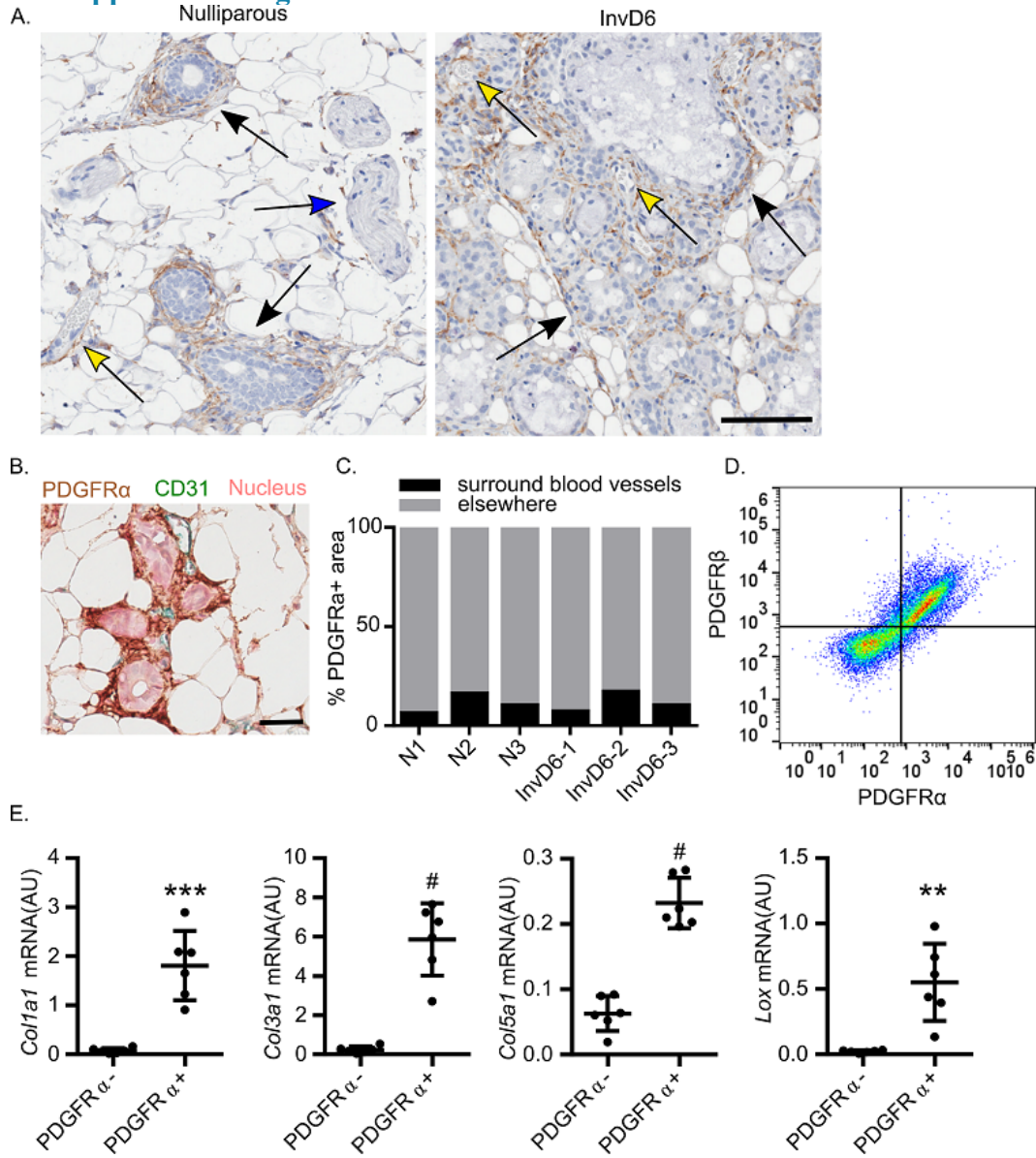
Monocyte derived cell migration assay. Fibroblast collagen pad culture was described above. 1.6×10^4 fibroblasts were mixed in 40 μ l of 2 mg/ml collagen and plated on a transwell insert with pore size of 5 μ m (Millipore, MCMP24H48), then placed inverted in a 12-well plate, and allowed to solidify for 1 hour in 37 °C incubator. The inserts were placed in 24-well plate right side up, supplied with fibroblast base medium, with addition of 1 ng/ml PGE₂, 1 μ g/ml CXCL12 neutralizing antibody (R&D, MAB310), and/or 1 μ g/ml mouse IgG1 isotype control (R&D, MAB002) and cultured for 24 hours prior to the addition of monocyte derived cells. The monocyte derived cells were generated as described above and labeled with CellTrace™ CFSE (Invitrogen, C34554) at a concentration of 1.25 μ M in PBS for 20 minutes at RT, and then 7.5×10^4 cells were plated on top of each insert. Medium was changed immediately after plating monocyte derived cells, using the same medium described above for fibroblasts but with the addition of 1% L929 conditioned medium in all conditions. After 15 hours, the cultures were fixed in Cytifix fixation buffer (BD, 554655) for 20 minutes. The number of fluorescently labelled monocytes that migrated to the bottom of the filter was detected using a Nikon Eclipse TE200 fluorescence microscope. Firstly, monocyte derived cells were visualized to assure monocyte plating at the same confluency across conditions. After removal of cells on the top of the insert by cotton swab,

4-5 pictures at 4x were taken for each insert to detect migrated cells. Images were processed by Image J software. Briefly, fluorescence intensity was measured by Image J and the fluorescence threshold was adjusted by mean intensity + 2 fold standard deviation. For images with high background, fluorescence threshold was adjusted by mean intensity + 3 fold standard deviation. Cell number was counted by Image J “Analyze particles” function. For images with severe background, cell numbers were counted by hand, with data independently verified under conditions where reader was blinded to study design. The same cell counting methods were used across groups in each experiment.

Statistical Analyses. Unpaired two-tailed *t*-test and One-Way ANOVA with Tukey correction were performed in GraphPad Prism, assuming independent samples and normal distributions. Only p values less than 0.05 were considered significant. Statistical analysis for the RNA seq data set is described above.

Study Approval. Animal procedures were approved with ethical consideration by the University of Colorado Anschutz Medical Campus and Oregon Health & Science University Institutional Animal Care and Use Committees.

• **Supplemental Figures.**



Supplemental figure 1. PDGFRα is expressed dominantly by stromal cells surrounding mammary ducts and alveoli.

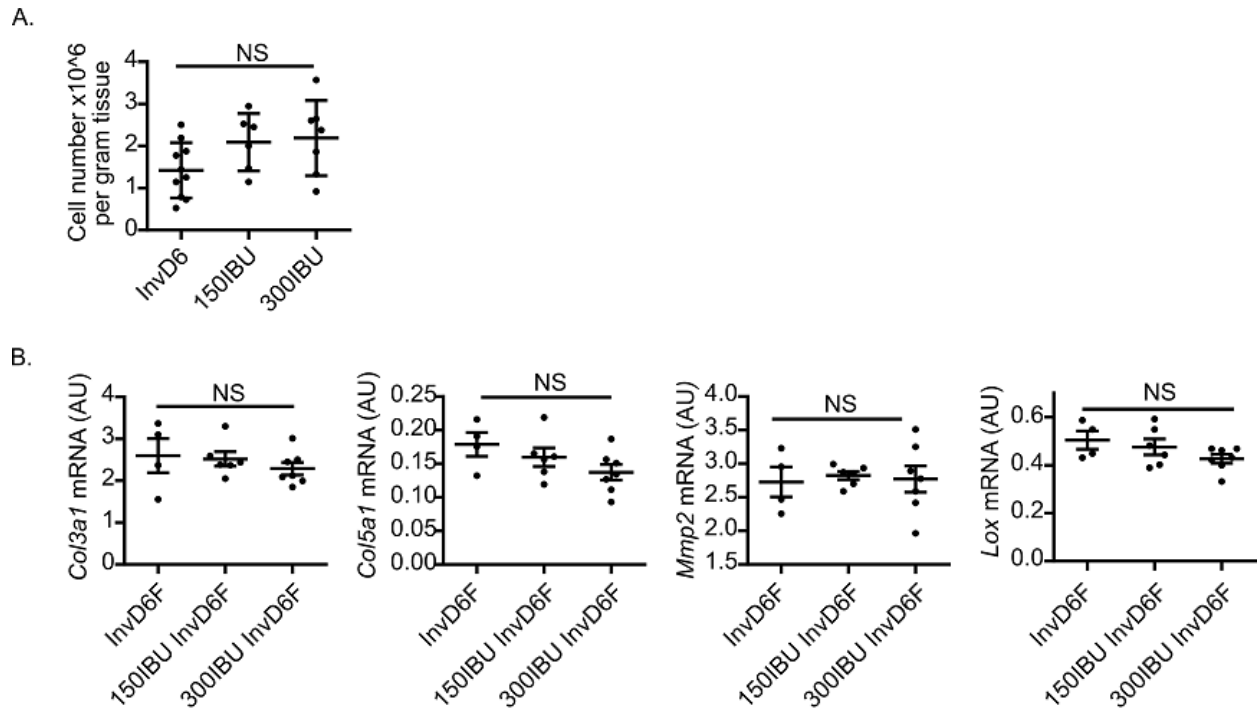
A) IHC staining of PDGFRα in nulliparous (left panel) and InvD6 mouse mammary glands (right panel). Black arrows: mammary ductal and alveolar structures; blue arrow: muscle; yellow arrows: blood vessel.

B) Co-staining for PDGFRα (brown) and CD31 (green) in nulliparous Balb/c mammary gland shows lack of dual positive cells. Counterstain: pink. Scale bar: 30 μm.

C) Quantification of PDGFRα positive area surround CD31⁺ blood vessels (black) or elsewhere (gray) in three mammary glands from nulliparous mice (N 1-3) and three InvD6 mammary glands (InvD6 1-3).

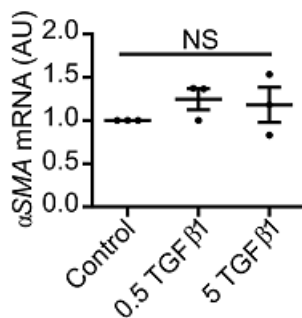
D) Flow cytometry for PDGFRα and PDGFRβ in nulliparous mouse mammary glands reveals significant dual positivity.

E) RT-qPCR for *Colla1*, *Col3a1*, *Col5a1* and *LOX* gene expression in sorted PDGFRα⁺ and PDGFRα⁻ cells. N=6. Scale bar: 100 μm. **P<0.01, ***P<0.001, #P<0.0001.



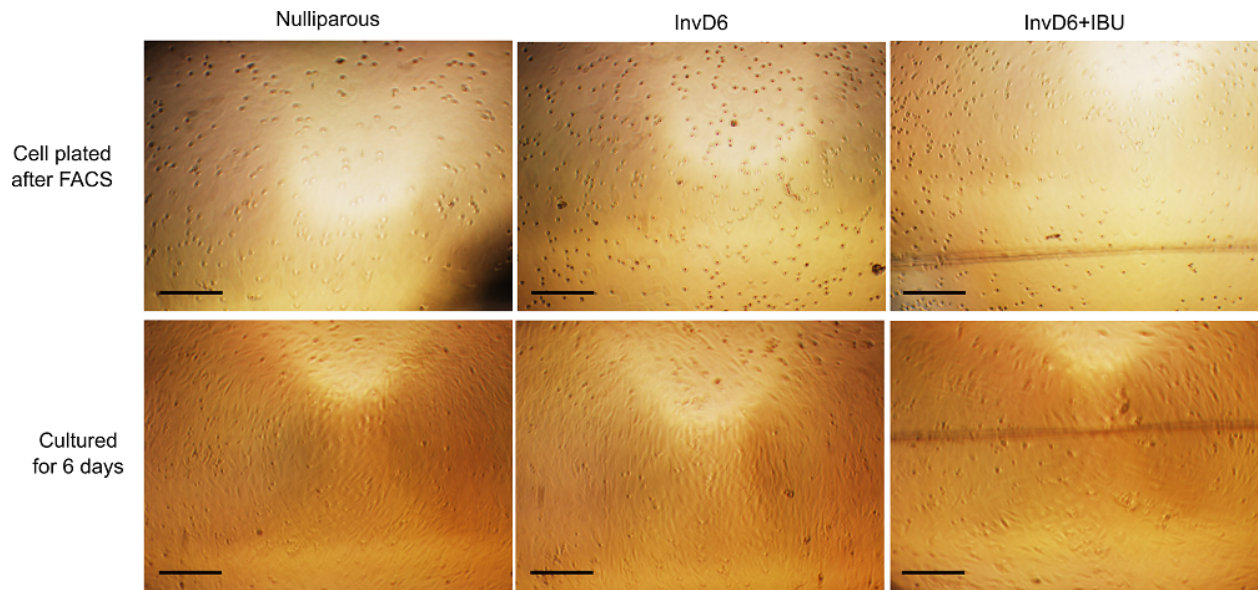
Supplemental figure 2. Effects of ibuprofen treatment on PDGFR α ⁺ cells in the InvD6 mammary gland.

A) PDGFR α ⁺ cell number per gram mammary gland tissue quantitated by FACS analysis, in the absence or presence of two doses of ibuprofen treatment (150IBU: 150 mg/kg and 300IBU: 300 mg/kg Ibuprofen in diet) for 6 days following weaning. N=6. **B)** RT-qPCR of *Col3a1*, *Col5a1*, *Lox* and *MMP2* gene expression in InvD6 fibroblasts in the absence or presence of ibuprofen. N=4-7. NS: not significant.



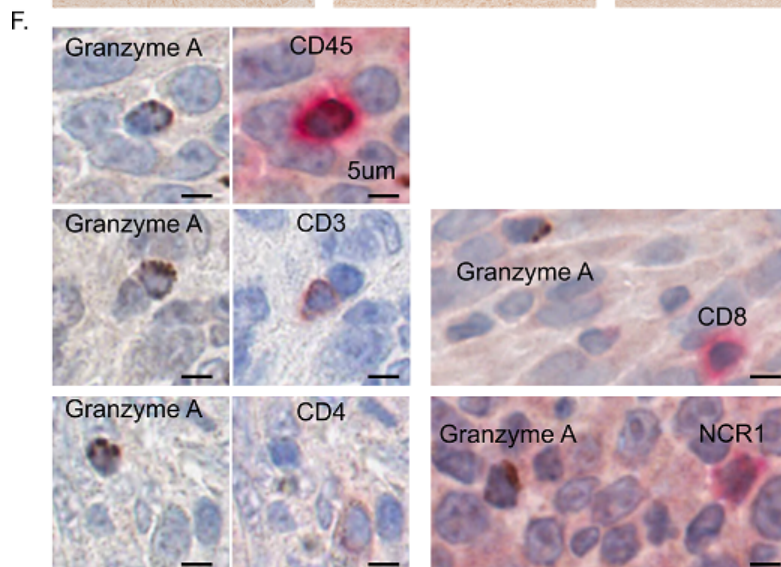
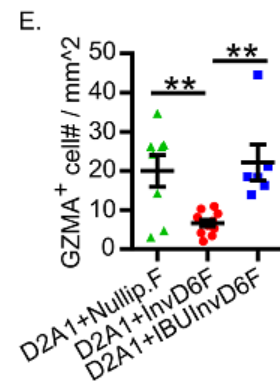
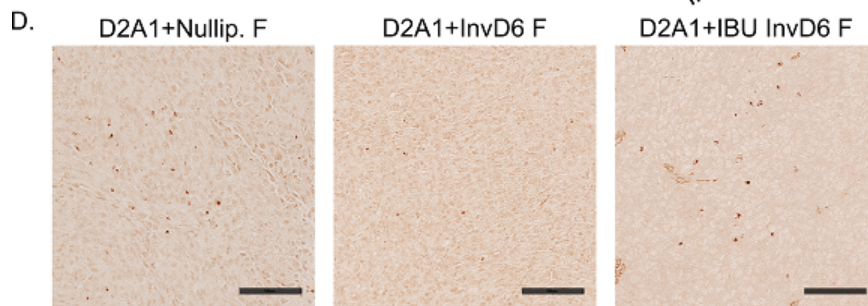
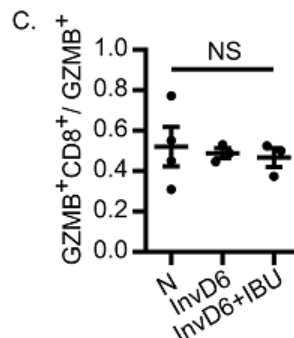
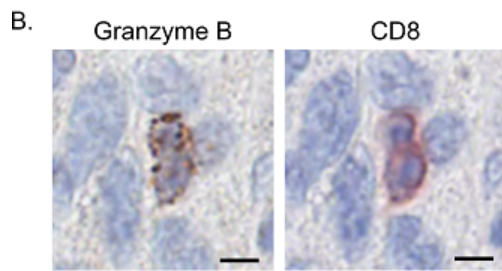
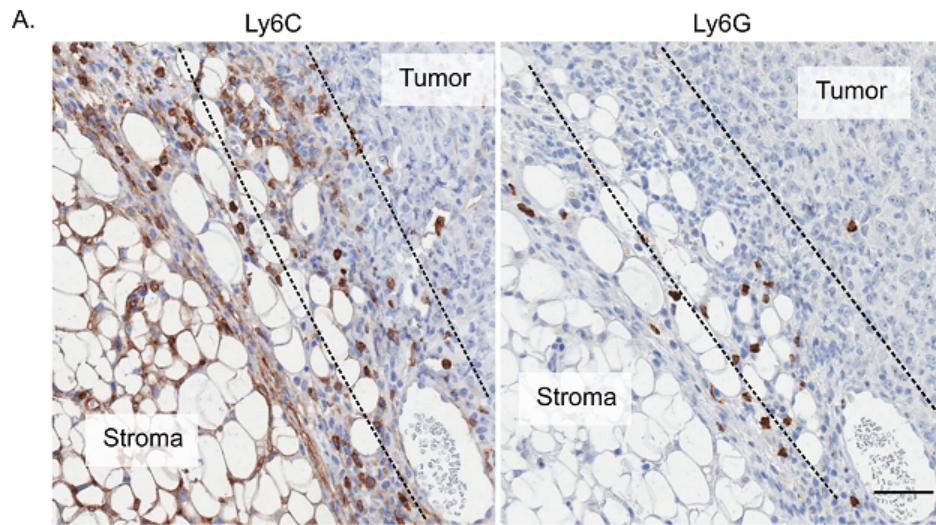
Supplemental figure 3. TGF β 1 does not induce fibroblast α SMA expression in floating collagen cultures.

RT-qPCR of *α SMA* in primary mammary fibroblasts without (Control) or with the treatment of 0.5 ng/ml TGF β 1 (0.5 TGF β 1) and 5 ng/ml TGF β 1 (5 TGF β 1). N=3. NS: not significant.



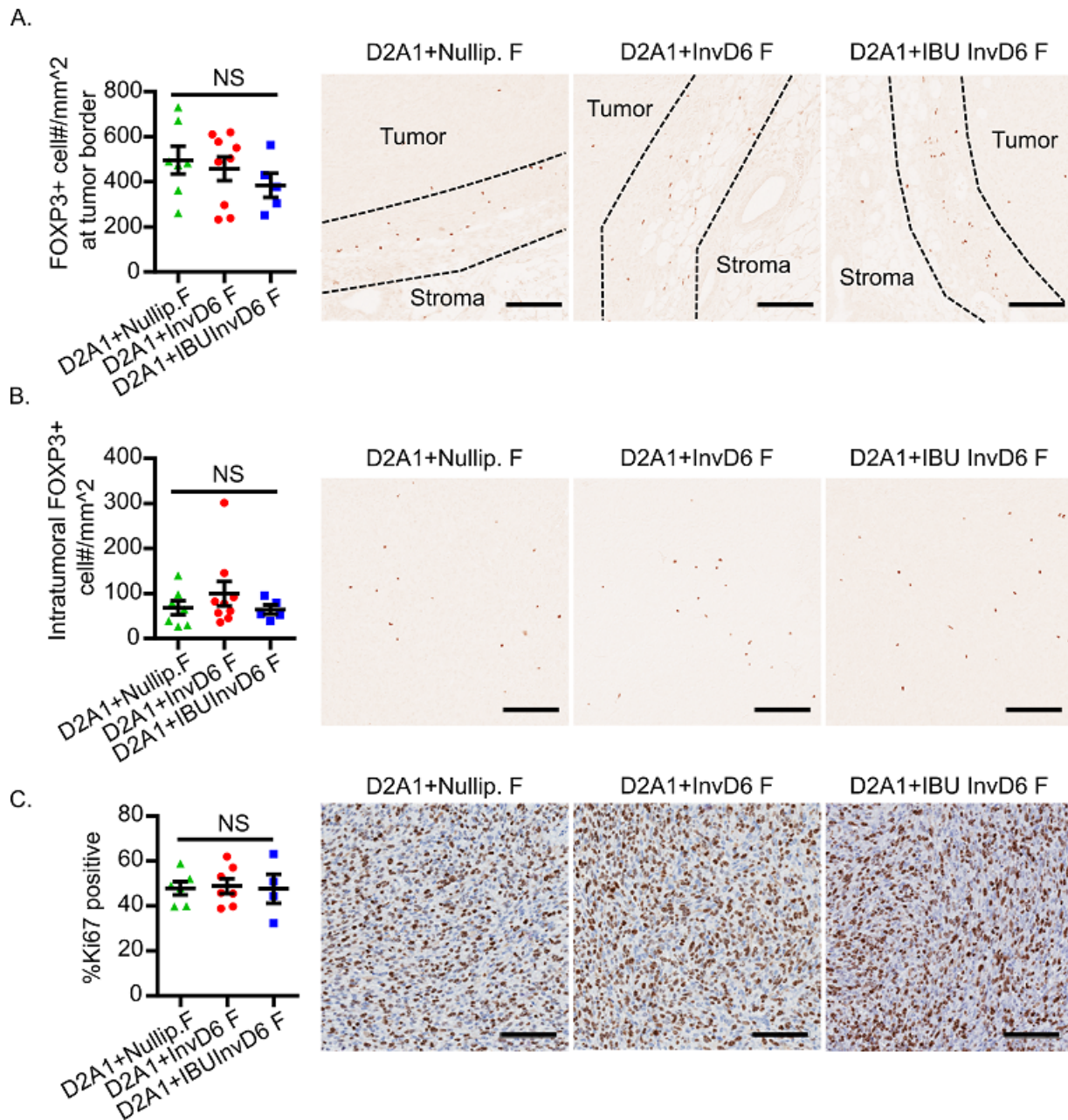
Supplemental figure 4. Fibroblast ex vivo adhesion and cell culture survival are independent of reproductive state.

Top panel: Sorted PDGFR α^+ mammary fibroblasts used in the D2A1 tumor cell co-injection experiments and plated at equal concentration. Bottom panel: cells in the top panel after 6 days of culture. Scale bar: 100 μ m.



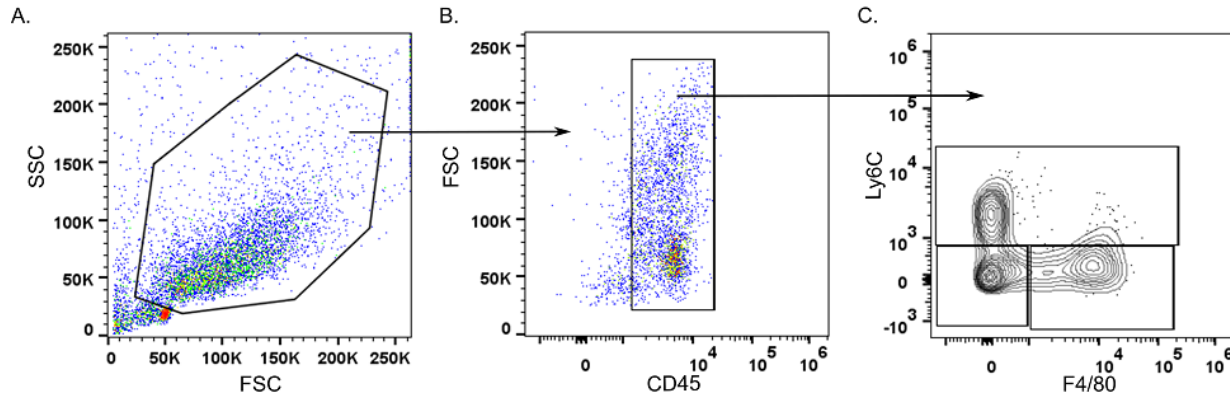
Supplemental figure 5. Immunohistochemical characterization of tumor infiltrating immune cells.

A) Ly6C and Ly6G staining in serial sections of representative D2A1+ InvD6 F tumor. Dashed lines show tumor border. Scale bar: 50 μm . **B)** IHC staining of granzyme B (left panel) and CD8 (right panel) of the same tumor section. **C)** Quantification the percentage of granzyme B⁺ cells that are CD8⁺. **D)** Representative images of granzyme A⁺ cells within tumors from each group. Scale bar: 100 μm . **E)** Quantification of IHC staining for intratumoral granzyme A⁺ cells by group. **F)** IHC co-staining for granzyme A and immune cell markers CD45, CD3, CD8, CD4, and NCR1, as indicated by labels. Scale bar: 5 μm .



Supplemental figure 6. FOXP3 and Ki67 IHC tumor analyses demonstrate no differences between fibroblast groups.

A) Left panel: Quantification of FOXP3⁺ cells at the tumor border. Right Panel: representative images of FOXP3⁺ cells at the tumor border. Scale bar: 100 μm . **B)** Left panel: Quantification of intratumoral FOXP3⁺ cells. Right Panel: representative images of intratumoral FOXP3⁺ cells. Scale bar: 100 μm . Counterstaining is not shown in A) and B) to enhance visualization of positive cells. **C)** Left panel: Quantification of Ki67⁺ cells in tumor. Right Panel: representative images of Ki67⁺ cells. Scale bar: 20 μm .



Supplemental figure 7. Characterization of monocyte derived cells by flow cytometry. A) Cells are gated by forward scatter and side scatter.

B) Immune cells are further gated by CD45 and forward scatter. C) CD45⁺ cells are further gated by F4/80 and Ly6C. Three populations are indicated. Monocyte: Ly6C⁺F4/80⁻. Macrophages: Ly6C⁻F4/80⁺. Immature myeloid progenitor cells: Ly6C⁻F480⁻

- **Supplemental method.**

Immunohistochemistry. 4 μm sections of formalin-fixed, paraffin-embedded mouse mammary glands were used for IHC. Slides were pretreated with Target Retrieval Solution (Dako S1699 or DAKO S2367). Then, slides were treated with 3% H₂O₂ in Methanol for 10 minutes, followed by protein block (Dako, X0909) for 1 hour. Primary and secondary antibody information are as follows:

| Targets | Primary Antibody vendor and catalog # | Dilution | Secondary antibody vendor and catalog # | Dilution | Chromogen and color |
|----------------|---------------------------------------|----------|---|----------|----------------------------|
| PDGFR α | R&D, AF1062 | 1:300 | Santa Cruz, SC2922 | 1:100 | DAKO, K3468, brown |
| CD31 | Abcam, ab28364 | 1:100 | ThermoFisher, 31461 | 1:100 | Bio SB, BSB0129, green |
| Ly6G | BD Biosciences, 551459 | 1:1000 | Biocare, RT517H | N/A | DAKO, K3468, brown |
| Granzyme A | Santa Cruz, SC5515 | 1:100 | Santa Cruz, SC2922 | 1:100 | DAKO, K3468, brown |
| CD45 | BD pharmingen, 550539 | 1:400 | Santa cruz, SC2021 | 1:100 | Biocare, WR806, red |
| CD3 | Abcam ab16669 | 1:100 | Histofine, Simple Stain, anti-rabbit | N/A | Vector, SK-4200, brick red |
| CD4 | eBioscience, 14-9766-82 | 1:100 | Histofine, Simple Stain, anti-rat | N/A | Vector, SK-4200, brick red |

| | | | | | |
|-------|-------------------------|-------|--------------------------------------|-------|---------------------|
| NCR1 | Abcam ab199128 | 1:50 | Histofine, Simple Stain, anti-rabbit | N/A | Biocare, WR806, red |
| FOXP3 | eBioscience, 14-5773-82 | 1:100 | Biocare, RT517H | N/A | DAKO, K3468, brown |
| Ki67 | Neo-markers, RM9106s | 1:100 | ThermoFisher, 31461 | 1:100 | DAKO, K3468, brown |

All primary antibodies were incubated for 1 hour at room temperature, and secondary antibodies were incubated for 30 minutes in room temperature. For dual co-staining slides, three methods were used based on the primary antibodies combination. Method-1: a combination of DAB (DAKO K3468, brown) with Warp Red (Biocare, WR806, red). Method-2: a combination of DAB (DAKO K3468, brown) with PolyDetector HRP Green kit (Bio SB, BSB0129, green). Method-3: AEC (Vector SK-4200) was used with antigen retrieval (BioGenex HK086) between each staining targets. For PDGFR α and CD31 dual staining, tissues were counterstained with Nuclear Fast Red (American MasterTech, STNFRPT) for 1 minutes. For other staining, tissues were counterstained with hematoxylin (DAKO, S3301) for 6 minutes.

Flow cytometry. 1×10^6 cells per sample were blocked with CD16/32 (eBioscience, 14-0161-81) for 30 minutes and cell surface markers were stained for 20 minutes. PDGFR α (BioLegend, 135910): 1:100 dilution, PDGFR β (BioLegend, 136007): 1:100 dilution, CD45 (eBioscience, 25-0451-82): 1:800 dilution, Ly6C (BioLegend, 128012): 1:400 dilution, F4/80 (BioLegend, 123108): 1:200 dilution. Cells were stained for 20 minutes. Experiments were performed on an LSRFortessa (BD Biosciences; Oregon Health and Science University Flow Cytometry Shared Resource) and analysis was performed using FlowJo (FlowJo, LLC Data Analysis Software, Ashland, OR).

CHAPTER IV. DISCUSSION AND FUTURE DIRECTIONS.

- **Summary of key findings.**

My graduate studies have focused on the characterization of mammary collagen remodeling and fibroblast activation under physiologic conditions. My focus has been on weaning-induced mammary gland involution, as involution promotes breast cancer progression, and collagen remodeling and fibroblast activation are implicated as potential mediators. In this thesis, I have characterized fibrillar collagen deposition and structural remodeling during weaning-induced involution using a variety of tools including RT-qPCR, SHG and trichrome staining. We found increased collagen abundance in the mammary lobular structures during weaning-induced involution in both rat mammary and human breast tissue. Fibrillar collagen, a structural protein that supports ductal and lobular structures in the gland, was not anticipated to increase during involution, since the major event during involution is clearance of the milk-secreting mammary lobules resulting in ~80% loss of mammary epithelium. Thus, one hypothesized mechanism to account for increased collagen abundance post-weaning is that the shrinkage of the mammary gland during involution concentrates this stable protein – collagen, into a smaller volume, resulting in a visually increased abundance. However, my collagen gene expression data, obtained from mammary tissues at distinct reproductive stages, do not support this hypothesis. All three of the major types of fibrillar collagen in the mammary glands, including collagen I, III and V, display increased gene expression during involution. Further, increased gene expression was found in the major non-fibrillar collagen genes too. These data suggest de novo collagen production in the mammary gland during involution, indicative of active stromal remodeling concurrent with epithelial cell death. The structure of collagen fibrils was also altered during involution, with more straight and tightly bundled collagen fibers and an increased percentage of collagen fibers being perpendicular to the mammary epithelial cells as compared to lactating or nulliparous glands.

These changes in collagen structure are consistent with a tumor-associated collagen signature, referred to as TACS3, that associate with decreased survival in breast cancer patients. The observed collagen structural remodeling of increased fiber linearity and perpendicular alignment to the ductal epithelium can be executed by many factors. A dominant mediator is the collagen crosslinking enzyme LOX, whose gene and protein expression were also increased during involution compared to lactation and nulliparous stages.

Mammary collagen deposition and structural remodeling during involution indicates the activation of fibroblasts, a cell type largely defined by collagen production and organization. However, the cell type responsible for collagen deposition within the mammary gland had not been definitively identified, and further, there are no exclusive markers for fibroblasts that are not also expressed by other cell types. Although there are biologically-imposed limitations in our approach of isolating mammary fibroblasts, we sought to isolate fibroblasts from the mammary gland to determine phenotypic changes of mammary fibroblasts during involution using PDGFR α as a positive section marker. PDGFR α had been previously found to be a relatively specific marker for fibroblasts in the mouse mammary gland and mammary tumors. By IHC, PDGFR α cells were found surrounding mammary ducts, alveoli, and blood vessels, and embedded within the fat pad. The PDGFR α ⁺ cells surrounding blood vessels were considered as perivascular fibroblasts. Perivascular fibroblasts share similar markers with stroma fibroblasts, so it is hard to optimize the isolation protocol to remove the contaminating perivascular fibroblasts. We confirmed that PDGFR α cells express collagen 1 by utilizing mammary tissue from the collagen 1a1 reporter mouse, where GFP is driven by the Col1a1 promoter. IHC staining of GFP and PDGFR α in the transgenic mouse mammary gland showed colocalization of GFP and PDGFR α . Quantification confirmed that 85-90% of these cells were found surrounding mammary ducts and alveoli with the perivascular fibroblasts

counting for only 10-15% of the total PDGFR α + cell population. Further, similar percentages of perivascular fibroblasts were found in both nulliparous and involution stages, suggesting PDGFR α can be used as a reliable marker to isolate mammary fibroblasts.

FACS was used to isolate mammary fibroblasts from nulliparous, involution day 4, 6, and 8 hosts. We did not perform fibroblast FACS isolation in the lactating gland, as the large amount of milk in the gland negatively influences the FACS procedure. However, fibroblasts in the lactating gland should serve as a better control compared to nulliparous for studying the functional shift of mammary fibroblasts during involution, as collagen level during lactation is very low.

RT-qPCR was performed to detect collagen gene expression in mammary fibroblasts isolated from different reproductive stages. Firstly, we found a ~2-fold increased number of fibroblasts in the involution day 6 and 8 groups, compared with the nulliparous group, which potentially contributes to the increased collagen deposition observed during involution. What's more, increased gene expression of the three types of major fibrillar collagen was found specifically in the involution-fibroblasts. Besides increased fibrillar collagen expression, the involution-fibroblasts also had increased gene expression of TGF β , MMP2, MMP3, and CXCL12. RNA-seq analysis was performed to further characterize involution stage mammary fibroblasts. Pathway analysis of the RNA-seq data comparing nulliparous-fibroblast and InvD6-fibroblasts showed InvD6-fibroblasts are enriched for ECM deposition, ECM remodeling, and immune related pathways, suggesting fibroblasts activation during weaning-induced involution and a critical role of fibroblasts in modifying the involution microenvironment. It is worth mentioning that although involution-fibroblasts had significantly increased ECM and cytokine gene expression, involution-fibroblasts were not α -SMA positive, providing evidence of a unique activation status of the involution-fibroblasts compared to classically activated fibroblasts in the wound healing setting.

The increased ECM and immune modulation pathways in the involution-fibroblasts are consistent with a tumor promotional phenotype. To directly test the effect of involution fibroblasts on tumor promotion, D2A1 tumor cells were co-injected with FACS isolated mammary fibroblasts from nulliparous and involution day 6 stages. Increased tumor growth was found in D2A1 cells co-injected with InvD6-fibroblasts compared with nulliparous-fibroblasts in the absence of changes in Ki67 staining. Further characterization of the tumors from this study showed decreased tumor cell death in the InvD6-fibroblast group. These data together with increased abundance of peritumoral Ly6C⁺ monocytes and decreased abundance of intratumoral CD8 T cells, suggest that InvD6-fibroblasts may recruit monocytes to the tumor, which then inhibit CD8 T cell cytotoxic functions, allowing for the observed enhanced tumor growth. Somewhat surprisingly, no differences in collagen abundance were detected in the end-stage tumors. It is possible we missed the window of detecting collagen differences by only analyzing end-stage tumors, which could be addressed in future studies.

Consistent with the reported function of NSAIDs in reducing collagen density during involution, we found that 6 days of ibuprofen treatment during involution reduced fibroblasts (IBU-involution-fibroblasts) expression of *Colla1*. What's more, the IBU-involution-fibroblasts had decreased TGF β 1, MMP3 and CXCL12 expression. More importantly, tumor co-injection studies with IBU-involution-fibroblasts showed that ibuprofen treatment decreased the tumor promotional capacity of involution-fibroblasts. The tumor growth curves of D2A1 cells co-injected with nulliparous-fibroblasts and with IBU-involution-fibroblasts were indistinguishable, indicating that ibuprofen treatment during the first 6 days of weaning-induced involution completely reversed the tumor promotional attributes of involution fibroblasts. A signature of relatively low peritumoral monocytes, high intratumoral CD8 T cells, and high tumor cell death was found in the tumors co-

injected with IBU-involution-fibroblasts. These data suggest that involution-fibroblasts can modify the tumor immune microenvironment, potentially by recruitment of immunosuppressive monocytes and T cell inhibition. Further, the immune regulation function of involution-fibroblasts can be targeted by ibuprofen treatment, which reverses their activation status and tumor supportive capabilities back to nulliparous levels. However, the mechanism of ibuprofen induced fibroblasts suppression is unknown. To test if ibuprofen can directly inhibit mammary fibroblast activation, we moved to an in vitro culture model. Fibroblasts are mechanically sensitive cells, and they can easily be activated by simply culturing on stiff plastic plates. To maintain fibroblasts in a relatively quiescent stage, so that we could experimentally manipulate their activation, we cultured primary mammary fibroblasts by embedding fibroblasts in floating mechanically soft collagen pads. TGF β 1 was used to induce fibroblast activation to mimic the presumed conditions of involution. Consistent with previously published data, TGF β 1 treatment induced fibroblasts activation, which was indicated by enlarged cell size with visual appearance of stress fibers, increased contractility, and enhanced collagen, COX2, and TGF β 1 gene expression. Ibuprofen treatment compromised TGF β 1 induced fibroblast activation, suggesting the COX enzymatic pathway, and presumably downstream products are necessary for fibroblast activation. To directly test this hypothesis, we treated fibroblasts with PGE2, which is a product of the COX pathway known to be upregulated in the involuting mammary gland, and which has been shown to have important roles in immune suppression and cancer progression. Treatment of fibroblasts with PGE2 in our cell culture model resulted in increased collagen I and CXCL12 gene expression, but did not induce morphological changes associated with activation (listed above). These data indicate both TGF β and COX pathways are potentially involved in fibroblasts activation during weaning-induced mammary gland involution.

The immune modulation function of involution-fibroblasts was supported by RNA-seq data and tumor characterization from the fibroblast and D2A1 tumor cell co-injection studies. Increased peritumoral monocytes in the involution-fibroblast co-injection group suggest the potential role of involution-fibroblast in monocyte recruitment. To test this, we performed a modified cell migration assay, where bone marrow derived monocytes were cultured on top of a transwell filter, with fibroblasts embedded in a collagen pad on the other side of the filter. Treatment of fibroblasts with PGE2 induced monocyte migration towards fibroblasts, and CXCL12 antibodies blocked the migratory effect. These data suggest that the increased monocyte recruitment capacity of involution-fibroblasts is potentially mediated by CXCL12, providing a therapeutic target for PPBC treatment.

In summary, I found increased collagen deposition, and structural reorganization during involution, which share similarities with tumor-associated collagen, indicating reproductive history as a potential modifiable factor in contributing breast density and breast cancer risk. I also found that mammary fibroblasts are uniquely activated during involution and significantly contribute to collagen remodeling and immune modulation, which together, help create the involution microenvironment that is supportive of tumor progression. Further, I also found that ibuprofen treatment inhibits involution-fibroblast activation and decreases their tumor promotional capacity. This finding supports the potential usage of ibuprofen in the preventive and therapeutic treatment of postpartum breast cancer.

- **Future perspectives and new questions.**

- Understand the immune modulation function of fibroblasts during involution.

I started my thesis work by characterizing mammary collagen in nulliparous and involuting hosts, and then turned my focus to the role of mammary fibroblasts, and determined they are the primary

collagen producing cells in the mammary gland. In further investigations of the tumor promotional function of involution-fibroblasts, we found another key component of fibroblast function, which is immune modulation. Specifically, I found the tumors formed by coinjection of D2A1 cells with involution-fibroblast had increased peritumoral monocytes infiltration and decreased intratumoral CD8 T cells. This immune cell signature suggests a role of involution-fibroblasts in immunosuppression leading to CD8 T cell suppression and tumor cell survival. Prior to my work, immune modulatory function in fibroblasts had been reported in a few recent reports on CAFs [101, 205, 235]. Here, we show for possibly the first time that physiologically activated fibroblasts modulate immune function in a manner consistent with tumor outcome.

The RNA-seq data on nulliparous- and involution-fibroblasts provide further support of the critical role of fibroblasts in immune modulation during weaning-induced involution. Analysis of RNA-seq data shows that mammary fibroblasts express a variety of cytokines and chemokines, including interleukins, C-X-C motif chemokine ligands and chemokine (C-C motif) ligands (Figure 4-1). Importantly, compared with nulliparous-fibroblasts, involution-fibroblasts have increased overall gene expression of various cytokines and chemokines, suggesting fibroblasts contribute to remodeling of the immune microenvironment during weaning-induced involution. Of note, involution-fibroblasts were found to highly-express the cytokines IL-6 and IL-33, which have been reported to be associated with suppressed Th1 response [242, 243]. These data further support the conclusion that fibroblasts contribute to the immunosuppressive microenvironment in the involuting mammary gland. Further, fibroblasts not only express cytokines, but also express a variety of cytokine receptors, suggesting that fibroblasts also can sense and respond to the immune microenvironment. The biological function of the cytokines and chemokines expressed by

involution fibroblast can be tested by fibroblast specific knockdown of those factors such as IL-33 and CXCL12, to investigate the influence to the mammary microenvironment during involution. Other important cytokines that fibroblasts can secrete and respond to are TGF β family members, including TGF β 1, TGF β 2, and TGF β 3. The *in vitro* culture studies of fibroblasts in my thesis suggest a role for TGF β in fibroblasts activation and ECM production during weaning-induced involution. In addition to being activated by TGF β , our *in vitro* studies suggest that involution fibroblasts may also contribute to the production of TGF β . Consistent with this observation, my data show that fibroblasts isolated from the involuting gland have increased *Tgfb1* gene expression compared with nulliparous-fibroblasts (Figure 3-1 H, and Figure 4-2 B). A 20% increase in *Tgfb3* expression was also found in involution-fibroblasts, whereas *Tgfb2* levels did not differ between nulliparous- and involution-fibroblasts (Figure 4-2 B), suggesting biological regulation of different TGF β isoforms in the involution fibroblasts. A fibroblast specific TGF β knockout mouse model can be used to test the function of fibroblast derived TGF β isoforms during weaning-induced involution.

TGF β has roles in regulating many biological processes that occur during involution. As mentioned in chapter I, TGF β has been shown to be one of the key mediators of epithelial cell death at the onsite of involution, with delayed cell death observed in TGF β 1 KO mice. Moreover, TGF β is potentially involved in inducing the clearance of apoptotic cells by phagocytic MECs, and dampening the proinflammatory response of the tissue to major cell death during involution [38]. TGF β has important roles in suppressing destructive immune activation in both the lymphoid and myeloid branches of immunity. TGF β is known to directly impair mature T cell proliferation, and induces differentiation of regulatory T cells (Tregs) [244], which actively impair the actions of cytotoxic T cells. In the myeloid branch of immunity, TGF β stimulates chemotaxis of immature

monocytes [245] and polarizes immature myeloid cells to an “M2” macrophage phenotype [246-248], which are known to produce the cytokines IL-4 and IL-13 [249]. These cytokines then further polarize the tissue microenvironment by driving differentiation of naïve T cells to a T helper 2 (Th2) differentiated state*. Given that fibroblasts may be putative producers of TGFβ during involution, this is another indicator of the involvement of involution-fibroblasts in mediating immunosuppression.

Based on flow cytometry data, involution day 6 is the peak of enhanced abundance of many types of immune cells during involution including macrophages, monocytes, CD4 and CD8 T cells. Coincidentally, the rapid increase in fibroblast number during involution is between day 4 and day 6, which suggests a potential cross-talk between immune cells and fibroblasts. The high levels of chemokines expressed by fibroblasts (Figure 4-2 C) suggests a potential function in immune cells recruitment. In the RNA-seq data, CXCL12 is the highest expressed chemokine by fibroblasts. The potential function of CXCL12 during involution is described in the monocytes migration assay in chapter III, which suggests CXCL12 is involved in fibroblast induced monocyte recruitment during involution. Another highly expressed chemokine that is known to enhance monocyte recruitment is CCL2 (Figure 4-2 C). Increased levels of CCL2 mRNA in the involution-fibroblasts suggests another potential mechanism of monocyte recruitment by fibroblasts. Further investigation is warranted in finding the critical cytokines and chemokines produced by involution-fibroblasts in inducing immune cell infiltration and immune modulation. It can potentially be performed by using fibroblast specific cytokine or chemokine knockout models, and test if fibroblasts have decreased immune cell recruitment function. These studies will shed light on the role of fibroblasts in regulation of the immune microenvironment during involution, which is

*Most of the function of TGFβ in immune regulation was re-printed with permission from the Journal of Clinical Medicine. (Guo Q, Betts C, Pennock N, Mitchell E, Schedin P. Mammary Gland Involution Provides a Unique Model to Study the TGF-β Cancer Paradox. J Clin Med. 2017 Jan 13;6(1).)

important in drug selection aimed at switching the immunosuppressive microenvironment toward a pro-inflammatory environment more keen to inhibit tumor progression.

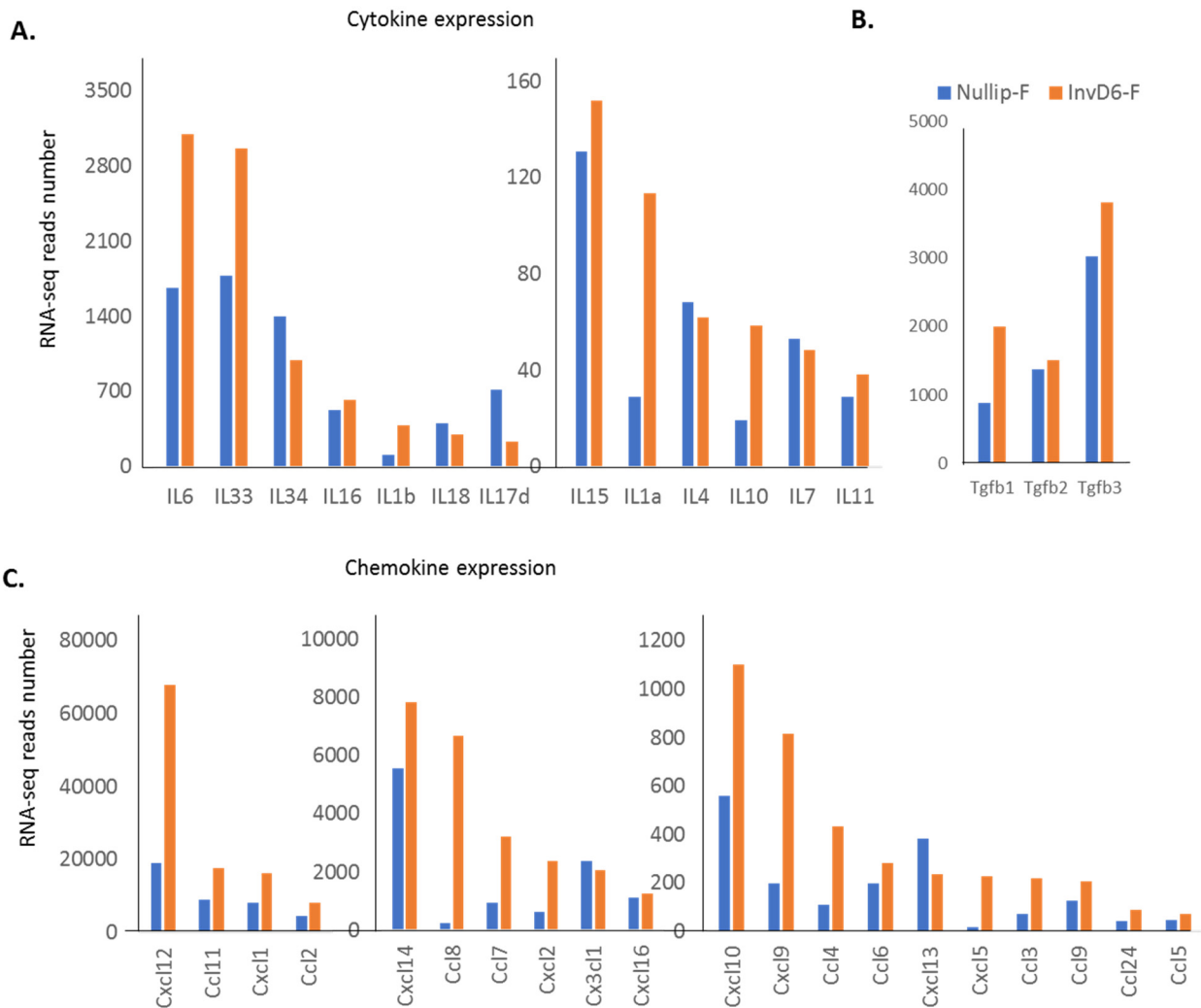


Figure 4- 1. Interleukins (A), TGFβs (B), C-X-C motif chemokines and C-C motif chemokines (C) gene expression in nulliparous-fibroblasts (blue) and involution-fibroblasts (orange). Data acquired by RNA-seq. Nulliparous-fibroblasts: n=2, InvD6-fibroblasts: n=3.

○ Macrophage RNA-seq data discussion.

The necessity of macrophages in the execution of involution and their potential contribution to the immunosuppressive microenvironment brought our attention to further characterize this cell type. Macrophages were isolated from mouse mammary glands by FACS for F4/80 positive cells. By flow cytometry, F4/80 positive cells in the mammary gland can be divided into 2 populations,

referred to as F4/80⁺, and F4/80⁺⁺ based on modest separation by F4/80 expression by flow and both populations exist in the nulliparous and involution day 6 mammary glands (Figure 4-2 A). By flow cytometry, one major difference between the F4/80⁺ and F4/80⁺⁺ populations is cell size. F4/80⁺⁺ population has higher in forward scatter and side scatter (figure 4-2 B and C), and on per cell basis, F4/80⁺⁺ cells contain more RNA than F4/80⁺ cells (Figure 4-2 D left panel). Although the F4/80⁺⁺ population seems to be higher for PDGFR α than F4/80⁺ population by flow cytometry, both of the two populations of macrophages have comparable low expression of PDGFR α by RNA-seq reads (Figure 4-2 D right panel). This is potentially a flow cytometry artifact due to large macrophages being more autofluorescence. Principal component analysis of RNA-seq data on both populations of macrophages confirmed differences between the two populations of macrophages (Figure 4-2 E). Further, both populations of macrophages have altered gene expression in the involuting mammary gland compared to the respective macrophages isolated from the nulliparous gland, as displayed by the volcano plot data (Figure 4-2 F and G). Pathway analysis and specific gene expression changes are still under investigation for the two populations of mammary macrophages in nulliparous and involuting hosts. Considering the gene expression alteration between two types of mammary macrophages in nulliparous and involution hosts, it will be interesting to test their tumor promotional function in a tumor cell co-injection study. What's more, it will be interesting to test if macrophages can induce fibroblast activation during involution, which can be done in the *in vitro* co-culture models described later.

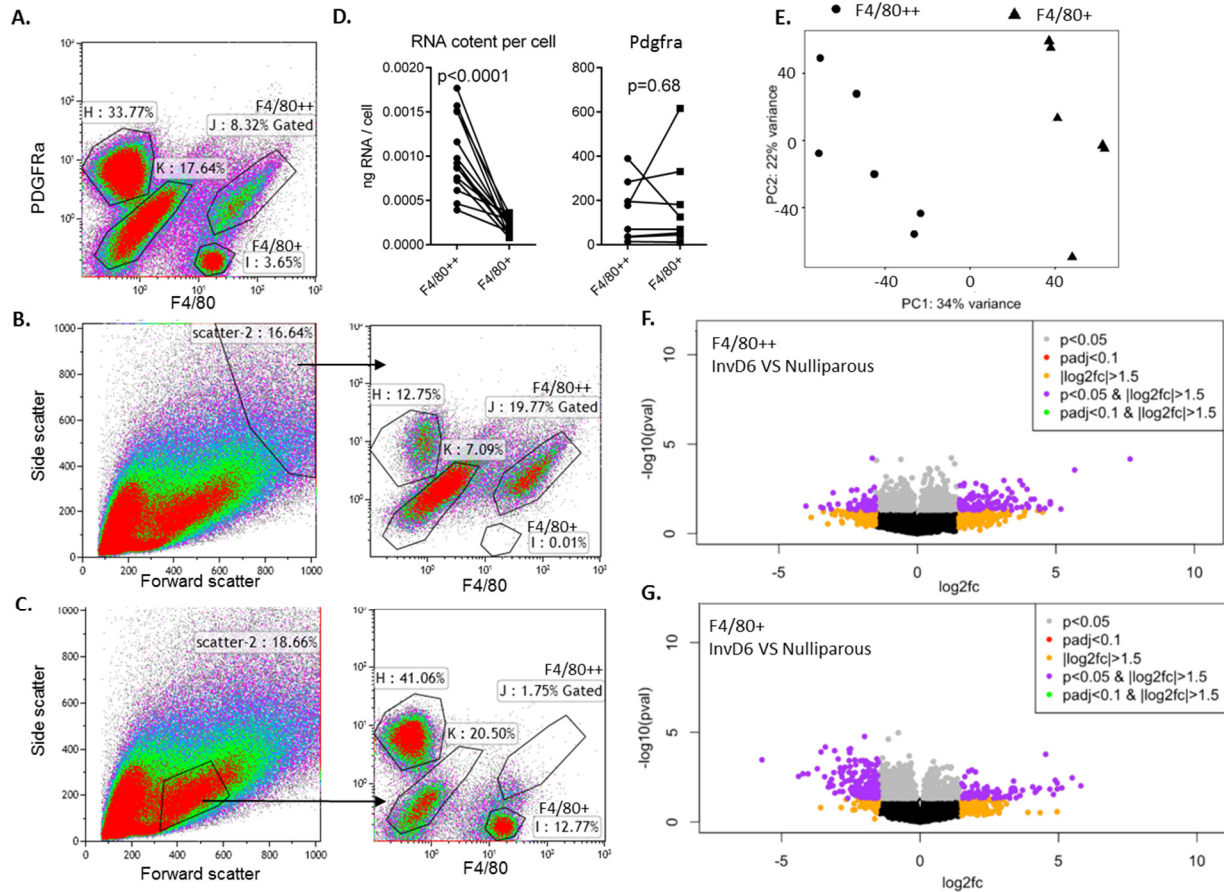


Figure 4- 2. Two populations of macrophages are present in the mammary gland and have altered gene expression during involution compared with nulliparous.

A. Flow cytometry plot of the nulliparous mammary gland stained for PDGFR α and F4/80. F4/80 $^{++}$ and F4/80 $^{+}$ macrophage populations are indicated in the figure. **B.** When high forward and side scatters were gated, F4/80 $^{+}$ population was lost in the plot. **C.** When low forward and side scatters were gated, F4/80 $^{++}$ population was lost in the plot. **D.** Left panel: RNA amount per cell in the two populations of macrophages. F4/80 $^{++}$ and F4/80 $^{+}$ from the same mouse mammary glands were considered as a group and paired t-test was used. Right panel: *Pdgfra* gene expression based on RNA-seq data for two populations of macrophages. **E.** Principal component analysis of two populations of macrophages. **F, G.** Analysis of the differentially expressed genes in both populations of macrophages, nulliparous and InvD6 were compared.

- 3D culture models development.

MEC apoptosis, immune cell infiltration and fibroblast activation during involution suggesting a potential crosstalk between those cells. To study cell crosstalk, simplified *in vitro* culture models are more amenable to reductionist mechanistic studies than the complex *in vivo* models. The disadvantage of 2D *in vitro* culturing model is that the lack of ECM changes cell behavior in a manner that can be less biologically relevant. Thus, the development of *in vitro* culture models

that can better mimic in vivo biology is needed. By using Matrigel, I have developed a unique 3D cell culture model to study the crosstalk between fibroblasts and macrophages and also a potential model that can be used to study weaning-induced involution. Matrigel is extracted from the Engelbreth-Holm-Swarm (EHS) mouse sarcoma, a tumor rich in the basement membrane protein laminin1 and also contains low amount of fibrillar collagens and other ECM proteins [250], which are important in supporting cell attachment and maintaining normal cell functionality, and likely contribute to why Matrigel works so well in 3D culture.

➤ *The crosstalk between macrophages and fibroblasts in a 3D culture model.*

Fibroblast activation during involution concur with macrophages infiltration, suggesting a potential role of macrophage in stimulating fibroblast activation. I have tested differentially polarized macrophages in inducing fibroblasts collagen production in a 3D culture model with some preliminary data acquired. Macrophages are the most abundant immune cells in the involuting mammary gland and are critical for the normal process of involution, as depletion of macrophages leads to decreased cell apoptosis and delayed involution. Macrophages have a spectrum of phenotypes in response to the surrounding cytokine milieu, ranging from antimicrobial and proinflammatory (M1) to tissue repair and immunosuppression (M2). M1 macrophages have been shown to aid host control of several bacterial infections and are associated with proinflammatory cytokine expression, i.e. IL-12. Macrophages in the involuting mammary gland have been characterized as M2 macrophages, which are positive for the classical M2 macrophage markers, such as arginase-1 (Arg-1) and mannose receptor (MR) and have high expression of the immunosuppressive cytokine IL-10 [19, 28].

Since macrophages can be a source of TGF β , and it has been shown that macrophages in response to apoptotic cells produce TGF β 1 [251-253], we hypothesized that during involution, clearance of apoptotic cells mediates macrophage M2 polarization and TGF β production, which leads to

fibroblasts activation and collagen production. To begin to test this hypothesis, I utilized a 3D culture model to coculture primary mouse mammary fibroblasts isolated from nulliparous mammary glands with macrophages in different polarization states. Bone marrow-derived macrophages (BMDMs) were treated with LPS and IFN γ to induce M1 polarization and IL-4 to induce M2 polarization (Figure 4-3 A). Macrophages and fibroblasts were mixed in a 1:1 ratio and embedded into Matrigel pads and cultured for 7 days. In these experiments, our first observation was that fibroblasts supported the survival of macrophages, as all three types of macrophages (M1, M2, BMDM) underwent cell death when cultured alone, and by 7 days of culturing, almost no viable macrophages could be detected. Culturing macrophages supplied with fibroblast conditioned medium supported the survival of macrophages, suggesting secreted factors from fibroblasts are critical for macrophage survival (Figure 4-3 B). What's more, strong physical interactions between macrophages and fibroblasts were found in the 3D coculture, with macrophages attached to the fibroblast cell bodies. In order to test the ability of macrophages to support fibroblast activation, collagen deposition was measured by immunofluorescence. Although our hypothesis is M2-polarized macrophages would induce fibroblast collagen production, to our surprise, the preliminary data showed the highest collagen abundance in the M1 and fibroblasts coculture condition (Figure 4-3 C). The results from the repeated experiment were not consistent with the first finding, largely due to lack of collagen expression under any conditions. Optimization should be done for this co-culture model and experiments should be repeated. However, it is possible that the inflammatory factors secreted by M1 macrophages stimulate fibroblast collagen production, such as IL-1 and TNF, which have been reported to enhance fibroblast collagen production in the absence of serum [254]. Further, macrophages are plastic cells that can potentially change their phenotypes when cultured with fibroblasts, so macrophage

phenotype at the end of the study and the linkage of the altered phenotype to fibroblast collagen production should be further investigated.

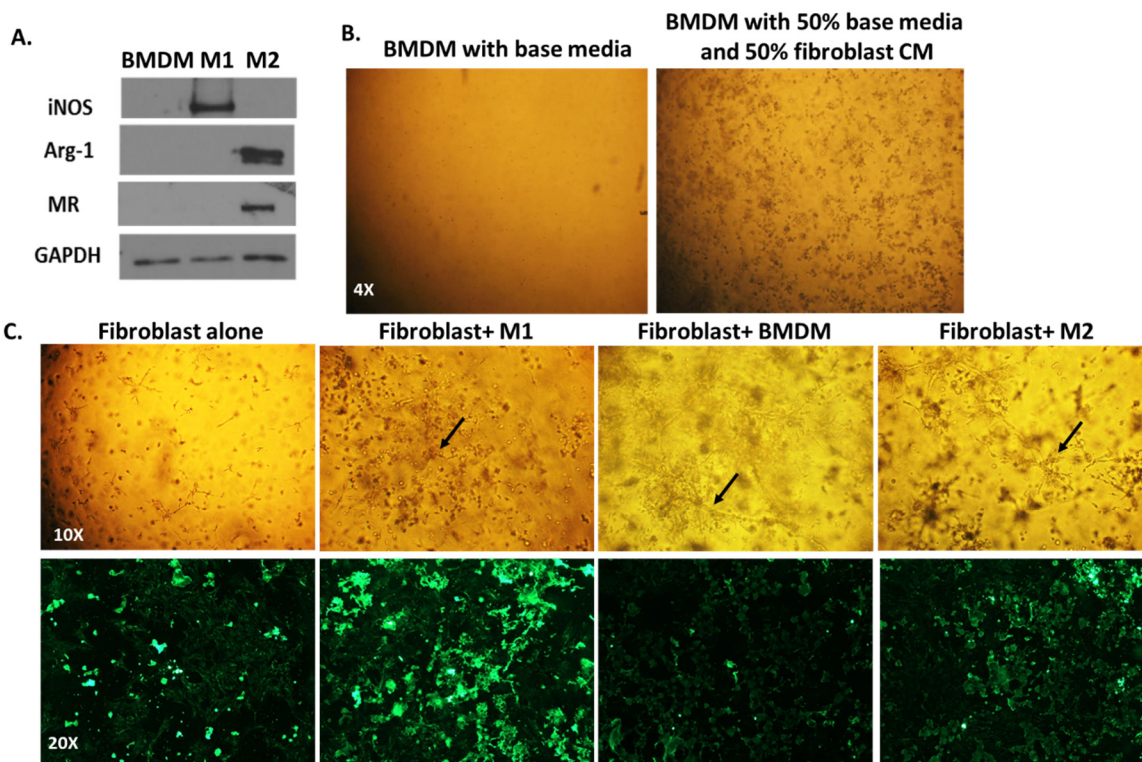


Figure 4- 3. M1 macrophages stimulate fibroblast collagen production in a 3D culture model.

A. BMDMs were stimulated with LPS and IFN- γ to polarize into a M1 phenotype and IL-4 to polarize into a M2 phenotype. Western blot was used to confirm macrophage phenotype after polarization. **B.** Left panel: BMDMs cultured in base medium with serum for 7 days fail to survive. Right panel: BMDMs cultured with 50% of fibroblast conditioned medium for 7 days are supported. **C.** Top panel: cell morphology of fibroblasts alone or co-cultured with three types of macrophages. Arrows show the interaction between macrophages and fibroblasts. Bottom panel: immunofluorescence staining of type I collagen in the Matrigel pads.

I also tested fibroblast-macrophage coculture model in the presence of apoptotic epithelial cells, as a means to further mimic the involution environment. In this study, a spontaneously immortalized mouse mammary epithelial cell line, EpH4 cells, were used to generate apoptotic cells. In my working experience with EpH4 cells, I found that lack of L-glutamine in the culture medium induced EpH4 cells to undergo caspase-mediated apoptosis (Figure 4-4 A and B). In the co-culture study, three types of macrophages (BMDM, M1, and M2 as described above) were pre-

incubated with apoptotic EpH4 cells for 30 minutes then mixed with fibroblasts and embedded in Matrigel and cultured for 4-6 days. M2 polarized macrophages showed the strongest interactions with fibroblasts in the presence of apoptotic cells, and formed more and larger cell clusters compared to the M1 and BMDM macrophages (Figure 4-4 C and D). These preliminary data suggest that M2 macrophages may be influenced by apoptotic cells in a manner that enhances the interactions with fibroblasts. Further investigations into the specific interactions between the three cell types, potential macrophage plasticity, and any effect on fibroblasts activation are warranted.

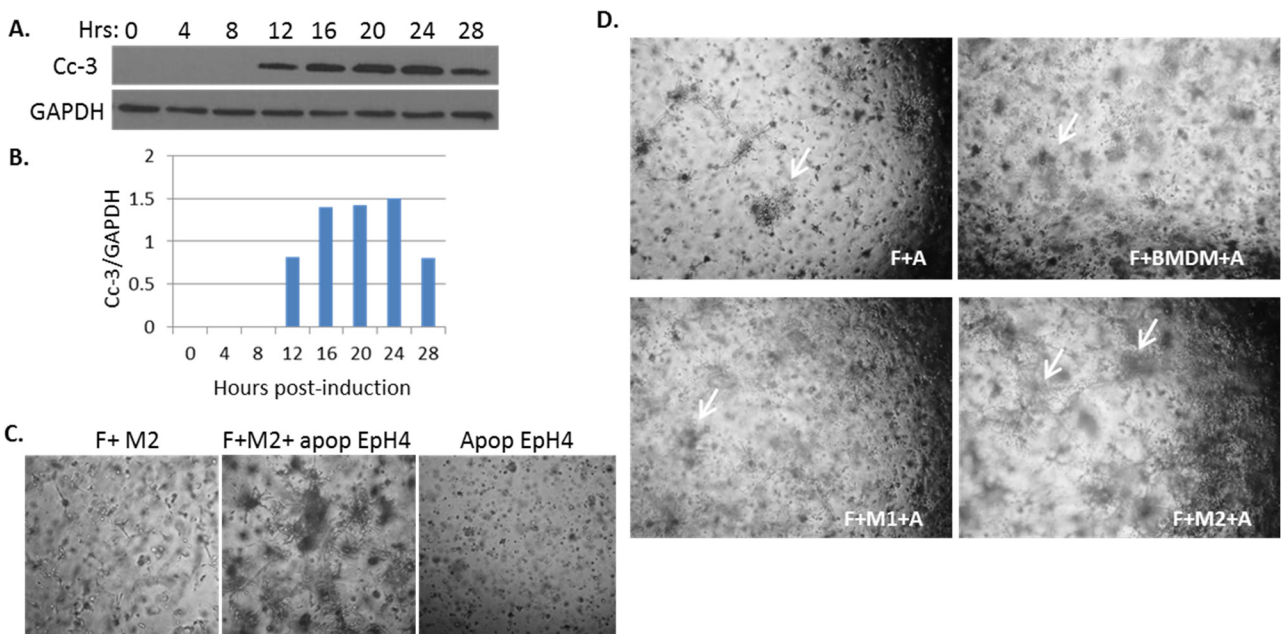


Figure 4- 4. Apoptotic EpH4 cells stimulate more fibroblast-macrophage interactions, especially in F-M2 co-culture conditions.

(A) Western blot for cleaved caspase 3 (cc-3) in EpH4 cell lysate after 0h-28h of glutamine removal showing the temporal induction of apoptosis. (B) Quantification of cleaved-caspase 3 normalized to GAPDH. (C) Left panel shows fibroblast-M2 coculture. Middle panel shows fibroblast, M2, and apoptotic EpH4 cell co-culture. Right panel shows apoptotic EpH4 cells alone in 3D culture. All pictures were taken after 4 days co-culture. 20,000, fibroblasts, 20,000 macrophages and 20,000 apoptotic cells were used in this culture system. (D) Fibroblasts and apoptotic EpH4 cells co-cultured with BMDM, M1 or M2 macrophages for 6 days. Arrows show cell-cell interactions. 30,000 fibroblasts, 7,000 macrophages, and 7,000 EpH4 cells were used in this co-culture system.

➤ *A 3D culture model development for potentially studying involution.*

Non-tumorigenic mammary epithelial cell lines, such as MCF10A cells, usually form a monolayer when culture on a 2D plastic plate, whereas when cultured on top of Matrigel they can form

multicellular mammospheres composed of polarized mammary epithelium with hollow apical centers, suggesting Matrigel supports mammary alveolar morphogenesis. However, not all types of mammary epithelial cells can form acini-like structures on Matrigel. The EpH4 cell line is a spontaneously immortalized mouse mammary epithelial cell line that form cell clusters when cultured on top of Matrigel, but without hollow centers (Figure 4-5 B). Interestingly, when fibroblasts were embedded in the Matrigel pad, EpH4 cells formed acini-like structure (Figure 4-5 A and B), suggesting a role for normal fibroblast in supporting EpH4 cell alveolar morphogenesis. This model can be potentially used to mimic mammary gland involution. The benefit for using this in vitro model is that we can avoid the complexity of the cellular and ECM environment in the mammary gland.

Firstly, this model can be used to test the functional switch of fibroblasts during involution. By embedding FACS isolated involution-fibroblasts, or by adding factors like TGF β or PGE2 to induce fibroblasts involution phenotype, we can test the functional alteration of involution-fibroblasts in supporting EpH4 cell morphogenesis compared to the nulliparous-fibroblasts.

This model can also be potentially used to study the crosstalk between apoptotic MECs to fibroblast activation. Apoptotic EpH4 cells can be directly added on the top of the fibroblasts pads to test the activation of the fibroblast. Alternatively, by adding specific lipids that have been reported to initiate MEC apoptosis during involution such as Arachidonic acid, we can induce organoid forming EpH4 cell apoptosis on the pad and investigate the influence to fibroblasts.

This in vitro model also can potentially be used to study the potential tumor promotional factors in the involution microenvironment. For example, by adding different ECM proteins that are upregulated during involution, we can monitor the morphological changes of the acini formed by EpH4 cells as a read out for the function of the ECM protein. Further, we can test the function of

involution associated ECM in tumor promotion by injection of tumor cells into the lumen formed by EpH4 cells cultured on top of the fibroblast pad mixed with different involution-ECM proteins.

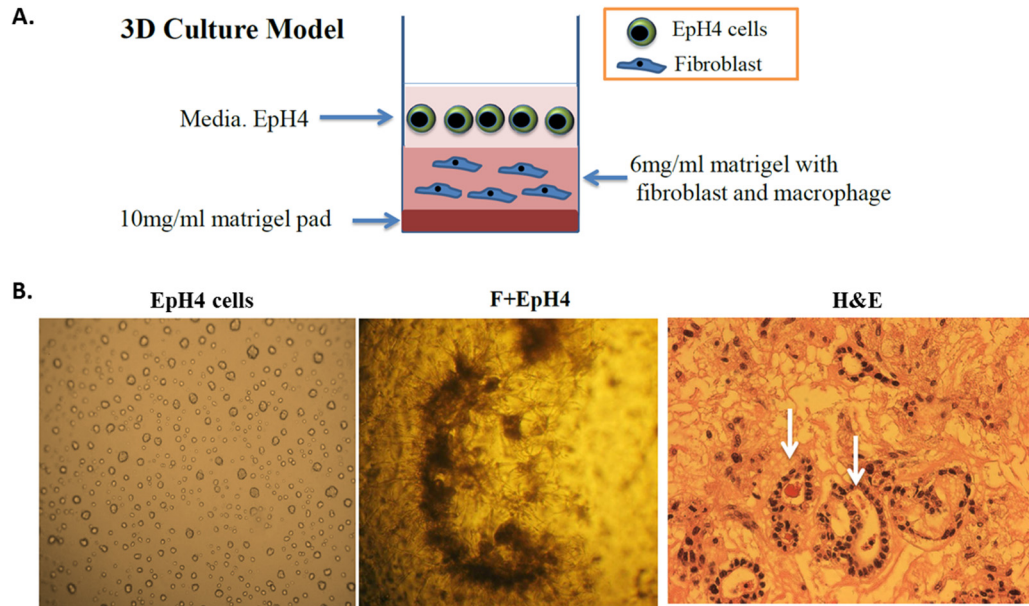


Figure 4- 5. Fibroblasts support EpH4 cellular morphogenesis.

A. Cartoon of 3D culture model, with fibroblast embedded in Matrigel pad and EpH4 cells placed on top of Matrigel pad. **B.** Left panel: EpH4 cells cultured on top of Matrigel pad without fibroblasts. Middle panel: EpH4 cells cultured on top of Matrigel pad with fibroblasts embedded. Right panel: H&E staining of sectioned pads from the EpH4 fibroblast co-cultures. Arrow indicate hollow acini-like structures formed by EpH4 cells when cultured with fibroblasts.

o **Method.**

RNA-seq. Details of data acquire and analysis are described in method section of chapter III.

Flow cytometry. 1×10^6 cells per sample were blocked with CD16/32 (eBioscience, 14-0161-81) for 30 minutes and cell surface markers were stained for 20 minutes. PDGFR α (BioLegend, 135910): 1:100 dilution, F4/80 (BioLegend, 123108): 1:200 dilution. Cells were stained for 20 minutes. Experiments were performed on an LSRFortessa (BD Biosciences; Oregon Health and Science University Flow Cytometry Shared Resource) and analysis was performed using FlowJo (FlowJo, LLC Data Analysis Software, Ashland, OR).

Cell culture. Primary mammary fibroblasts isolation and culturing condition are described in chapter III method section. EpH4 cells were maintained in DMEM high glucose with no L-glutamine or sodium pyruvate (Sigma D5671), containing 1% 1M HEPES and 1% penicillin/streptomycin and 1mM L-glutamine.

Generation of L-cell Conditioned Media. L929 murine fibrosarcoma cells were cultured in DMEM high glucose containing 10% FBS and 2 mM L-glutamine. For maintaining culturing, cells were split 1:4-1:8 at 80% confluency. For generation of L-cell conditioned media, media was collected 5-7 days after cells reached 100% confluency, filter sterilized, and stored in aliquots at -20 degree.

Bone marrow derived macrophages polarization. Bone marrow was harvested from tibia and femurs of 6-8 week old BALB/c mice. Macrophages were matured from bone marrow by plating 750,000 bone marrow cells in 10 cm tissue culture plates in 10 mL of initial macrophage media (RPMI 1640 containing 30% L-cell conditioned media, 10% FBS, and 1% penicillin/streptomycin) (maturation day 0), medium changed at maturation day 3. On day 5, medium was switched to 10 mL pre-activation media (DMEM low glucose containing 30% L-cell conditioned media, 10% FBS, 1% non-essential amino acids, and 1% penicillin/streptomycin). After 24 hours of pre-activation, media was removed and polarization media were applied. For BMDM, DMEM low glucose containing 30% L-cell conditioned media (BMDM media) was used for 48 hours. After 24 hours in BMDM medium, medium was removed and replaced with BMDM medium with 5 ng/mL lipopolysaccharide (LPS) and 12 ng/ml IFN- γ (M1 media) or BMDM medium plus 10 ng/mL IL-4 (M2 media) for 24 hours. After 24 hours, macrophages were washed with PBS, and harvested using a cell scraper. Cells from each well were split into two equal aliquots and pelleted

by centrifugation at 1500 rpm for 2 minutes for RNA and protein, or used in 3D co-culture assays with primary mammary fibroblasts.

Generation of Apoptotic EpH4 cells. EpH4 cells at 95% confluency were harvested with 0.25% trypsin-EDTA, and re-seeded 1:2 on tissue culture plates in 10 mL apoptosis induction media (DMEM high glucose with no L-glutamine or sodium pyruvate (Sigma D5671), containing 1% 1M HEPES and 1% penicillin/streptomycin) for different time points at 37 degree in 5% CO₂. After desired hours, floating and loosely adherent cells were collected by pipetting up and down and pelleted by centrifugation at 1500 rpm for 2 minutes.

Western Blot. EpH4 cell lysates were prepared by harvesting cells directly into 100 µL Radio Immuno Precipitation Assay (RIPA) buffer (10 µM Tris pH 7.4, 150 µM NaCl, 0.1% SDS, 1% sodium deoxycholate, and 1% Triton X-100) containing protease and phosphatase inhibitors (1x Protease Inhibitor Cocktail (Sigma), 200 µg/mL PMSF, 1 mM Na₃VO₄, and 50 mM NaF). 30 µL of total protein were separated by SDS-PAGE using a 10% acrylamide gel. Membranes were blocked in 5% non-fat dry milk in TBS-T (10 mM Tris-HCl, pH 8.0, 150 mM NaCl, 0.1% Tween 20) for 1 hour at room temperature. Primary antibody incubation was performed overnight in 4 degree. Cleaved Caspase-3 (1: 500; Cell Signaling, 9661S), GAPDH (1:1000; G9545, Sigma-Aldrich, St. Louis, MO; 1 hour, RT), AIF-1 (1:100; Wako), iNOS (1:100; Abcam ab15323), Arg-1 (1:120; Santa Cruz), mannose receptor (1:100; Sigma), followed by anti-rabbit HRP-conjugated secondary antibody (Santa Cruz Biotechnologies, Santa Cruz, CA and Bio-Rad Laboratories, Hercules, CA, respectively; 30 minutes, RT) with detection using with detection using ECL Western Blotting Substrate (Thermo Fisher Scientific, Waltham, MA). Densitometry was performed using Image J Software¹⁷⁵.

- **Significance.**

Young women’s breast cancer has a major impact on women worldwide. Although breast cancer is more frequent in women 65 years of age and older, breast cancer in women younger than 45 years (young women’s breast cancer) accounts for more than 40% of all cancer in women in this age group [255]. Furthermore, around 50% of the young women’s breast cancer cases are associated with a recent pregnancy [4], called postpartum breast cancer. Postpartum breast cancer patients have significantly increased metastasis and decreased survival rates compared to young nulliparous women with breast cancer, even after adjusting for breast cancer biologic subtype, tumor stage, year and age of diagnosis [4]. Further, increased age at first birth is associated with increased risk of postpartum breast cancer [3]. According to the National Vital Statistics System, the mean age of first-time mothers in the United States is increasing from 23 years old in 1980 to 26 years old in 2012 (Figure 4-6), and most recently to 26.3 in 2014. With this continued delayed childbearing, an increase in postpartum breast cancer is anticipated, so finding prevention and treatment strategies is of ever-increasing importance.

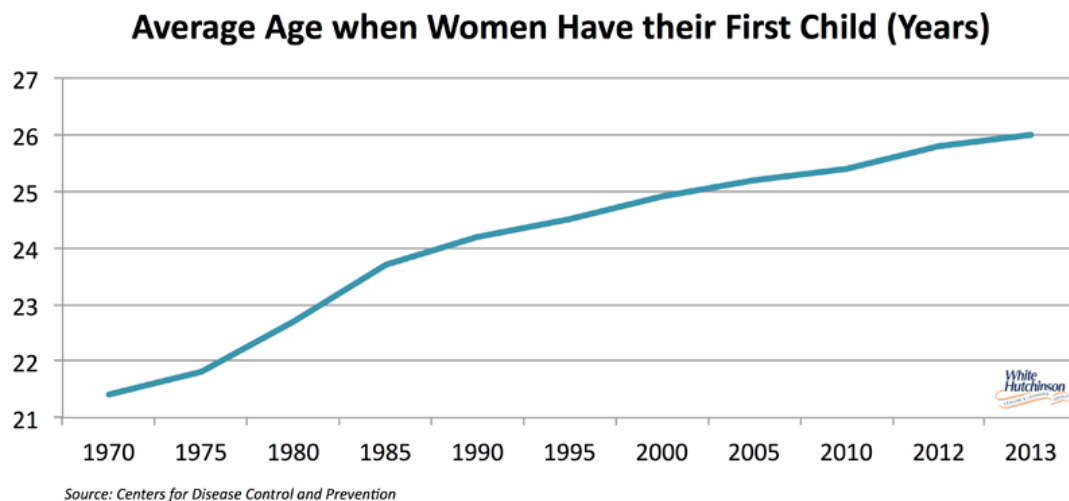


Figure 4- 6. Average age when women have their first child in United States.

Data adapted from “White Hutchinson Leisure & Learning Group, Kansas City, MO, USA”

Since breast cancer diagnosed during pregnancy does not carry a poorer prognosis than when diagnosed in nulliparous patients [9-11], a postpartum event likely contributes to the poor prognosis of postpartum breast cancer. The postpartum event of mammary involution has been shown in rodent models to support enhanced tumor growth and progression to metastasis [14, 19]. These rodent models serve as useful tools in understanding the mechanisms underlying the aggressiveness of PPBC. In my thesis work, I found increased collagen abundance in the involuting mammary gland, suggesting increased breast density, which is strongly correlated with increased risk and increased aggressiveness of breast cancer. I also found that the increased collagen during involution is coincident with fibroblast activation, which includes acquisition of immune suppressive activates. The involution-fibroblasts promote tumor growth when co-injecting with tumor cells. Furthermore, we found ibuprofen treatment during involution suppresses fibroblast activation and tumor promotional capacities. In sum, this work provides a rationale for targeting fibroblast during the postpartum window and justifies the potential benefit to use NSAIDs during the postpartum weaning for the prevention and treatment of postpartum breast cancer.

REFERENCE.

1. Fan, F. and P. Thomas, *Common Benign Conditions of Low Concern, in Breast Cancer and its Precursor Lesions. Making Sense and Making It Early*, P. Thomas, Editor., Springer New York Dordrecht Heidelberg London.
2. Janerich, D.T. and M.B. Hoff, *Evidence for a crossover in breast cancer risk factors*. Am J Epidemiol, 1982. **116**(5): p. 737-42.
3. Schedin, P., *Pregnancy-associated breast cancer and metastasis*. Nat Rev Cancer, 2006. **6**(4): p. 281-91.
4. Callihan, E.B., et al., *Postpartum diagnosis demonstrates a high risk for metastasis and merits an expanded definition of pregnancy-associated breast cancer*. Breast Cancer Res Treat, 2013. **138**(2): p. 549-59.
5. Matthews, T.J. and B.E. Hamilton, *Delayed childbearing: more women are having their first child later in life*. NCHS Data Brief, 2009(21): p. 1-8.
6. Andersson, T.M., et al., *Increasing incidence of pregnancy-associated breast cancer in Sweden*. Obstet Gynecol, 2009. **114**(3): p. 568-72.
7. Matsuda, T., et al., *Cancer incidence and incidence rates in Japan in 2006: based on data from 15 population-based cancer registries in the monitoring of cancer incidence in Japan (MCIJ) project*. Jpn J Clin Oncol, 2012. **42**(2): p. 139-47.
8. Borges, V.F., *Management of the patient with postpartum breast cancer*. Oncology (Williston Park), 2014. **28**(9): p. 768-70.
9. Stensheim, H., et al., *Cause-specific survival for women diagnosed with cancer during pregnancy or lactation: a registry-based cohort study*. J Clin Oncol, 2009. **27**(1): p. 45-51.
10. Johansson, A.L., et al., *Increased Mortality in Women with Breast Cancer Detected during Pregnancy and Different Periods Postpartum*. Cancer Epidemiol Biomarkers Prev, 2011. **20**(9): p. 1865-72.
11. Amant, F., et al., *Prognosis of women with primary breast cancer diagnosed during pregnancy: results from an international collaborative study*. J Clin Oncol, 2013. **31**(20): p. 2532-9.
12. Henderson, B.E., R. Ross, and L. Bernstein, *Estrogens as a cause of human cancer: the Richard and Hinda Rosenthal Foundation award lecture*. Cancer Res, 1988. **48**(2): p. 246-53.
13. Rossouw, J.E., et al., *Risks and benefits of estrogen plus progestin in healthy postmenopausal women: principal results From the Women's Health Initiative randomized controlled trial*. JAMA, 2002. **288**(3): p. 321-33.
14. Lyons, T.R., et al., *Postpartum mammary gland involution drives progression of ductal carcinoma in situ through collagen and COX-2*. Nat Med, 2011. **17**(9): p. 1109-15.
15. Puckridge, P.J., et al., *Breast cancer and pregnancy: a diagnostic and management dilemma*. ANZ J Surg, 2003. **73**(7): p. 500-3.
16. Woo, J.C., T. Yu, and T.C. Hurd, *Breast cancer in pregnancy: a literature review*. Arch Surg, 2003. **138**(1): p. 91-8; discussion 99.
17. Daling, J.R., et al., *The relation of reproductive factors to mortality from breast cancer*. Cancer Epidemiol Biomarkers Prev, 2002. **11**(3): p. 235-41.
18. Whiteman, M.K., et al., *Reproductive history and mortality after breast cancer diagnosis*. Obstet Gynecol, 2004. **104**(1): p. 146-54.
19. Martinson, H.A., et al., *Wound healing-like immune program facilitates postpartum mammary gland involution and tumor progression*. Int J Cancer, 2015. **136**(8): p. 1803-13.
20. Lyons, T.R., et al., *Cyclooxygenase-2-dependent lymphangiogenesis promotes nodal metastasis of postpartum breast cancer*. J Clin Invest, 2014. **124**(9): p. 3901-12.

21. Quarrie, L.H., C.V. Addey, and C.J. Wilde, *Programmed cell death during mammary tissue involution induced by weaning, litter removal, and milk stasis*. J Cell Physiol, 1996. **168**(3): p. 559-69.
22. Lund, L.R., et al., *Two distinct phases of apoptosis in mammary gland involution: proteinase-independent and -dependent pathways*. Development, 1996. **122**(1): p. 181-93.
23. Strange, R., et al., *Apoptotic cell death and tissue remodelling during mouse mammary gland involution*. Development, 1992. **115**(1): p. 49-58.
24. Stein, T., et al., *Involution of the mouse mammary gland is associated with an immune cascade and an acute-phase response, involving LBP, CD14 and STAT3*. Breast Cancer Res, 2004. **6**(2): p. R75-91.
25. Clarkson, R.W., et al., *Gene expression profiling of mammary gland development reveals putative roles for death receptors and immune mediators in post-lactational regression*. Breast Cancer Res, 2004. **6**(2): p. R92-109.
26. Walker, N.I., R.E. Bennett, and J.F. Kerr, *Cell death by apoptosis during involution of the lactating breast in mice and rats*. Am J Anat, 1989. **185**(1): p. 19-32.
27. Alexander, C.M., et al., *Stromelysin-1 regulates adipogenesis during mammary gland involution*. J Cell Biol, 2001. **152**(4): p. 693-703.
28. O'Brien, J., et al., *Alternatively activated macrophages and collagen remodeling characterize the postpartum involuting mammary gland across species*. Am J Pathol, 2010. **176**(3): p. 1241-55.
29. O'Brien, J.H., et al., *Rat mammary extracellular matrix composition and response to ibuprofen treatment during postpartum involution by differential GeLC-MS/MS analysis*. J Proteome Res, 2012. **11**(10): p. 4894-905.
30. Sargeant, T.J., et al., *Stat3 controls cell death during mammary gland involution by regulating uptake of milk fat globules and lysosomal membrane permeabilization*. Nat Cell Biol, 2014. **16**(11): p. 1057-68.
31. Marti, A., et al., *Mouse mammary gland involution is associated with cytochrome c release and caspase activation*. Mech Dev, 2001. **104**(1-2): p. 89-98.
32. Sakamoto, K., et al., *Janus Kinase 1 Is Essential for Inflammatory Cytokine Signaling and Mammary Gland Remodeling*. Mol Cell Biol, 2016. **36**(11): p. 1673-90.
33. Schere-Levy, C., et al., *Leukemia inhibitory factor induces apoptosis of the mammary epithelial cells and participates in mouse mammary gland involution*. Exp Cell Res, 2003. **282**(1): p. 35-47.
34. Bagci, H., et al., *Impaired cell death and mammary gland involution in the absence of Dock1 and Rac1 signaling*. Cell Death Dis, 2014. **5**: p. e1375.
35. Nguyen, A.V. and J.W. Pollard, *Transforming growth factor beta3 induces cell death during the first stage of mammary gland involution*. Development, 2000. **127**(14): p. 3107-18.
36. Baxter, F.O., et al., *IKKbeta/2 induces TWEAK and apoptosis in mammary epithelial cells*. Development, 2006. **133**(17): p. 3485-94.
37. Monks, J., et al., *Epithelial cells remove apoptotic epithelial cells during post-lactation involution of the mouse mammary gland*. Biol Reprod, 2008. **78**(4): p. 586-94.
38. Fornetti, J., et al., *Mammary epithelial cell phagocytosis downstream of TGF-beta3 is characterized by adherens junction reorganization*. Cell Death Differ, 2016. **23**(2): p. 185-96.
39. Stein, T., N. Salomonis, and B.A. Gusterson, *Mammary gland involution as a multi-step process*. J Mammary Gland Biol Neoplasia, 2007. **12**(1): p. 25-35.
40. Watson, C.J., *Involution: apoptosis and tissue remodelling that convert the mammary gland from milk factory to a quiescent organ*. Breast Cancer Res, 2006. **8**(2): p. 203.
41. Schedin, P., et al., *Fibronectin fragments induce MMP activity in mouse mammary epithelial cells: evidence for a role in mammary tissue remodeling*. J Cell Sci, 2000. **113** (Pt 5): p. 795-806.

42. Schedin, P., et al., *Microenvironment of the involuting mammary gland mediates mammary cancer progression*. J Mammary Gland Biol Neoplasia, 2007. **12**(1): p. 71-82.
43. McDaniel, S.M., et al., *Remodeling of the mammary microenvironment after lactation promotes breast tumor cell metastasis*. Am J Pathol, 2006. **168**(2): p. 608-20.
44. Goddard, E.T., et al., *Quantitative extracellular matrix proteomics to study mammary and liver tissue microenvironments*. Int J Biochem Cell Biol, 2016.
45. Schedin, P., et al., *Fibronectin fragments induce MMP activity in mouse mammary epithelial cells: evidence for a role in mammary tissue remodeling*. Journal of Cell Science, 2000.
46. Schedin, P., et al., *Mammary ECM composition and function are altered by reproductive state*. Mol Carcinog, 2004. **41**(4): p. 207-20.
47. Bemis, L.T. and P. Schedin, *Reproductive State of Rat Mammary Gland Stroma Modulates Human Breast Cancer Cell Migration and Invasion*. CANCER RESEARCH, 2000.
48. O'Brien, J., et al., *Non-steroidal anti-inflammatory drugs target the pro-tumorigenic extracellular matrix of the postpartum mammary gland*. Int J Dev Biol, 2011. **55**(7-9): p. 745-55.
49. Maller, O., et al., *Collagen architecture in pregnancy-induced protection from breast cancer*. J Cell Sci, 2013. **126**(Pt 18): p. 4108-10.
50. Goddard, E.T., et al., *Quantitative extracellular matrix proteomics to study mammary and liver tissue microenvironments*. Int J Biochem Cell Biol, 2016. **81**(Pt A): p. 223-232.
51. Bissell, M.J., H.G. Hall, and G. Parry, *How does the extracellular matrix direct gene expression?* J Theor Biol, 1982. **99**(1): p. 31-68.
52. Lauber, K., et al., *Clearance of apoptotic cells: getting rid of the corpses*. Mol Cell, 2004. **14**(3): p. 277-87.
53. Rosen, A. and L. Casciola-Rosen, *Autoantigens as substrates for apoptotic proteases: implications for the pathogenesis of systemic autoimmune disease*. Cell Death Differ, 1999. **6**(1): p. 6-12.
54. O'Brien, J., et al., *Macrophages are crucial for epithelial cell death and adipocyte repopulation during mammary gland involution*. Development, 2012. **139**(2): p. 269-75.
55. Stein, T., et al., *A mouse mammary gland involution mRNA signature identifies biological pathways potentially associated with breast cancer metastasis*. J Mammary Gland Biol Neoplasia, 2009. **14**(2): p. 99-116.
56. Guo, Q., et al., *Mammary Gland Involution Provides a Unique Model to Study the TGF-beta Cancer Paradox*. J Clin Med, 2017. **6**(1).
57. Smith, W.L., R.M. Garavito, and D.L. DeWitt, *Prostaglandin endoperoxide H synthases (cyclooxygenases)-1 and -2*. J Biol Chem, 1996. **271**(52): p. 33157-60.
58. Singh-Ranger, G. and K. Mokbel, *The role of cyclooxygenase-2 (COX-2) in breast cancer, and implications of COX-2 inhibition*. Eur J Surg Oncol, 2002. **28**(7): p. 729-37.
59. Waddell, W.R. and R.W. Loughry, *Sulindac for polyposis of the colon*. J Surg Oncol, 1983. **24**(1): p. 83-7.
60. Thun, M.J., et al., *Aspirin use and risk of fatal cancer*. Cancer Res, 1993. **53**(6): p. 1322-7.
61. Reddy, B.S., et al., *Prevention of colon cancer by low doses of celecoxib, a cyclooxygenase inhibitor, administered in diet rich in omega-3 polyunsaturated fatty acids*. Cancer Res, 2005. **65**(17): p. 8022-7.
62. Wang, Z., *The role of COX-2 in oral cancer development, and chemoprevention/ treatment of oral cancer by selective COX-2 inhibitors*. Curr Pharm Des, 2005. **11**(14): p. 1771-7.
63. Wang, D. and R.N. Dubois, *The role of COX-2 in intestinal inflammation and colorectal cancer*. Oncogene, 2010. **29**(6): p. 781-8.
64. Boland, G.P., et al., *COX-2 expression is associated with an aggressive phenotype in ductal carcinoma in situ*. Br J Cancer, 2004. **90**(2): p. 423-9.

65. Denkert, C., et al., *Elevated expression of cyclooxygenase-2 is a negative prognostic factor for disease free survival and overall survival in patients with breast carcinoma*. *Cancer*, 2003. **97**(12): p. 2978-87.
66. Ristimaki, A., et al., *Prognostic significance of elevated cyclooxygenase-2 expression in breast cancer*. *Cancer Res*, 2002. **62**(3): p. 632-5.
67. Kwan, M.L., et al., *NSAIDs and breast cancer recurrence in a prospective cohort study*. *Cancer Causes Control*, 2007. **18**(6): p. 613-20.
68. Holmes, M.D., et al., *Aspirin intake and survival after breast cancer*. *J Clin Oncol*, 2010. **28**(9): p. 1467-72.
69. Kalinski, P., et al., *IL-12-deficient dendritic cells, generated in the presence of prostaglandin E2, promote type 2 cytokine production in maturing human naive T helper cells*. *J Immunol*, 1997. **159**(1): p. 28-35.
70. van der Pouw Kraan, T.C., et al., *Prostaglandin-E2 is a potent inhibitor of human interleukin 12 production*. *J Exp Med*, 1995. **181**(2): p. 775-9.
71. Muthuswamy, R., et al., *PGE(2) transiently enhances DC expression of CCR7 but inhibits the ability of DCs to produce CCL19 and attract naive T cells*. *Blood*, 2010. **116**(9): p. 1454-9.
72. Sheng, H., et al., *Prostaglandin E2 increases growth and motility of colorectal carcinoma cells*. *J Biol Chem*, 2001. **276**(21): p. 18075-81.
73. Fornetti, J., et al., *Physiological COX-2 expression in breast epithelium associates with COX-2 levels in ductal carcinoma in situ and invasive breast cancer in young women*. *Am J Pathol*, 2014. **184**(4): p. 1219-29.
74. Provenzano, P.P., et al., *Collagen density promotes mammary tumor initiation and progression*. *BMC Med*, 2008. **6**: p. 11.
75. Conklin, M.W., et al., *Aligned collagen is a prognostic signature for survival in human breast carcinoma*. *Am J Pathol*, 2011. **178**(3): p. 1221-32.
76. Provenzano, P.P., et al., *Collagen reorganization at the tumor-stromal interface facilitates local invasion*. *BMC Med*, 2006. **4**(1): p. 38.
77. Sahai, E., et al., *Simultaneous imaging of GFP, CFP and collagen in tumors in vivo using multiphoton microscopy*. *BMC Biotechnol*, 2005. **5**: p. 14.
78. Fleischmajer, R., et al., *Dermal collagen fibrils are hybrids of type I and type III collagen molecules*. *J Struct Biol*, 1990. **105**(1-3): p. 162-9.
79. Fleischmajer, R., et al., *Type I and type III collagen interactions during fibrillogenesis*. *Ann N Y Acad Sci*, 1990. **580**: p. 161-75.
80. Romanic, A.M., et al., *Copolymerization of pNcollagen III and collagen I. pNcollagen III decreases the rate of incorporation of collagen I into fibrils, the amount of collagen I incorporated, and the diameter of the fibrils formed*. *J Biol Chem*, 1991. **266**(19): p. 12703-9.
81. Liu, X., et al., *Type III collagen is crucial for collagen I fibrillogenesis and for normal cardiovascular development*. *Proc Natl Acad Sci U S A*, 1997. **94**(5): p. 1852-6.
82. Clore, J.N., I.K. Cohen, and R.F. Diegelmann, *Quantitation of collagen types I and III during wound healing in rat skin*. *Proc Soc Exp Biol Med*, 1979. **161**(3): p. 337-40.
83. Volk, S.W., et al., *Diminished type III collagen promotes myofibroblast differentiation and increases scar deposition in cutaneous wound healing*. *Cells Tissues Organs*, 2011. **194**(1): p. 25-37.
84. Birk, D.E., et al., *Collagen type I and type V are present in the same fibril in the avian corneal stroma*. *J Cell Biol*, 1988. **106**(3): p. 999-1008.
85. Wenstrup, R.J., et al., *Type V collagen controls the initiation of collagen fibril assembly*. *J Biol Chem*, 2004. **279**(51): p. 53331-7.

86. Wenstrup, R.J., et al., *Regulation of collagen fibril nucleation and initial fibril assembly involves coordinate interactions with collagens V and XI in developing tendon.* J Biol Chem, 2011. **286**(23): p. 20455-65.
87. Williams, R.M., W.R. Zipfel, and W.W. Webb, *Interpreting Second-Harmonic Generation Images of Collagen I Fibrils.* Biophysical Journal, 2005. **88**(2): p. 1377-1386.
88. Cay M. Kielty, *Type VI Collagen Microfibrils: Evidence for a Structural Association with Hyaluronan.* The Journal of Cell Biology, 1992.
89. Kuo, H.J., et al., *Type VI collagen anchors endothelial basement membranes by interacting with type IV collagen.* J Biol Chem, 1997. **272**(42): p. 26522-9.
90. Bober, M., et al., *Collagen VI is a subepithelial adhesive target for human respiratory tract pathogens.* J Innate Immun, 2010. **2**(2): p. 160-6.
91. Karousou, E., et al., *Collagen VI and hyaluronan: the common role in breast cancer.* Biomed Res Int, 2014. **2014**: p. 606458.
92. Cescon, M., et al., *Collagen VI at a glance.* J Cell Sci, 2015. **128**(19): p. 3525-31.
93. Iyengar, P., et al., *Adipocyte-derived collagen VI affects early mammary tumor progression in vivo, demonstrating a critical interaction in the tumor/stroma microenvironment.* J Clin Invest, 2005. **115**(5): p. 1163-76.
94. Tao, G., et al., *Collagen XIV is important for growth and structural integrity of the myocardium.* Journal of Molecular and Cellular Cardiology, 2012. **53**(5): p. 626-638.
95. Ansoorge, H.L., et al., *Type XIV Collagen Regulates Fibrillogenesis: PREMATURE COLLAGEN FIBRIL GROWTH AND TISSUE DYSFUNCTION IN NULL MICE.* Journal of Biological Chemistry, 2008. **284**(13): p. 8427-8438.
96. Lu, P., M.D. Sternlicht, and Z. Werb, *Comparative mechanisms of branching morphogenesis in diverse systems.* J Mammary Gland Biol Neoplasia, 2006. **11**(3-4): p. 213-28.
97. Esbona, K., et al., *COX-2 modulates mammary tumor progression in response to collagen density.* Breast Cancer Res, 2016. **18**(1): p. 35.
98. Lu, Y., et al., *Do Different Cyclooxygenase Inhibitors Impair Rotator Cuff Healing in a Rabbit Model?* Chin Med J (Engl), 2015. **128**(17): p. 2354-9.
99. Muscara, M.N., et al., *Wound collagen deposition in rats: effects of an NO-NSAID and a selective COX-2 inhibitor.* Br J Pharmacol, 2000. **129**(4): p. 681-6.
100. Virchow, R., *Die Cellularpathologie in ihrer Begründung auf physiologische und pathologische Gewebelehre.* 1858, Berlin: Hirschwald.
101. Kalluri, R. and M. Zeisberg, *Fibroblasts in cancer.* Nat Rev Cancer, 2006. **6**(5): p. 392-401.
102. Tarin, D. and C.B. Croft, *Ultrastructural features of wound healing in mouse skin.* J Anat, 1969. **105**(Pt 1): p. 189-90.
103. Osterreicher, C.H., et al., *Fibroblast-specific protein 1 identifies an inflammatory subpopulation of macrophages in the liver.* Proc Natl Acad Sci U S A, 2011. **108**(1): p. 308-13.
104. Strutz, F., et al., *Identification and characterization of a fibroblast marker: FSP1.* J Cell Biol, 1995. **130**(2): p. 393-405.
105. Lam, S., et al., *Secretion of collagen type IV by human renal fibroblasts is increased by high glucose via a TGF-beta-independent pathway.* Nephrol Dial Transplant, 2004. **19**(7): p. 1694-701.
106. Zou, Y., et al., *Muscle interstitial fibroblasts are the main source of collagen VI synthesis in skeletal muscle: implications for congenital muscular dystrophy types Ullrich and Bethlem.* J Neuropathol Exp Neurol, 2008. **67**(2): p. 144-54.
107. Shuttleworth, C.A., L. Berry, and N. Wilson, *Collagen synthesis in rabbit dental pulp fibroblast cultures.* Arch Oral Biol, 1980. **25**(3): p. 201-5.
108. Prockop, D.J., *How does a skin fibroblast make type I collagen fibers?* J Invest Dermatol, 1982. **79** **Suppl 1**: p. 3s-6s.

109. Narayanan, A.S. and R.C. Page, *Synthesis of type V collagen by fibroblasts derived from normal, inflamed and hyperplastic human connective tissues*. Coll Relat Res, 1985. **5**(4): p. 297-304.
110. Frantz, C., K.M. Stewart, and V.M. Weaver, *The extracellular matrix at a glance*. J Cell Sci, 2010. **123**(Pt 24): p. 4195-200.
111. Albert, B., et al., *Molecular Biology of The Cell*. 1989, Garland Publishing, Inc.
112. Murad, S., A. Sivarajah, and S.R. Pinnell, *Serum stimulation of lysyl hydroxylase activity in cultured human skin fibroblasts*. Connect Tissue Res, 1985. **13**(2): p. 181-6.
113. Layman, D.L., A.S. Narayanan, and G.R. Martin, *The production of lysyl oxidase by human fibroblasts in culture*. Arch Biochem Biophys, 1972. **149**(1): p. 97-101.
114. Lindner, D., et al., *Differential expression of matrix metalloproteases in human fibroblasts with different origins*. Biochem Res Int, 2012. **2012**: p. 875742.
115. Ravanti, L., et al., *Induction of collagenase-3 (MMP-13) expression in human skin fibroblasts by three-dimensional collagen is mediated by p38 mitogen-activated protein kinase*. J Biol Chem, 1999. **274**(4): p. 2446-55.
116. Pinnell, S.R. and G.R. Martin, *The cross-linking of collagen and elastin: enzymatic conversion of lysine in peptide linkage to alpha-aminoadipic-delta-semialdehyde (allysine) by an extract from bone*. Proc Natl Acad Sci U S A, 1968. **61**(2): p. 708-16.
117. Shoulders, M.D. and R.T. Raines, *Collagen structure and stability*. Annu Rev Biochem, 2009. **78**: p. 929-58.
118. Kim, Y., C.D. Boyd, and K. Csiszar, *A new gene with sequence and structural similarity to the gene encoding human lysyl oxidase*. J Biol Chem, 1995. **270**(13): p. 7176-82.
119. Cox, T.R. and J.T. Erler, *Lysyl oxidase in colorectal cancer*. Am J Physiol Gastrointest Liver Physiol, 2013. **305**(10): p. G659-66.
120. Shaw, T.J. and P. Martin, *Wound repair at a glance*. J Cell Sci, 2009. **122**(Pt 18): p. 3209-13.
121. Gosain, A. and L.A. DiPietro, *Aging and wound healing*. World J Surg, 2004. **28**(3): p. 321-6.
122. Hendricks, T., et al., *Inhibition of basal and TGF beta-induced fibroblast collagen synthesis by antineoplastic agents. Implications for wound healing*. Br J Cancer, 1993. **67**(3): p. 545-50.
123. Velnar, T., T. Bailey, and V. Smrkolj, *The wound healing process: an overview of the cellular and molecular mechanisms*. J Int Med Res, 2009. **37**(5): p. 1528-42.
124. Schreier, T., E. Degen, and W. Baschong, *Fibroblast migration and proliferation during in vitro wound healing. A quantitative comparison between various growth factors and a low molecular weight blood dialysate used in the clinic to normalize impaired wound healing*. Res Exp Med (Berl), 1993. **193**(4): p. 195-205.
125. Atit, R.P., et al., *The Nf1 tumor suppressor regulates mouse skin wound healing, fibroblast proliferation, and collagen deposited by fibroblasts*. J Invest Dermatol, 1999. **112**(6): p. 835-42.
126. Lewis, J.H. and C.L. Jeffreys, *Effects of clotting and clot lysis on platelet thromboplastic activity*. Proc Soc Exp Biol Med, 1961. **108**: p. 382-5.
127. Kurkinen, M., et al., *Sequential appearance of fibronectin and collagen in experimental granulation tissue*. Lab Invest, 1980. **43**(1): p. 47-51.
128. Edward, M., J.A. Quinn, and W. Sands, *Keratinocytes stimulate fibroblast hyaluronan synthesis through the release of stratifin: a possible role in the suppression of scar tissue formation*. Wound Repair Regen, 2011. **19**(3): p. 379-86.
129. Montesano, R. and L. Orci, *Transforming growth factor beta stimulates collagen-matrix contraction by fibroblasts: implications for wound healing*. Proc Natl Acad Sci U S A, 1988. **85**(13): p. 4894-7.
130. Werner, S., T. Krieg, and H. Smola, *Keratinocyte-fibroblast interactions in wound healing*. J Invest Dermatol, 2007. **127**(5): p. 998-1008.

131. Wang, Z., et al., *Enhanced keratinocyte proliferation and migration in co-culture with fibroblasts*. PLoS One, 2012. **7**(7): p. e40951.
132. Hinz, B., *Formation and function of the myofibroblast during tissue repair*. J Invest Dermatol, 2007. **127**(3): p. 526-37.
133. Ulrich, M.M., et al., *Expression profile of proteins involved in scar formation in the healing process of full-thickness excisional wounds in the porcine model*. Wound Repair Regen, 2007. **15**(4): p. 482-90.
134. Dvorak, H.F., *Tumors: wounds that do not heal. Similarities between tumor stroma generation and wound healing*. N Engl J Med, 1986. **315**(26): p. 1650-9.
135. Olumi, A.F., et al., *Carcinoma-associated fibroblasts direct tumor progression of initiated human prostatic epithelium*. Cancer Res, 1999. **59**(19): p. 5002-11.
136. Dimanche-Boitrel, M.T., et al., *In vivo and in vitro invasiveness of a rat colon-cancer cell line maintaining E-cadherin expression: an enhancing role of tumor-associated myofibroblasts*. Int J Cancer, 1994. **56**(4): p. 512-21.
137. Orimo, A., et al., *Stromal fibroblasts present in invasive human breast carcinomas promote tumor growth and angiogenesis through elevated SDF-1/CXCL12 secretion*. Cell, 2005. **121**(3): p. 335-48.
138. Jia, C.C., et al., *Cancer-associated fibroblasts from hepatocellular carcinoma promote malignant cell proliferation by HGF secretion*. PLoS One, 2013. **8**(5): p. e63243.
139. Bhowmick, N.A., E.G. Neilson, and H.L. Moses, *Stromal fibroblasts in cancer initiation and progression*. Nature, 2004. **432**(7015): p. 332-7.
140. Karagiannis, G.S., et al., *Cancer-associated fibroblasts drive the progression of metastasis through both paracrine and mechanical pressure on cancer tissue*. Mol Cancer Res, 2012. **10**(11): p. 1403-18.
141. Le, Q.T., et al., *Validation of lysyl oxidase as a prognostic marker for metastasis and survival in head and neck squamous cell carcinoma: Radiation Therapy Oncology Group trial 90-03*. J Clin Oncol, 2009. **27**(26): p. 4281-6.
142. Cox, T.R., et al., *The hypoxic cancer secretome induces pre-metastatic bone lesions through lysyl oxidase*. Nature, 2015. **522**(7554): p. 106-10.
143. Nilsson, M., et al., *High Lysyl Oxidase (LOX) in the Non-Malignant Prostate Epithelium Predicts a Poor Outcome in Prostate Cancer Patient Managed by Watchful Waiting*. PLoS One, 2015. **10**(10): p. e0140985.
144. Lochter, A., et al., *Matrix metalloproteinase stromelysin-1 triggers a cascade of molecular alterations that leads to stable epithelial-to-mesenchymal conversion and a premalignant phenotype in mammary epithelial cells*. J Cell Biol, 1997. **139**(7): p. 1861-72.
145. Paunescu, V., et al., *Tumour-associated fibroblasts and mesenchymal stem cells: more similarities than differences*. J Cell Mol Med, 2011. **15**(3): p. 635-46.
146. Kim, J.H., et al., *The role of myofibroblasts in upregulation of S100A8 and S100A9 and the differentiation of myeloid cells in the colorectal cancer microenvironment*. Biochem Biophys Res Commun, 2012. **423**(1): p. 60-6.
147. Allaoui, R., et al., *Cancer-associated fibroblast-secreted CXCL16 attracts monocytes to promote stroma activation in triple-negative breast cancers*. Nat Commun, 2016. **7**: p. 13050.
148. Augsten, M., et al., *Cancer-associated fibroblasts expressing CXCL14 rely upon NOS1-derived nitric oxide signaling for their tumor-supporting properties*. Cancer Res, 2014. **74**(11): p. 2999-3010.
149. Bleul, C.C., et al., *A highly efficacious lymphocyte chemoattractant, stromal cell-derived factor 1 (SDF-1)*. J Exp Med, 1996. **184**(3): p. 1101-9.

150. Karin, N., *The multiple faces of CXCL12 (SDF-1alpha) in the regulation of immunity during health and disease*. J Leukoc Biol, 2010. **88**(3): p. 463-73.
151. Chatterjee, M., et al., *Platelet-derived CXCL12 regulates monocyte function, survival, differentiation into macrophages and foam cells through differential involvement of CXCR4-CXCR7*. Cell Death Dis, 2015. **6**: p. e1989.
152. Frydenlund, N., et al., *Tumoral PD-L1 expression in desmoplastic melanoma is associated with depth of invasion, tumor-infiltrating CD8 cytotoxic lymphocytes and the mixed cytomorphological variant*. Mod Pathol, 2017.
153. Chen, L. and X. Han, *Anti-PD-1/PD-L1 therapy of human cancer: past, present, and future*. J Clin Invest, 2015. **125**(9): p. 3384-91.
154. Nazareth, M.R., et al., *Characterization of human lung tumor-associated fibroblasts and their ability to modulate the activation of tumor-associated T cells*. J Immunol, 2007. **178**(9): p. 5552-62.
155. Boyd, N.F., et al., *Mammographic densities and breast cancer risk*. Cancer Epidemiol Biomarkers Prev, 1998. **7**(12): p. 1133-44.
156. Boyd, N.F., et al., *Mammographic breast density as an intermediate phenotype for breast cancer*. Lancet Oncol, 2005. **6**(10): p. 798-808.
157. Vacek, P.M. and B.M. Geller, *A prospective study of breast cancer risk using routine mammographic breast density measurements*. Cancer Epidemiol Biomarkers Prev, 2004. **13**(5): p. 715-22.
158. Vachon, C.M., et al., *Mammographic breast density as a general marker of breast cancer risk*. Cancer Epidemiol Biomarkers Prev, 2007. **16**(1): p. 43-9.
159. Kerlikowske, K., et al., *Breast cancer risk by breast density, menopause, and postmenopausal hormone therapy use*. J Clin Oncol, 2010. **28**(24): p. 3830-7.
160. Boyd, N.F., et al., *Quantitative classification of mammographic densities and breast cancer risk: results from the Canadian National Breast Screening Study*. J Natl Cancer Inst, 1995.
161. Engmann, N.J., et al., *Population-Attributable Risk Proportion of Clinical Risk Factors for Breast Cancer*. JAMA Oncol, 2017.
162. Checka, C.M., et al., *The relationship of mammographic density and age: implications for breast cancer screening*. AJR Am J Roentgenol, 2012. **198**(3): p. W292-5.
163. Pike, M.C., et al., *'Hormonal' risk factors, 'breast tissue age' and the age-incidence of breast cancer*. Nature, 1983. **303**(5920): p. 767-70.
164. Martin, L.J., et al., *Family history, mammographic density, and risk of breast cancer*. Cancer Epidemiol Biomarkers Prev, 2010. **19**(2): p. 456-63.
165. Ziv, E., et al., *Mammographic breast density and family history of breast cancer*. J Natl Cancer Inst, 2003. **95**(7): p. 556-8.
166. Boyd, N.F., et al., *Mammographic density: a heritable risk factor for breast cancer*. Methods Mol Biol, 2009. **472**: p. 343-60.
167. Fair, A.M., et al., *Increased vitamin D and calcium intake associated with reduced mammographic breast density among premenopausal women*. Nutr Res, 2015. **35**(10): p. 851-7.
168. Li, T., et al., *The association of measured breast tissue characteristics with mammographic density and other risk factors for breast cancer*. Cancer Epidemiol Biomarkers Prev, 2005. **14**(2): p. 343-9.
169. Huo, C.W., et al., *High mammographic density is associated with an increase in stromal collagen and immune cells within the mammary epithelium*. Breast Cancer Res, 2015. **17**: p. 79.
170. Boyd, N.F., et al., *Breast tissue composition and susceptibility to breast cancer*. J Natl Cancer Inst, 2010. **102**(16): p. 1224-37.

171. Mockus, M., et al., *First Pregnancy Characteristics, Postmenopausal Breast Density, and Salivary Sex Hormone Levels in a Population at High Risk for Breast Cancer*. BBA Clin, 2015. **3**: p. 189-195.
172. Goddard, E.T., et al., *The Rodent Liver Undergoes Weaning-Induced Involution and Supports Breast Cancer Metastasis*. Cancer Discov, 2016.
173. Izu, Y., et al., *Dysfunctional tendon collagen fibrillogenesis in collagen VI null mice*. Matrix Biol, 2011. **30**(1): p. 53-61.
174. Ansorge, H.L., et al., *Type XIV Collagen Regulates Fibrillogenesis: PREMATURE COLLAGEN FIBRIL GROWTH AND TISSUE DYSFUNCTION IN NULL MICE*. J Biol Chem, 2009. **284**(13): p. 8427-38.
175. Villone, D., et al., *Supramolecular interactions in the dermo-epidermal junction zone: anchoring fibril-collagen VII tightly binds to banded collagen fibrils*. J Biol Chem, 2008. **283**(36): p. 24506-13.
176. Amenta, P.S., et al., *Proteoglycan-collagen XV in human tissues is seen linking banded collagen fibers subjacent to the basement membrane*. J Histochem Cytochem, 2005. **53**(2): p. 165-76.
177. Franzke, C.W., P. Bruckner, and L. Bruckner-Tuderman, *Collagenous transmembrane proteins: recent insights into biology and pathology*. J Biol Chem, 2005. **280**(6): p. 4005-8.
178. Jindal, S., et al., *Postpartum breast involution reveals regression of secretory lobules mediated by tissue-remodeling*. Breast Cancer Res, 2014.
179. Chen, J., et al., *Multiphoton microscopy study of the morphological and quantity changes of collagen and elastic fiber components in keloid disease*. J Biomed Opt, 2011. **16**(5): p. 051305.
180. Xiao, Q. and G. Ge, *Lysyl oxidase, extracellular matrix remodeling and cancer metastasis*. Cancer Microenviron, 2012. **5**(3): p. 261-73.
181. Barker, H.E., T.R. Cox, and J.T. Erler, *The rationale for targeting the LOX family in cancer*. Nat Rev Cancer, 2012. **12**(8): p. 540-52.
182. Nagase, H., R. Visse, and G. Murphy, *Structure and function of matrix metalloproteinases and TIMPs*. Cardiovasc Res, 2006. **69**(3): p. 562-73.
183. Ingman, W.V., et al., *Macrophages promote collagen fibrillogenesis around terminal end buds of the developing mammary gland*. Developmental Dynamics, 2006. **235**(12): p. 3222-3229.
184. Amant, F., et al., *Prognosis of Women With Primary Breast Cancer Diagnosed During Pregnancy: Results From an International Collaborative Study*. J Clin Oncol, 2013.
185. Gillitzer, R. and M. Goebeler, *Chemokines in cutaneous wound healing*. J Leukoc Biol, 2001. **69**(4): p. 513-21.
186. Midwood, K.S., L.V. Williams, and J.E. Schwarzbauer, *Tissue repair and the dynamics of the extracellular matrix*. Int J Biochem Cell Biol, 2004. **36**(6): p. 1031-7.
187. Wilgus, T.A., *Immune cells in the healing skin wound: influential players at each stage of repair*. Pharmacol Res, 2008. **58**(2): p. 112-6.
188. Schafer, M. and S. Werner, *Cancer as an overhealing wound: an old hypothesis revisited*. Nat Rev Mol Cell Biol, 2008. **9**(8): p. 628-38.
189. Dumont, N., et al., *Breast fibroblasts modulate early dissemination, tumorigenesis, and metastasis through alteration of extracellular matrix characteristics*. Neoplasia, 2013. **15**(3): p. 249-62.
190. Gascard, P. and T.D. Tlsty, *Carcinoma-associated fibroblasts: orchestrating the composition of malignancy*. Genes Dev, 2016. **30**(9): p. 1002-19.
191. Threatt, B., et al., *Association between mammographic parenchymal pattern classification and incidence of breast cancer*. Cancer, 1980. **45**(10): p. 2550-6.
192. Martin, L.J. and N.F. Boyd, *Mammographic density. Potential mechanisms of breast cancer risk associated with mammographic density: hypotheses based on epidemiological evidence*. Breast Cancer Res, 2008. **10**(1): p. 201.

193. Butcher, D.T., T. Alliston, and V.M. Weaver, *A tense situation: forcing tumour progression*. Nat Rev Cancer, 2009. **9**(2): p. 108-22.
194. Barcus, C.E., et al., *Stiff collagen matrices increase tumorigenic prolactin signaling in breast cancer cells*. J Biol Chem, 2013. **288**(18): p. 12722-32.
195. Goswami, S., et al., *Macrophages promote the invasion of breast carcinoma cells via a colony-stimulating factor-1/epidermal growth factor paracrine loop*. Cancer Res, 2005. **65**(12): p. 5278-83.
196. Bates, G.J., et al., *Quantification of regulatory T cells enables the identification of high-risk breast cancer patients and those at risk of late relapse*. J Clin Oncol, 2006. **24**(34): p. 5373-80.
197. Gao, D., et al., *Myeloid progenitor cells in the premetastatic lung promote metastases by inducing mesenchymal to epithelial transition*. Cancer Res, 2012. **72**(6): p. 1384-94.
198. Reiser, J. and A. Banerjee, *Effector, Memory, and Dysfunctional CD8(+) T Cell Fates in the Antitumor Immune Response*. J Immunol Res, 2016. **2016**: p. 8941260.
199. Ali, H.R., et al., *Association between CD8+ T-cell infiltration and breast cancer survival in 12,439 patients*. Ann Oncol, 2014. **25**(8): p. 1536-43.
200. Liu, S., et al., *CD8+ lymphocyte infiltration is an independent favorable prognostic indicator in basal-like breast cancer*. Breast Cancer Res, 2012. **14**(2): p. R48.
201. Huang, Y., et al., *CD4+ and CD8+ T cells have opposing roles in breast cancer progression and outcome*. Oncotarget, 2015. **6**(19): p. 17462-78.
202. Gallina, G., et al., *Tumors induce a subset of inflammatory monocytes with immunosuppressive activity on CD8+ T cells*. J Clin Invest, 2006. **116**(10): p. 2777-90.
203. Williams, C.B., E.S. Yeh, and A.C. Soloff, *Tumor-associated macrophages: unwitting accomplices in breast cancer malignancy*. NPJ Breast Cancer, 2016. **2**.
204. Ward, R., et al., *Monocytes and macrophages, implications for breast cancer migration and stem cell-like activity and treatment*. Oncotarget, 2015. **6**(16): p. 14687-99.
205. Silzle, T., et al., *Tumor-associated fibroblasts recruit blood monocytes into tumor tissue*. Eur J Immunol, 2003. **33**(5): p. 1311-20.
206. Erez, N., et al., *Cancer-Associated Fibroblasts Are Activated in Incipient Neoplasia to Orchestrate Tumor-Promoting Inflammation in an NF-kappaB-Dependent Manner*. Cancer Cell, 2010. **17**(2): p. 135-47.
207. Yata, Y., et al., *DNase I-hypersensitive sites enhance alpha1(I) collagen gene expression in hepatic stellate cells*. Hepatology, 2003. **37**(2): p. 267-76.
208. Sharon, Y., et al., *Isolation of normal and cancer-associated fibroblasts from fresh tissues by Fluorescence Activated Cell Sorting (FACS)*. J Vis Exp, 2013(71): p. e4425.
209. Mosunjac, M.B., et al., *Use of a novel marker, calponin, for myoepithelial cells in fine-needle aspirates of papillary breast lesions*. Diagn Cytopathol, 2000. **23**(3): p. 151-5.
210. Bertolami, C. and R.B. Donoff, *The effect of full-thickness skin grafts on the actomyosin content of contracting wounds*. J Oral Surg, 1979. **37**(7): p. 471-6.
211. Su, G., et al., *Functional screen of paracrine signals in breast carcinoma fibroblasts*. PLoS One, 2012. **7**(10): p. e46685.
212. Administration, U.S.D.o.H.a.H.S.F.a.D. *Guidance for Industry. Estimating the Maximum Safe Starting Dose in Initial Clinical Trials for Therapeutics in Adult Healthy Volunteers*. 2005.
213. Seluanov, A., A. Vaidya, and V. Gorbunova, *Establishing primary adult fibroblast cultures from rodents*. J Vis Exp, 2010(44).
214. Nakagawa, S., P. Pawelek, and F. Grinnell, *Long-term culture of fibroblasts in contracted collagen gels: effects on cell growth and biosynthetic activity*. J Invest Dermatol, 1989. **93**(6): p. 792-8.

215. Gorska, A.E., et al., *Transgenic mice expressing a dominant-negative mutant type II transforming growth factor-beta receptor exhibit impaired mammary development and enhanced mammary tumor formation*. Am J Pathol, 2003. **163**(4): p. 1539-49.
216. Roberts, A.B. and M.B. Sporn, *Transforming growth factor-beta: potential common mechanisms mediating its effects on embryogenesis, inflammation-repair, and carcinogenesis*. Int J Rad Appl Instrum B, 1987. **14**(4): p. 435-9.
217. Uria, J.A., et al., *Differential effects of transforming growth factor-beta on the expression of collagenase-1 and collagenase-3 in human fibroblasts*. J Biol Chem, 1998. **273**(16): p. 9769-77.
218. Lijnen, P., et al., *Transforming growth factor-beta 1 promotes contraction of collagen gel by cardiac fibroblasts through their differentiation into myofibroblasts*. Methods Find Exp Clin Pharmacol, 2003. **25**(2): p. 79-86.
219. Dewland, P.M., S. Reader, and P. Berry, *Bioavailability of ibuprofen following oral administration of standard ibuprofen, sodium ibuprofen or ibuprofen acid incorporating poloxamer in healthy volunteers*. BMC Clin Pharmacol, 2009. **9**: p. 19.
220. Boyd, N.F., et al., *Mammographic density and breast cancer risk: current understanding and future prospects*. Breast Cancer Res, 2011.
221. Gillette, M., et al., *P190B RhoGAP overexpression in the developing mammary epithelium induces TGFbeta-dependent fibroblast activation*. PLoS One, 2013. **8**(5): p. e65105.
222. Blackstock, C.D., et al., *Insulin-like growth factor-1 increases synthesis of collagen type I via induction of the mRNA-binding protein LARP6 expression and binding to the 5' stem-loop of COL1a1 and COL1a2 mRNA*. J Biol Chem, 2014. **289**(11): p. 7264-74.
223. Takabatake, Y., et al., *Lactation opposes pappalysin-1-driven pregnancy-associated breast cancer*. EMBO Mol Med, 2016. **8**(4): p. 388-406.
224. Iliopoulos, D., H.A. Hirsch, and K. Struhl, *An epigenetic switch involving NF-kappaB, Lin28, Let-7 MicroRNA, and IL6 links inflammation to cell transformation*. Cell, 2009. **139**(4): p. 693-706.
225. Acerbi, I., et al., *Human breast cancer invasion and aggression correlates with ECM stiffening and immune cell infiltration*. Integr Biol (Camb), 2015. **7**(10): p. 1120-34.
226. Hughes, K., et al., *Conditional deletion of Stat3 in mammary epithelium impairs the acute phase response and modulates immune cell numbers during post-lactational regression*. J Pathol, 2012. **227**(1): p. 106-17.
227. Cotechini, T., T.R. Medler, and L.M. Coussens, *Myeloid Cells as Targets for Therapy in Solid Tumors*. Cancer J, 2015. **21**(4): p. 343-50.
228. Li, H., et al., *Low/negative expression of PDGFR-alpha identifies the candidate primary mesenchymal stromal cells in adult human bone marrow*. Stem Cell Reports, 2014. **3**(6): p. 965-74.
229. Bartol, A., A. Laib, and H. Augustin, *Tumor vessel associated-pericytes, in Tumor-Associated Fibroblasts and their Matrix*. 2011. p. 91-97.
230. Viski, C., et al., *Endosialin-Expressing Pericytes Promote Metastatic Dissemination*. Cancer Res, 2016. **76**(18): p. 5313-25.
231. Palucka, A.K. and L.M. Coussens, *The Basis of Oncoimmunology*. Cell, 2016. **164**(6): p. 1233-47.
232. O'Connell, J.T., et al., *VEGF-A and Tenascin-C produced by S100A4+ stromal cells are important for metastatic colonization*. Proc Natl Acad Sci U S A, 2011. **108**(38): p. 16002-7.
233. Elkabets, M., et al., *Human tumors instigate granulysin-expressing hematopoietic cells that promote malignancy by activating stromal fibroblasts in mice*. J Clin Invest, 2011. **121**(2): p. 784-99.
234. Pazolli, E., et al., *Chromatin remodeling underlies the senescence-associated secretory phenotype of tumor stromal fibroblasts that supports cancer progression*. Cancer Res, 2012. **72**(9): p. 2251-61.

235. Ozdemir, B.C., et al., *Depletion of carcinoma-associated fibroblasts and fibrosis induces immunosuppression and accelerates pancreas cancer with reduced survival*. *Cancer Cell*, 2014. **25**(6): p. 719-34.
236. Kim, S., et al., *Lifetime use of nonsteroidal anti-inflammatory drugs and breast cancer risk: results from a prospective study of women with a sister with breast cancer*. *BMC Cancer*, 2015. **15**: p. 960.
237. Storey, J.D., *A direct approach to false discovery rates*. *J. R. Statist.*, 2002(Series B): p. 479–498.
238. Francke, A., et al., *Generation of mature murine monocytes from heterogeneous bone marrow and description of their properties*. *J Histochem Cytochem*, 2011. **59**(9): p. 813-25.
239. Martinez, F.O., et al., *Macrophage activation and polarization*. *Front Biosci*, 2008. **13**: p. 453-61.
240. Reddy, S.M., et al., *Phagocytosis of apoptotic cells by macrophages induces novel signaling events leading to cytokine-independent survival and inhibition of proliferation: activation of Akt and inhibition of extracellular signal-regulated kinases 1 and 2*. *J Immunol*, 2002. **169**(2): p. 702-13.
241. Helft, J., et al., *GM-CSF Mouse Bone Marrow Cultures Comprise a Heterogeneous Population of CD11c(+)MHCII(+) Macrophages and Dendritic Cells*. *Immunity*, 2015. **42**(6): p. 1197-211.
242. Murakami-Satsutani, N., et al., *IL-33 promotes the induction and maintenance of Th2 immune responses by enhancing the function of OX40 ligand*. *Allergol Int*, 2014. **63**(3): p. 443-55.
243. Rincon, M., et al., *Interleukin (IL)-6 directs the differentiation of IL-4-producing CD4+ T cells*. *J Exp Med*, 1997. **185**(3): p. 461-9.
244. Peng, Y., et al., *TGF-beta regulates in vivo expansion of Foxp3-expressing CD4+CD25+ regulatory T cells responsible for protection against diabetes*. *Proc Natl Acad Sci U S A*, 2004. **101**(13): p. 4572-7.
245. Wahl, S.M., et al., *Transforming growth factor type beta induces monocyte chemotaxis and growth factor production*. *Proc Natl Acad Sci U S A*, 1987. **84**(16): p. 5788-92.
246. Turley, J.M., et al., *Transforming growth factor beta 1 functions in monocytic differentiation of hematopoietic cells through autocrine and paracrine mechanisms*. *Cell Growth Differ*, 1996. **7**(11): p. 1535-44.
247. Gong, D., et al., *TGFbeta signaling plays a critical role in promoting alternative macrophage activation*. *BMC Immunol*, 2012. **13**: p. 31.
248. Stein, M., et al., *Interleukin 4 potently enhances murine macrophage mannose receptor activity: a marker of alternative immunologic macrophage activation*. *J Exp Med*, 1992. **176**(1): p. 287-92.
249. Bonecchi, R., et al., *Divergent effects of interleukin-4 and interferon-gamma on macrophage-derived chemokine production: an amplification circuit of polarized T helper 2 responses*. *Blood*, 1998. **92**(8): p. 2668-71.
250. Hansen, K.C., et al., *An in-solution ultrasonication-assisted digestion method for improved extracellular matrix proteome coverage*. *Mol Cell Proteomics*, 2009. **8**(7): p. 1648-57.
251. Fadok, V.A., et al., *Macrophages that have ingested apoptotic cells in vitro inhibit proinflammatory cytokine production through autocrine/paracrine mechanisms involving TGF-beta, PGE2, and PAF*. *J Clin Invest*, 1998. **101**(4): p. 890-8.
252. Voll, R.E., et al., *Immunosuppressive effects of apoptotic cells*. *Nature*, 1997. **390**(6658): p. 350-1.
253. McDonald, P.P., et al., *Transcriptional and translational regulation of inflammatory mediator production by endogenous TGF-beta in macrophages that have ingested apoptotic cells*. *J Immunol*, 1999. **163**(11): p. 6164-72.
254. Elias, J.A., et al., *Regulation of human lung fibroblast collagen production by recombinant interleukin-1, tumor necrosis factor, and interferon-gamma*. *Ann N Y Acad Sci*, 1990. **580**: p. 233-44.
255. Anders, C.K., et al., *Breast cancer before age 40 years*. *Semin Oncol*, 2009. **36**(3): p. 237-49.